PONTIFICIA UNIVERSIDAD CATÓLICA DEL PERÚ

Escuela de Posgrado

Heavy neutrino production and decay at DUNE Near Detector

Tesis para optar el grado académico de Doctor en Física que presenta:

Saneli Alcides Carbajal Vigo

Asesor:

Alberto Martin Gago Medina

Lima, 2024

Informe de Similitud

Yo, Alberto Gago Medina, docente de la Escuela de Posgrado de la Pontificia Universidad Católica del Perú, asesor(a) de la tesis/el trabajo de investigación titulado Heavy neutrino production and decay at DUNE Near Detector, del autor Saneli Carbajal, dejo constancia de lo siguiente:

- El mencionado documento tiene un índice de puntuación de similitud de 29 %. Así lo consigna el reporte de similitud emitido por el software *Turnitin* el 05/07/2024
- He revisado con detalle dicho reporte y el índice real de similitud de la Tesis de doctorado y este corresponde al 18 % ya que un poco más del 11% corresponden a autorreferencias de trabajos publicados sobre esta tesis, de tal manera no se advierten indicios de plagio.
- Las citas a otros autores y sus respectivas referencias cumplen con las pautas académicas.

Lugar y fecha:
Lima, 07-07-2024

Apellidos y nombres del asesor / de la asesora: Gago Medina Alberto Martin.	
DNI: 07835422	Firma
ORCID: 0000-0002-0019-9692	

A mi madre.
Gracias por todo.

iv

Acknowledgements

v

Resumen

En la presente tesis se estudia el potencial del DUNE Near Detector (DUNEND) para establecer límites a neutrinos pesados (HNL). Esto es realizado a través de un estudio de cómo los HNL afectan las tasas de producción y las distribuciones angulares de los neutrinos activos. Se demuestra que la producción de HNL en DUNE produce un déficit de eventos de corriente cargada (CC) en el Liquid Argon Time Proyection Chamber (LArTPC) de DUNEND y se utiliza esto para estimar la sensibilidad de DUNE a HNLs. Nuestro análisis revela que la sensibilidad depende fuertemente de las incertidumbres sistemáticas en las predicciones del flujo de neutrinos de DUNE. Asumiendo 10 años de operación (5 en modo neutrino y 5 en modo antineutrino) se obtienen los límites $|U_{\mu 4}|^2 < 9 \times 10^{-3}(4 \times 10^{-2})$ y $|U_{e4}|^2 < 7 \times 10^{-3}(3 \times 10^{-2})$ para masas por debajo de 10 MeV y una incertidumbre del 5%(20%) en la normalización de la predicción de los eventos de corriente cargada de neutrinos. Estos límites son mejores que aquellos que pueden ser alcanzados por las búsquedas directas en DUNE para masas por debajo de los 2(10) MeV. Para el caso de una incertidumbre conservadora del 20%, los límites obtenidos solo pueden mejorar los límites experimentales actuales en $|U_{e4}|^2$ por un factor de 3 en una pequeña región alrededor de 5 eV y establecer límites en $|U_{\mu 4}|^2$ en una región de masas libre de restricciones (40 eV - 1 MeV)

Palabras clave: Fenomenología de neutrinos, neutrinos pesados, experimento DUNE.

Abstract

In the present thesis we study the potential of the DUNE Near Detector (DUNEND) for establishing bounds for heavy neutral leptons (HNL). This is achieved by studying how the presence of HNLs affects the production rates and angular distributions of active neutrinos. We show that HNL production at DUNE creates a deficit in the neutrino charged current (CC) events at the Liquid Argon Time Proyection Chamer (LArTPC) of the DUNEND and use this to estimate the sensitivity of DUNE to HNLs. Our analysis reveals that the sensitivity is heavily dependent on the systematic uncertainties in the DUNE neutrino flux predictions. For 10 years of operation (5 in neutrino and antineutrino mode) we obtain limits of $|U_{\mu4}|^2 < 9 \times 10^{-3} (4 \times 10^{-2})$ and $|U_{e4}|^2 < 7 \times 10^{-3} (3 \times 10^{-2})$ for masses below 10 MeV and a 5%(20%) overall normalization uncertainty in the neutrino charged current event rates prediction. These limits are better than those that can be achieved by DUNE direct searches for the case of a 5%(20%) uncertainty within the region of masses below 2(10) MeV. When a conservative 20% uncertainty is present, the limits obtained can only improve current experimental constraints on $|U_{e4}|^2$ by up to a factor of 3 in a small region around 5 eV and set limits on $|U_{\mu4}|^2$ in a mass region free of constraints (40 eV - 1 MeV).

Keywords: Neutrino phenomenology, heavy neutral leptons, DUNE experiment.

Publication List

1. S. Carbajal and A.M. Gago (2021). Setting limits on heavy neutral leptons using the neutrino CC events at the DUNE near detector. J. Phys. Conf. Ser., 2156, 012237. doi:10.1088/1742-6596/2156/1/012237

2. Asli M Abdullahi et al (2023). The present and future status of heavy neutral leptons. J. Phys. G: Nucl. Part. Phys. 50 020501. doi: 10.1088/1361-6471/ac98f9

3. S. Carbajal and A. M. Gago (2024). Indirect search of heavy neutral leptons using the DUNE near detector. Frontiers in Physics 12. doi:10.3389/fphy.2024.1398070.

Table of contents

List of figures

List of tables

Introduction

The study of the fundamental composition of matter has been a recurring subject in the history of the Western world. The "physicists" of ancient Greece tried to give rational explanations for the existence of matter and its properties based mostly on clever reasoning and deduction. However, it was not until the XVI century, with the development of the scientific method, that an empirically rigorous study of the microscopic world truly began. This endeavor over centuries eventually gave birth to one of the most precise theories in the history of science: the Standard Model (SM) of particle physics. The Standard Model is a quantum field theory framework formulated within the context of the local gauge symmetry group $SU(3)_c \times SU(2)_L \times U(1)_Y$. The fields of the SM are composed of six quarks (up, down, charm, strange, top, bottom), three charged leptons (electron, muon and tau), three neutrinos (electron, muon and tau neutrino), six gauge bosons (photon, $W^\pm$, Z and eight gluons) and the Higgs field. Although the SM has proven to be a very successful and precise theory, there are still some open questions about the nature of some interactions and particle properties. For instance, neutrinos are considered to be massless in the SM. However, it has been observed that neutrinos can spontaneously change their flavors, a phenomenon known as neutrino oscillations [12, 13, 39]. These oscillations can be explained if one considers that the neutrino states that participate in the weak interactions (weak eigenstates) are different from the eigenstates of the neutrino Hamiltonian (mass eigenstates). This gives rise to neutrino mixing, where each weak eigenstate is a superposition of the mass eigenstates. This mixing cannot occur if all neutrinos are massless. The analysis of neutrino oscillations has led to the conclusion that not all neutrinos can have a zero mass [54].

To account for the existence of neutrino mass, one must add neutrino mass terms to the SM lagrangian. The most straightforward way to achieve this is to add a coupling between the Higgs field and the neutrino fields in a way that is similar to what is done in the quark sector for the d, s and b quarks. In principle, the introduction of this Dirac mass can explain the existence of neutrino masses and should solve the neutrino mass problem completely. However, experiments have shown that the values of the neutrino masses are very small, on the order of 0.1 eV [61], and these mass scales can only be achieved if the couplings between

the Higgs and neutrino fields are several orders of magnitude smaller than the couplings of the Higgs to the rest particles of the SM. These unnaturally small coupling constants suggest that there might be another mechanism responsible for the generation of neutrino masses that does not require fine-tuning of the coupling constants. There is another way to introduce neutrino masses to the SM lagrangian. Since neutrinos are not charged under the electromagnetic interaction, it is possible to directly add to the lagrangian a term that couples two neutrino fields. To preserve the $SU(2)_L$ symmetry of the SM, these neutrino fields must be right-handed, so that they do not directly participate in the weak interaction. This so-called Majorana mass term can explain the existence of neutrino masses, but at the same time violates lepton number conservation by two units. Majorana neutrinos would also be their own antiparticles, so their existence would open the possibility for new interesting physics beyond the SM.

In general, one can add both Dirac and Majorana mass terms to the SM lagrangian, and the values of the physical neutrino masses can be obtained from the diagonalization of the neutrino mass matrix. However, the problem of the smallness of neutrino masses remains open and one still needs a mechanism to generate very small neutrino masses to avoid fine tuning. This can be achieved if one adds extra neutrino fields to the SM lagrangian with masses that are much larger than the masses of the three neutrinos of the SM. These extra neutrino fields must be also sterile in the sense that, in contrast to the active neutrinos of the SM, they do not participate in the weak interaction, a condition that can be achieved if they have right-handed chirality. After the diagonalization of the mass matrix, the presence of these sterile neutrinos affects the mass of the active neutrinos of the SM in a way that the active neutrino masses decrease as the sterile neutrino masses increase. This seesaw mechanism [62] can naturally explain the smallness of the active neutrino masses if one admits the existence of heavier sterile neutrino states. However, the scale of the masses of the sterile neutrinos is not completely fixed because it depends on the scale of their coupling constants. If the coupling constants are of order 1, then the scale of the new physics is very large, around 10^{14} GeV. This high-scale seesaw is attractive because it might be connected to GUT theories and leptogenesis, but it also introduces a destabilization of the Higgs mass and is not testable in the near future. On the other hand, if the coupling constants are sufficiently small, then the scale of new physics can be small enough to get sterile neutrinos with masses that range from eV to TeV. This low-scale seesaw is particularly interesting because the sterile neutrinos can be produced at energies that are accessible to experiment in the present or near future. In particular, if the sterile neutrino has a mass much larger than 1 eV, then it can also decay into other SM particles and its decay products can in principle be detected in current accelerator experiments. These heavy neutral leptons (HNL) have become increasingly more

interesting because they might be detected in next-generation neutrino experiments. The confirmation of the existence of HNLs or sterile neutrinos, in general, would be a giant step towards the understanding of the mechanisms for mass generation in nature beyond the standard model.

One of the more promising experiments for the study of HNLs is the Deep Underground Neutrino Experiment (DUNE) [4]. DUNE will produce the world's most intense neutrino beam, which will be pointed towards two liquid argon detectors: the Near Detector (DUNEND) and the Far Detector (DUNEFD), located at 574 m and 1300 km from the DUNE target, respectively. The main goal of the DUNE experiment is to study neutrino oscillations and precisely measure the parameters involved in the neutrino physics of the SM. However, the high intensity of the DUNE neutrino beam will also let us study neutrino physics beyond the SM. DUNE will be able to produce a significant amount of HNLs with masses up to GeV. If these HNLs decay inside one of the DUNE detectors, it would be possible to detect their decay products, confirming their existence and opening a window beyond standard model physics. However, the production of HNLs at DUNE will also have other effects that can indirectly detect the presence of HNLs. For instance, the production of one HNL can only be possible if it replaces the production of an active neutrino. Therefore, if HNLs are produced at DUNE, then the number of active neutrinos produced necessarily decreases. This phenomenon, which is independent of neutrino oscillations, translates into a deficit of neutrino charged current (CC) events at the DUNE detectors. In this work, we conduct a detailed study of this possible CC events deficit at the DUNEND due to HNL production. We show that this CC deficit can be interpreted as an indirect signal of the presence of HNLs at DUNE. We calculate the significance of this deficit in different configurations and show that, if no significant CC deficit is found at DUNE, this can be used to estimate limits on the HNL's mass and mixing to active neutrinos.

This thesis is organized as follows. In the first chapter, we make a brief review of the standard model and then proceed to explain some possible mechanisms for neutrino mass generations and neutrino oscillations. In the second chapter, we focus on HNLs and review how these particles might be created from meson and lepton decays, their possible decay products, lifetimes and also neutrino oscillations that involve HNLs. In the third chapter, we explain the configuration for our simulations of the DUNE neutrino flux, as well as the implementation of HNL production and decay. In the fourth chapter, we show our results for the change in the neutrino flux at DUNE due to the production of HNLs. We also estimate the sensitivity of DUNE to HNLs and the possible limits that DUNE might be able to set to the HNL mass and its mixing with active neutrinos. Finally, in the last section, we show our conclusions and the possible extensions of our work.
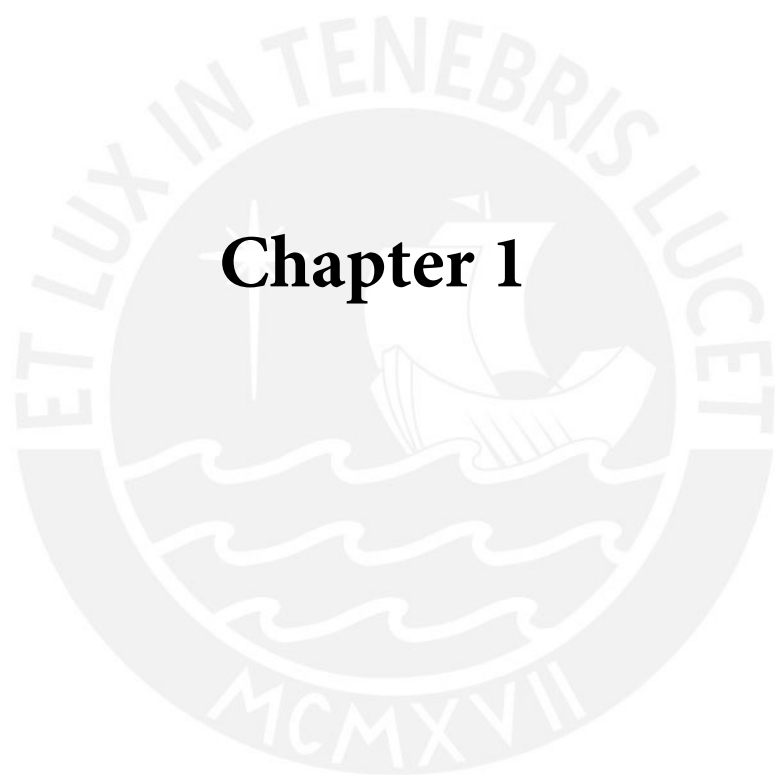
Chapter 1

Chapter 1

Neutrinos and the Standard Model

1.1   The Standard Model

The standard model (SM) of particle physics is considered one of the most successful theories of physics and at present represents our most fundamental understanding of the phenomena observed in particle physics. The Standard Model is a quantum field theory framework formulated within the context of local gauge symmetries, specifically the group $SU(3)_c \times SU(2)_L \times U(1)_Y$ that describes the electromagnetic, weak, and strong nuclear forces and their interactions with matter fields. The subscripts C, L and Y refer to the color, left-handed (LH) chirality and weak hypercharge, respectively. The weak interaction related to the $SU(2)_L$ symmetry affects only left-handed chiral particle estates, which are organized in doublets, while the right-handed chiral states are organized in singles and hence are not affected by the symmetry transformation The SM postulates the existence of fermionic matter fields, which include six quark flavors and three generations of leptons, each with associated antiparticles. The matter fields interact through the exchange of gauge bosons produced by the gauge invariance of the theory: photons (γ), W ($W^\pm$) and Z bosons, and eight gluons. Also, the model incorporates the Higgs mechanism, characterized by a scalar Higgs field with a non-zero vacuum expectation value, which spontaneously breaks the electroweak symmetry and gives mass to the fermion fields. Figure 1.1 shows all the particles that are part of the standard model, where fermions participate in the weak interaction, only charged particles interact electromagnetically and all quarks participate in the strong interaction.

In the standard model, all left-handed leptons transform trivially under $SU(3)_C$ (and therefore do not participate in the strong interaction) and transform as a doublet under $SU(2)_L$. On the other hand, the quarks transform as a triplet under $SU(3)$, where the components are labeled as colors red, green and blue. Due to the nature of the $SU(2)_L$ symmetry, which treats LH and right-handed (RH) chiral states differently, the SM partity is explicitly broken.
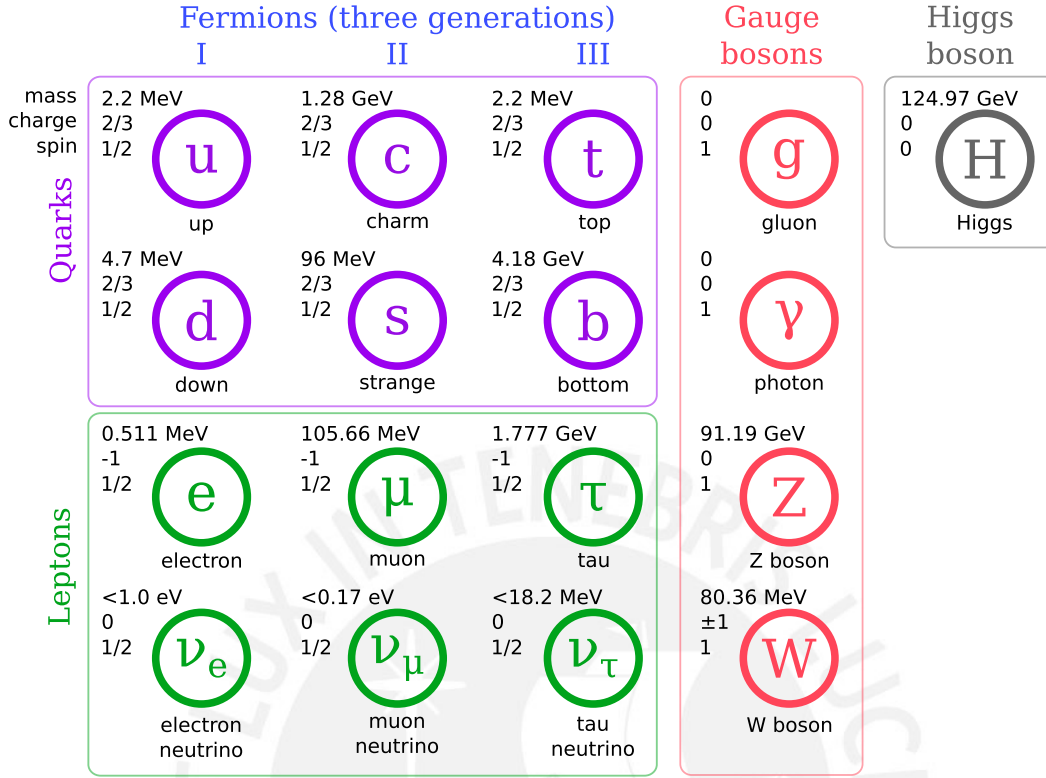
Fig. 1.1 Particles of the Standard Model of Particle Physics. The figure is based on Ref. [60]

This is particularly important for neutrinos because in the SM they are massless and hence the right-handed chiral components are not required to appear in the Lagrangian.

The standard model Lagrangian can be written as

$$\mathcal{L}_{SM} = \mathcal{L}_{Gauge} + \mathcal{L}_{Fermion} + \mathcal{L}_{Higgs} + \mathcal{L}_{Yukawa}, . \tag{1.1}$$

The term $\mathcal{L}_{Gauge}$ represents the kinetic terms of the gauge fields and is explicitly given by

$$\mathcal{L}_{Gauge} = -\frac{1}{4} B_{\mu\nu} B^{\mu\nu} - \frac{1}{4} W^i_{\mu\nu} W^{i,\mu\nu} - \frac{1}{4} G^a_{\mu\nu} G^{a,\mu\nu}, \tag{1.2}$$

where

$$\begin{aligned}
B_{\mu\nu} &= \partial_\mu B_\nu - \partial_\nu B_\mu, \\
W^i_{\mu\nu} &= \partial_\mu W^i_\nu - \partial_\nu W^i_\mu + g \varepsilon_{ijk} W^j_\mu W^k_\nu, \\
G^a_{\mu\nu} &= \partial_\mu G^a_\nu - \partial_\nu G^a_\mu + g_s f_{abc} G^b_\mu G^c_\nu.
\end{aligned} \tag{1.3}$$

The fields B_μ and W^i_μ represent the gauge fields of the $SU(2)_L \times U(1)_Y$ electroweak symmetry and the g the $SU(2)_L$ coupling constant. The fields G^a_μ represent the gauge fields of the

$SU(3)_C$ symmetry and G_s the coupling constant of the strong interaction. The terms ε_{ijk} and f_{abc} are the structure constants of the $SU(2)$ and $SU(3)$ groups, respectively. These gauge fields are spin-one bosons that are necessary to maintain the symmetry of the SM lagrangian under $SU(3)_C \times SU(2)_L \times U(1)_Y$.

The term $\mathcal{L}_{\text{Fermion}}$ represents the kinetic term of the fermions. Due to the $SU(2)_L$ symmetry of the SM lagrangian, the LH chiral components of leptons are organized in isospin doublets of the form

$$L^\ell = \begin{pmatrix} v_L^\ell \\ \ell_L \end{pmatrix} \tag{1.4}$$

and the RH chiral components are organized in the singlets ℓ_R, where the index $\ell = e, \mu, \tau$ represents the flavour of the lepton. The LH chiral components of quarks are also organized in the isospin doublets

$$Q_a^i = \begin{pmatrix} u_{L,a}^i \\ d_{L,a}^i \end{pmatrix}, \tag{1.5}$$

where the index i represents the generation of the quark, a its color and one must remember that the doublets contain the weak eigenstates of the quarks. Additionally, the remaining quarks are organized in isospin singlets of the form $u_{R,a}^i$ and $d_{R,a}^i$. The gauge fields must also be present in the $\mathcal{L}_{\text{Fermion}}$ term because the spacetime derivates are replaced by the corresponding covariant derivatives that maintain the lagrangian invariant under local transformations. The total expression for the kinetic term of fermions is

$$\begin{aligned}
\mathcal{L}_{\text{Fermion}} &= \sum_{\ell=1}^{3} i\bar{L}^\ell \gamma^\mu \left(\partial_\mu - ig'Y_L B_\mu - ig\frac{\tau_i}{2}W_\mu^i \right) L^\ell \\
&+ \sum_{q=1}^{3} i\bar{Q}^q \gamma^\mu \left(\partial_\mu - ig'Y_Q B_\mu - ig\frac{\tau_i}{2}W_\mu^i - ig_s\frac{\lambda_a}{2}G_\mu^a \right) Q^q \\
&+ \sum_{\ell=1}^{3} i\overline{\ell_R}\gamma^\mu \left(\partial_\mu - iY_{\ell_R}g'B_\mu \right) \ell_R + \sum_{q=1}^{6} i\overline{q_R}\gamma^\mu \left(\partial_\mu - iY_{q_R}g'B_\mu \right) q_R,
\end{aligned} \tag{1.6}$$

where τ_i and λ_a are the generators of $SU(2)$ and $SU(3)$, respectively, g' the coupling constant of $SU(1)_Y$ and Y_L the hypercharge of the field. So far, all the fields have been considered massless but we know from experiments that the charged fermions and the W and Z bosons are massive (as well as the neutrinos, which we will treat in more detail later). One might be tempted to add terms of the form $m^2\bar{L}L$ to the SM lagrangian. However, these terms would violate the gauge invariance of the theory because they couple left and right-handed chiral states, which are part of different representations. This problem is solved by the introduction

of the Higgs field H, which is a scalar field with a non-zero vacuum expectation value that couples to the gauge bosons and the fermions. The term $\mathcal{L}_{\text{Higgs}}$ in the SM lagrangian, which contains the kinetic term of the Higgs field as well as its couplings to the gauge bosons and its potential, is given by

$$
\begin{aligned}
\mathcal{L}_{\text{Higgs}} =& H^\dagger \left(\partial_\mu + \frac{i}{2} g' B_\mu + i g \frac{\tau_a}{2} W^a_\mu \right) \left(\partial^\mu - \frac{i}{2} g' B^\mu - i g \frac{\tau^b}{2} W^{b,\mu} \right) H \\
& - \mu^2 H^\dagger H + \lambda \left(H^\dagger H \right)^2 ,
\end{aligned}
\tag{1.7}
$$

where λ and μ^2 represent two parameters that define the shape of the Higgs potential, which has a minimum when the field takes the vacuum expectation value $\langle H \rangle = v = \dfrac{\mu}{\sqrt{\lambda}}$. In principle, the Higgs field has an infinite number of states where the Higgs potential takes its minimum value. However, in practice, nature randomly selects one of these states as the physical vacuum and therefore the symmetry of the final state does not have the same symmetry as the lagrangian. This process is known as spontaneous symmetry breaking and is responsible for the generation of mass in the standard model. The final form of the SM lagrangian after symmetry breaking can be obtained by making the substitution

$$
H(x) = \frac{1}{\sqrt{2}} \begin{pmatrix} 0 \\ v + h(x) \end{pmatrix} ,
\tag{1.8}
$$

where h is a real scalar field that represents the physical Higgs field. After substitution in (1.7), the Higgs sector of the SM lagrangian takes the form

$$
\begin{aligned}
\mathcal{L}_{\text{Higgs}} =& \frac{1}{2} \partial_\mu h \partial^\mu h - \lambda v^2 h^2 - \lambda v h^3 - \frac{1}{4} \lambda h^4 \\
& + \frac{1}{8} (h+v)^2 \left[2 g^2 v^2 W^{+,\mu} W^-_\mu + \left(g W^3_\mu - g' B_\mu \right) \left(g W^{3,\mu} - g' B^\mu \right) \right] .
\end{aligned}
\tag{1.9}
$$

From (1.9) we can conclude that the Higgs mass is $m_H = \sqrt{2\lambda}\, v$. The physical gauge bosons of the weak interactions are

$$
\begin{aligned}
W^\pm_\mu &= \frac{1}{\sqrt{2}} \left(W^1_\mu \mp W^2_\mu \right) \\
Z_\mu &= \frac{1}{\sqrt{g^2 + g'^2}} \left(g W^3_\mu - g' B_\mu \right)
\end{aligned}
\tag{1.10}
$$

and have masses $m_W = \frac{1}{2}gv$ and $m_Z = \frac{1}{2}v\sqrt{g^2 + g'^2}$. The experimental values of the masses of the Higgs and the weak bosons are [61]:

$$
\begin{aligned}
m_H &= 125.11 \pm 0.11 \text{ GeV}, \\
m_W &= 80.377 \pm 0.012 \text{ GeV}, \\
m_Z &= 91.187 \pm 0.0021 \text{ GeV}.
\end{aligned}
\tag{1.11}
$$

The physical photon is also present in the Higgs sector (1.9) as the field

$$
A_\mu = \frac{1}{\sqrt{g^2 + g'^2}}\left(g'W_\mu^3 + B_\mu\right)
\tag{1.12}
$$

which, as required, remains massless after the electroweak symmetry breaking. The gluons also remain massless since they are not affected by $SU(2)_L$.

Finally, the term $\mathcal{L}_{\text{Yukawa}}$ in (1.1) represents the Yukawa interactions between the Higgs field and the fermion fields. After electroweak symmetry breaking, the Yukawa sector has the form

$$
\mathcal{L}_{\text{Yukawa}} = -\sum_{\ell=1}^{3} m_\ell \bar{\ell}_L \ell_R - \sum_{i,j=1}^{3} m_{ij}^u \bar{u}_L^i u_R^j - \sum_{i,j=1}^{3} m_{ij}^d \bar{d}_L^i d_R^j + \text{ h.c. },
\tag{1.13}
$$

where m_ℓ are the lepton masses and m_{ij}^u and m_{ij}^d are 3×3 matrices. The quark fields present in (1.13) are the weak eigenstates and hence are not eigenstates of the Hamiltonian, also known as mass eigenstates. These mass eigenstates can be obtained by diagonalizing the matrices present in (1.13). Rewriting the Yukawa quark sector in terms of the mass eigenstates has a particularly important effect on the charged current weak interaction of quarks. For instance, the coupling of the quark fields with the W^- boson takes the form

$$
\begin{aligned}
\sum_{i=1}^{3} \frac{g}{\sqrt{2}} W_\mu^- \bar{d}_L^i \gamma^\mu u_L^i + \text{ h.c. } &\rightarrow \sum_{i=1}^{3} \frac{g}{\sqrt{2}} W_\mu^- \overline{\left(\sum_{m=1}^{3} U_{im}^{dL} d_L'\right)} \gamma^\mu \left(\sum_{n=1}^{3} U_{in}^{uL} u_L'^n\right) \\
&\quad + \text{ h.c. } \\
&= \sum_{m,n=1}^{3} \frac{g}{\sqrt{2}} \left[\sum_{i=1}^{3} U_{im}^{dL*} U_{in}^{uL}\right] W_\mu^- \bar{d}_L'^m \gamma^\mu u_L'^n + \text{ h.c. },
\end{aligned}
\tag{1.14}
$$

where the matrices U are unitary matrices that transform the weak eigenstates into mass eigenstates represented by the primed fields. Equation (1.14) shows that it is possible to have transitions between an up and a strange quark although they belong to different generations. The amplitude of this transition is proportional to the elements of the matrix between brackets

in Eq. (1.14), which is known as the Cabibbo-Kobayashi-Maskawa (CKM) matrix:

$$V_{\text{CKM}} = U^{dL\dagger} \cdot U^{uL}. \tag{1.15}$$

This matrix represents the observable effects of the mixing in the quark sector and can be parametrized by three real mixing angles ($\theta_{12} \geq 0$, θ_{13} and $\theta_{23} \leq \pi/2$) and one complex phase $0 \leq \delta_{\text{CP}} \leq 2\pi$:

$$V_{\text{CKM}} = \begin{pmatrix} c_{12}c_{13} & s_{12}c_{13} & s_{13}e^{-i\delta_{CP}} \\ -s_{12}c_{23} - c_{12}s_{13}s_{23}e^{i\delta_{CP}} & c_{12}c_{23} - s_{12}s_{13}s_{23}e^{i\delta_{CP}} & c_{13}s_{23} \\ s_{12}s_{23} - c_{12}s_{13}c_{23}e^{i\delta_{CP}} & -c_{12}S_{23} - s_{12}s_{13}c_{23}e^{i\delta_{CP}} & c_{13}c_{23} \end{pmatrix}, \tag{1.16}$$

where $s_{ij} = \sin\theta_{ij}$ and $c_{ij} = \cos\theta_{ij}$.

1.2   Neutrino mass generation

Neutrinos are considered massless in the Standard Model. However, the observation of neutrino oscillations implies that they cannot be massless, an indication that the standard model is incomplete. The most straightforward way to introduce neutrino masses is to add a neutrino mass term to the lagrangian similar to the up-quark mass terms. This requires the introduction of three RH neutrino states ν_R, which are not present in the standard model. After electroweak symmetry breaking, the mass term for the neutrinos has the form

$$\mathcal{L}_D = -\sum_{i,j=1}^{3} m_{ij}^{\nu} \bar{\nu}_L^i \nu_R^j + \text{h.c.} , \tag{1.17}$$

where m_{ij}^{ν} represents a 3×3 matrix. Equation (1.17) is known as a neutrino Dirac mass term and it is originated by the Yukawa coupling of the Higgs field to the neutrino field. In order to express the lagrangian in terms of the mass eigenstates ν' we have to diagonalize the matrix m_{ij}. This process affects the weak interaction charged current:

$$\begin{aligned} \sum_{i=1}^{3} \frac{g}{\sqrt{2}} W_\mu^+ \bar{\ell}_L^i \gamma^\mu \nu_L^i + \text{h.c.} &\rightarrow \sum_{i=1}^{3} \frac{g}{\sqrt{2}} W_\mu^+ \overline{\left(\sum_{m=1}^{3} U_{im}^{\ell L} \ell_L'^m\right)} \gamma^\mu \left(\sum_{n=1}^{3} U_{in}^{\nu L} \nu_L'^n\right) + \text{h.c.} \\ &= \sum_{m,n=1}^{3} \frac{g}{\sqrt{2}} \left[\sum_{i=1}^{3} U_{im}^{\ell L*} U_{in}^{\nu L}\right] W_\mu^+ \bar{\ell}_L'^m \gamma^\mu \nu_L'^n + \text{h.c.} , \end{aligned} \tag{1.18}$$

where the matrix

$$U_{\text{PMNS}} = U^{\ell L\dagger} \cdot U^{\nu L} \tag{1.19}$$

is known as the Pontecorvo–Maki–Nakagawa–Sakata (PMNS) matrix. In the standard model, we take $U^{\ell L} = \text{diag}(1,1,1)$ and therefore the PMNS matrix relates the neutrino flavor eigenstates to the mass eigenstates

$$\begin{pmatrix} \nu_e \\ \nu_\mu \\ \nu_\tau \end{pmatrix} = \begin{pmatrix} U_{e1} & U_{e2} & U_{e3} \\ U_{\mu 1} & U_{\mu 2} & U_{\mu 3} \\ U_{\tau 1} & U_{\tau 2} & U_{\tau 3} \end{pmatrix} \cdot \begin{pmatrix} \nu_1 \\ \nu_2 \\ \nu_3 \end{pmatrix}, \tag{1.20}$$

where $U_{\alpha i}$ represent the elements of the PMNS matrix and ν_i represent the mass eigenstates. Equation (1.20) is usually written in the form

$$\nu_\alpha = \sum_i U_{\alpha i} \nu_i, \tag{1.21}$$

where α denotes the flavor of the neutrino. The PMNS matrix can be parametrized by three real mixing angles ($\theta_{12} \geq 0$, θ_{13} and $\theta_{23} \leq \pi/2$) and one complex phase $0 \leq \delta_{\text{CP}} \leq 2\pi$:

$$U_{\text{PMNS}} = \begin{pmatrix} c_{12}c_{13} & s_{12}c_{13} & s_{13}e^{-i\delta_{CP}} \\ -s_{12}c_{23} - c_{12}S_{13}s_{23}e^{i\delta_{CP}} & c_{12}c_{23} - s_{12}s_{13}s_{23}e^{i\delta_{CP}} & c_{13}S_{23} \\ s_{12}S_{23} - c_{12}S_{13}c_{23}e^{i\delta_{CP}} & -c_{12}S_{23} - s_{12}s_{13}c_{23}e^{i\delta_{CP}} & c_{13}c_{23} \end{pmatrix}, \tag{1.22}$$

where $s_{ij} = sin(\theta_{ij})$, $c_{ij} = cos(\theta_{ij})$.

The Dirac mass term in Eq. (1.17) introduces a RH neutrino field. However, it is also possible to construct a mass term for neutrinos that only involves LH chiral fields. We define the charge-conjugated spinor as

$$\Psi^c = C\bar{\Psi}^T, \tag{1.23}$$

where $C = i\gamma_0\gamma_2$ is the charge conjugation matrix. We can now build a Majorana mass term of the form

$$\mathcal{L}_M = \frac{1}{2}\sum_{i,j=1}^{3} m_{ij}^\nu \overline{\nu_L^c}^i \nu_L^j + \text{h.c.} = \frac{1}{2}\sum_{i,j=1}^{3} m_{ij}^\nu \nu_L^{i,T} C \nu_L^j + \text{h.c.}, \tag{1.24}$$

where the m^ν is a symmetric complex 3×3 mass matrix and the sum is over all the lepton generations. We see that the Majorana mass in (1.24) couples neutrinos with antineutrinos and hence violates lepton number conservation by 2 units. We can follow a procedure similar

to the Dirac case and diagonalize the Majorana mass matrix as

$$\text{diag}\left(m_{\nu_1}, m_{\nu_2}, m_{\nu_3}\right) = U^{\nu,T} \cdot m^{\nu} \cdot U^{\nu}, \tag{1.25}$$

where U^{ν} is a 3×3 unitary matrix. In this case, the Majorana PMNS matrix is given by

$$U_{\text{PMNS}}^{\text{Majorana}} = U_{\text{PMNS}}^{\text{Dirac}} \cdot \text{diag}\left(1, e^{i\phi_1}, e^{i\phi_2}\right), \tag{1.26}$$

where $0 \leq \phi_{1,2} \leq 2\pi$ are two Majorana phases. Equation (1.24) includes only LH chiral fields, but it cannot be introduced directly in the SM lagrangian because left-handed leptons must be organized in isospin doublets. This would imply adding a term of the form $m_{ij}L^{iT}L^j$ to the SM lagrangian, which would also add a Majorana mass term for the electrons and break electric charge conservation. One alternative is to add to the SM lagrangian the dimension-5 effective Weinberg operator[59] given by

$$\mathcal{L}_{\text{Weinberg}} = \frac{1}{2} \sum_{i,j=1}^{3} \frac{c_{ij}}{\Lambda_{\text{NP}}} \left(L^i \cdot H\right)^T \left(L^j \cdot H\right) + \text{h.c.}, \tag{1.27}$$

where c_{ij} are dimensionless coupling constants and Λ_{NP} is an effective operator scale related to new physics. After electroweak symmetry breaking, the Weinberg operator becomes

$$\frac{1}{2} \sum_{i,j=1}^{3} \frac{c_{ij}}{\Lambda_{\text{NP}}} \left(L^i \cdot H\right)^T \left(L^j \cdot H\right) + \text{h.c.} \rightarrow \frac{1}{2} \sum_{i,j=1}^{3} m_{ij}^{\nu} \nu_L^{i,T} C \nu_L^j + \text{h.c.}, \tag{1.28}$$

which is identical to the Majorana mass of Eq. (1.24). The Weinberg operator is gauge invariant and generates the neutrino masses

$$m^{\nu} = \frac{v^2}{2\Lambda_{\text{NP}}} c, \tag{1.29}$$

where v is the vacuum expectation value of the Higgs field. The neutrino masses depend inversely on the new physics scale Λ_{NP} and can be made as small as desired provided the value of Λ_{NP} is very large. For instance, for $c \sim 1$, in order order get $m^{\nu} \sim 0.1$ GeV one needs $\Lambda_{NP} \sim \mathcal{O}(10^{14})$ GeV.

The Majorana mass term in (1.24) was built using LH chiral neutrino fields. However, one could also introduce to the SM lagrangian a bare mass term for RH chiral fields of the

form

$$\mathcal{L}_M = \frac{1}{2}\sum_{i,j=1}^{3} m_{ij}^{\nu}\overline{\nu_R^{c}}^{i}\nu_R^{j} + \text{h.c.} = \frac{1}{2}\sum_{i,j=1}^{3} m_{ij}^{\nu}\left(\nu_R^{i}\right)^{T}C\nu_R^{j} + \text{h.c.} \ . \tag{1.30}$$

Since RH particles and LH antiparticles transform as singlets under $SU(2)_L$, the mass term in (1.30) is gauge invariant, although it still couples particles with antiparticles and hence violates lepton number conservation by two units. In general, one can combine (1.17) and (1.30) to build a mass term for neutrinos that, after electroweak symmetry breaking, has the form

$$\mathcal{L}_{\text{Seesaw}} = -\sum_{ij} m_{ij}^{D}\bar{\nu}_L^{i}\nu_R^{j} + \frac{1}{2}\sum_{ij} M_{ij}\left(\nu_R^{i}\right)^{T}C\nu_R^{j} + \text{h.c.} \ , \tag{1.31}$$

where m_D is called the Dirac neutrino mass mixing. If we define the 6-dimensional vector

$$n = \begin{pmatrix} \nu_L^{i} \\ \nu_R^{i} \end{pmatrix} \tag{1.32}$$

we can write the Seesaw lagrangian of (1.31) as

$$\mathcal{L}_{\text{Seesaw}} = \begin{pmatrix} \nu_L^{i} \\ \nu_R^{i} \end{pmatrix}^{T} \cdot \underbrace{\begin{pmatrix} 0 & m^{D} \\ \left(m^{D}\right)^{T} & M \end{pmatrix}}_{\mathcal{M}} \cdot \begin{pmatrix} \nu_L^{i} \\ \nu_R^{i} \end{pmatrix}, \tag{1.33}$$

where the matrix $\mathcal{M}$ is a 6×6 matrix. We can diagonalize this matrix in order to obtain the mass eigenstates n' of the Seesaw lagrangian

$$\mathcal{U}^{T} \cdot \mathcal{M} \cdot \mathcal{U} = \text{diag}\left(m_{\nu_1}, m_{\nu_2}, m_{\nu_3}, m_{N_1}, m_{N_2}, m_{N_3}\right), \tag{1.34}$$

where $n = \mathcal{U}n'$, the m_{ν_i} are the light neutrinos masses and the m_{N_i} are the heavy neutrino masses. If one considers only one generation it is easy to show that the diagonalization of the mass matrix can be expressed as

$$\begin{pmatrix} \cos\theta & \sin\theta \\ -\sin\theta & \cos\theta \end{pmatrix} \cdot \begin{pmatrix} 0 & m_D \\ m_D & M \end{pmatrix} \cdot \begin{pmatrix} \cos\theta & -\sin\theta \\ \sin\theta & \cos\theta \end{pmatrix} = \begin{pmatrix} m_\nu & 0 \\ 0 & m_N \end{pmatrix} \tag{1.35}$$

and its eigenvalues are

$$m_\nu = \frac{1}{2}\left(M - \sqrt{M^2 + 4m_D^2}\right), \quad m_N = \frac{1}{2}\left(M + \sqrt{M^2 + 4m_D^2}\right). \tag{1.36}$$

Phenomenologically, the value of M is expected to be much larger than the light neutrino mass m_D, which is expected to be of the order of the electroweak scale, $m_D \lesssim 100\text{GeV}$. In this case, we have

$$m_\nu = -\frac{m_D^2}{M} + \mathcal{O}\left(\frac{m_D^4}{M^3}\right), \quad m_N = M + \frac{m_D^2}{M} - \mathcal{O}\left(\frac{m_D^4}{M^3}\right) \tag{1.37}$$

and

$$\theta \approx \tan\theta = \frac{m_D}{M} - \mathcal{O}\left(\frac{m_D^3}{M^3}\right). \tag{1.38}$$

Using $m_D \sim 100$ GeV we have a relation between the light and heavy neutrino masses

$$\frac{m_\nu}{0.1\text{eV}} = \frac{10^{14}\text{GeV}}{M}, \tag{1.39}$$

which means that the light neutrino mass decreases as the heavy neutrino mass increases. This is known as the seesaw mechanism. In this limit, the mixing angle θ is very small and the weak eigenstates are

$$\begin{aligned} \nu_L &= \cos\theta\, \nu - \sin\theta\, N \approx \nu - \theta N, \\ \nu_R &= \sin\theta\, \nu + \cos\theta\, N \approx N + \theta\nu. \end{aligned} \tag{1.40}$$

This implies that the RH neutrinos are not truly sterile and couple to the SM charged current, although the coupling is heavily suppressed by the small mixing angle. For the more general case of three neutrino generations, although the algebra is much more complex, it is also possible to diagonalize the mass matrix

$$m^\nu = -m^D \cdot M^{-1} \cdot \left(m^D\right)^T \tag{1.41}$$

and also obtain an expression for the mixing angles between the gauge eigenstates of the active neutrinos and the sterile neutrinos,

$$\Theta = m^D \cdot M^{-1}. \tag{1.42}$$

Again, if the RH neutrinos have $M_{N_i} \sim 10^{14}\text{GeV}$, it is possible to obtain very small values for the masses of the light neutrinos.

There are alternative mechanisms similar to the type-I seesaw mechanism that modify the SM lagrangian in order to generate Weinberg operators at the tree level. For instance, the Type-II seesaw mechanism adds a heavy scalar $\Delta = \left(\Delta^0, \Delta^+, \Delta^{++}\right)^T$ that transforms as

an $SU(2)_L$ triplet. This scalar field couples to the SM electroweak gauge bosons. After electroweak symmetry breaking, the component Δ^0 gains a nonzero vacuum expectation value

$$\left\langle \Delta^0 \right\rangle = \frac{\mu v^2}{2m_\Delta^2}, \tag{1.43}$$

where v represents the Higgs VEV and m_Δ the bare mass of the triplet. This in turn induces a Majorana mass term for the neutrinos with

$$m^\nu = y^\Delta \left\langle \Delta^0 \right\rangle = \frac{\mu v^2}{m_\Delta^2} y^\Delta, \tag{1.44}$$

where y^Δ is a matrix of Yukawa couplings of the triplet scalar with the SM lepton doublets and μ is a coupling constant between the Higgs and the scalar triplet. Finally, in the type-III seesaw mechanism, three triplet fermions $F^i = \left(F^-, F^0, F^+ \right)$ that couple to the SM leptons and the Higgs are added to the SM lagrangian:

$$\mathcal{L}_{SM} \rightarrow \mathcal{L}_{SM} + \sum_{i,j} y_{ij}^F \left(L^i \right)^T \cdot F^j \cdot H + \sum_{i,j} m_{ij}^F \left(F^i \right)^T F^j. \tag{1.45}$$

If the fermion mass term m^F is much larger than the electroweak scale, we obtain an effective Majorana mass matrix for the light neutrinos

$$m^\nu = \left(y^F \right)^T \cdot \left(m^F \right)^{-1} \cdot y^F. \tag{1.46}$$

1.3 Neutrino oscillations

The neutrino mass generation mechanisms discussed in the previous section show that the neutrino weak eigenstates that participate in the weak interaction are not the mass eigenstates of the Hamiltonian. In the standard model, the weak and mass eigenstates are related by the equation

$$\nu_\alpha = \sum_{i=1}^3 U_{\alpha i} \nu_i, \tag{1.47}$$

where $\alpha = e, \mu, \tau$ represents the flavour of the neutrino, $U_{\alpha i}$ are the elements of the PMNS matrix and the index $i = 1, 2, 3$ refer to the three mass eingestates. Since neutrinos are stable particles, the mixing in the neutrino sector makes it possible for oscillation between different flavor states. These oscillations have been observed in

The phenomenon of neutrino oscillation can be easily understood in the two-generation framework, where only electron and muon neutrinos are considered. In this case, the mixing matrix can be parametrized by only one parameter θ:

$$\begin{pmatrix} v_e \\ v_\mu \end{pmatrix} = \begin{pmatrix} \cos\theta & \sin\theta \\ -\sin\theta & \cos\theta \end{pmatrix} \begin{pmatrix} v_1 \\ v_2 \end{pmatrix}. \tag{1.48}$$

If the initial state of the particle is given by

$$|\psi(0)\rangle = |v_e\rangle \equiv \cos\theta\,|v_1\rangle + \sin\theta\,|v_2\rangle \tag{1.49}$$

then at time T, when the neutrino has traveled a distance L, the wave function has the form

$$|\psi(\mathbf{x},t)\rangle = \cos\theta\,|v_1\rangle\,e^{-i\phi_1} + \sin\theta\,|v_2\rangle\,e^{-i\phi_2}, \tag{1.50}$$

where $\phi_i = p_i \cdot x$ and p_i represent the momenta of the mass eigenstates. Inverting Eq. (1.48) one can express the mass eigenstates in terms of the weak eigenstates and replace them in Eq. (1.50) to obtain

$$\begin{aligned}
|\psi(L,T)\rangle &= \cos\theta\left(\cos\theta\,|v_e\rangle - \sin\theta\,|v_\mu\rangle\right)e^{-i\phi_1} + \sin\theta\left(\sin\theta\,|v_e\rangle + \cos\theta\,|v_\mu\rangle\right)e^{-i\phi_2} \\
&= e^{-i\phi_1}\left[\left(\cos^2\theta + e^{i\Delta\phi_{12}}\sin^2\theta\right)|v_e\rangle - \left(1 - e^{i\Delta\phi_{12}}\right)\cos\theta\sin\theta\,|v_\mu\rangle\right],
\end{aligned} \tag{1.51}$$

where $\Delta\phi_{12} = \phi_1 - \phi_2 = (E_1 - E_2)T - (p_1 - p_2)L$. We see in Eq. (1.51) that the wave function that was initially an electron neutrino now can develop a muon neutrino component as long as $\Delta\phi_{12} \neq 0$. The oscillation probability of $v_e \to v_\mu$ is defined as

$$P\left(v_e \to v_\mu\right) = \langle v_\mu|\Psi(L,T)\rangle = \sin^2(2\theta)\sin^2\left(\frac{\Delta\phi_{12}}{2}\right). \tag{1.52}$$

The term $\Delta\phi_{12}$ can be expressed in terms of the masses of eigenstates. This can be achieved by a wave-packet treatment or, equivalently, by setting $p_1 = p_2$, $E_1 = E_2$ or $\beta_1 = \beta_2$, where β_i are the Lorentz factors of the mass eigenstates. In each case one obtains

$$\Delta\phi_{12} \approx \frac{m_1^2 - m_2^2}{2E}L \tag{1.53}$$

and the two-flavour oscillation probability becomes

$$P\left(v_e \to v_\mu\right) = \sin^2(2\theta)\sin^2\left(\frac{(m_1^2 - m_2^2)L}{4E_v}\right). \tag{1.54}$$

If we express L in km, $\Delta m^2 = m_1^2 - m_2^2$ in eV^2 and E_v in GeV we have

$$P\left(v_e \to v_\mu\right) = \sin^2(2\theta) \sin^2\left(1.27 \frac{\Delta m^2 \left[\text{eV}^2\right] L[\text{ km}]}{E_v[\text{GeV}]}\right). \tag{1.55}$$

By conservation of probability, the neutrino survival probability, $P\left(v_e \to v_e\right)$, takes the form

$$P\left(v_e \to v_e\right) = 1 - \sin^2(2\theta) \sin^2\left(\frac{\left(m_1^2 - m_2^2\right) L}{4E_v}\right). \tag{1.56}$$

In both cases, the wavelengths of the oscillations are given by

$$\lambda_{\text{osc}}[\text{km}] = \frac{\pi E_v[\text{GeV}]}{1.27 \Delta m^2 \left[\text{eV}^2\right]}. \tag{1.57}$$

In the case of three generations of neutrinos, one must use the 3×3 PMNS matrix

$$\begin{pmatrix} v_e \\ v_\mu \\ v_\tau \end{pmatrix} = \begin{pmatrix} U_{e1} & U_{e2} & U_{e3} \\ U_{\mu 1} & U_{\mu 2} & U_{\mu 3} \\ U_{\tau 1} & U_{\tau 2} & U_{\tau 3} \end{pmatrix} \begin{pmatrix} v_1 \\ v_2 \\ v_3 \end{pmatrix}. \tag{1.58}$$

The mixing matrix in the three neutrino framework can be parametrized in terms of three mixing angles θ_{13} and one angle δ presenting CP violation

$$
\begin{aligned}
U &= \begin{pmatrix} U_{e1} & U_{e2} & U_{e3} \\ U_{\mu 1} & U_{\mu 2} & U_{\mu 3} \\ U_{\tau 1} & U_{\tau 2} & U_{\tau 3} \end{pmatrix} \\
&= \begin{pmatrix} 1 & 0 & 0 \\ 0 & c_{23} & s_{23} \\ 0 & -s_{23} & c_{23} \end{pmatrix} \begin{pmatrix} c_{13} & 0 & s_{13}e^{-i\delta} \\ 0 & 1 & 0 \\ -s_{13}e^{-i\delta} & 0 & c_{13} \end{pmatrix} \begin{pmatrix} c_{12} & s_{12} & 0 \\ -s_{12} & c_{12} & 0 \\ 0 & 0 & 1 \end{pmatrix} \begin{pmatrix} e^{i\alpha_1/2} & 0 & 0 \\ 0 & e^{i\alpha_2/2} & 0 \\ 0 & 0 & 1 \end{pmatrix} \\
&= \begin{pmatrix} c_{12}c_{13} & s_{12}c_{13} & s_{13}e^{-i\delta} \\ -s_{12}c_{23} - c_{12}s_{23}s_{13}e^{i\delta} & c_{12}c_{23} - s_{12}s_{23}s_{13}e^{i\delta} & s_{23}c_{13} \\ s_{12}s_{23} - c_{12}c_{23}s_{13}e^{i\delta} & -c_{12}s_{23} - s_{12}c_{23}s_{13}e^{i\delta} & c_{23}c_{13} \end{pmatrix} \begin{pmatrix} e^{i\alpha_1/2} & 0 & 0 \\ 0 & e^{i\alpha_2/2} & 0 \\ 0 & 0 & 1 \end{pmatrix},
\end{aligned}
\tag{1.59}
$$

where $c_{ij} = \cos\theta_{ij}$, $s_{ij} = \sin\theta_{ij}$, δ determines CP violation and the phases α_i are relevant if neutrinos are Majorada because they contribute to CP violation. However, in neutrino oscillations, these act as global phases and hence they do not affect the results of neutrino oscillations.

The neutrino oscillation and survival probabilities in the three-generation scenario can be calculated following the same procedure used in the case of two generations. In general, the formula for the oscillation probability in the three flavors scenario is given by [42]:

$$
P_{\nu_\alpha \to \nu_\beta}(L, E_\nu) = \delta_{\alpha\beta} - 4 \sum_{k>j} \Re\mathfrak{e} \left[U_{\alpha k}^* U_{\beta k} U_{\alpha j} U_{\beta j}^* \right] \sin^2 \left(1.27 \frac{\Delta m_{kj}^2 \left[\text{eV}^2 \right] L[\text{km}]}{E_\nu[\text{GeV}]} \right)
$$
$$
+ 2 \sum_{k>j} \Im\mathfrak{m} \left[U_{\alpha k}^* U_{\beta k} U_{\alpha j} U_{\beta j}^* \right] \sin \left(2.54 \frac{\Delta m_{kj}^2 \left[\text{eV}^2 \right] L[\text{km}]}{E_\nu[\text{GeV}]} \right).
$$

(1.60)

Figure 1.2 shows the survival probabilities $P(\nu_\mu \to \nu_\mu)$ and $P(\nu_e \to \nu_e)$ of muon and electron neutrinos as a function of the neutrino energy for $L = 574$ m and $L = 1300$ km, which are the positions of the two detectors of the DUNE experiment. We see that the largest oscillations will be present for muon neutrinos, particularly at around 2.5 GeV, which, as we will see in the next sections, is exactly the position of the peak of the muon neutrino flux at DUNE.

In principle, the labelings of ν_1, ν_2 and ν_3 are arbitrary. However, it is conventional to label the mass states in order of increasing content of ν_e, where ν_1 has the most ν_e content and ν_3 the least. Historically, oscillations were first studied using neutrino fluxes coming from the Sun and the Earth's atmosphere. The studies of atmospheric neutrinos are sensitive to θ_{23} and Δm_{32}^2, where the sign of the mass splitting cannot be measured. On the other hand, solar neutrinos are sensitive to θ_{12} and Δm_{21}^2 and the matter effects on the oscillation make it possible to set the sign of Δm_{21}^2. This uncertainty in the sign of the mass expliting in atmospheric neutrinos opens the possibility for two neutrino mass orderings, which are shown in Figure 1.3. In the normal ordering (NO) $\Delta m_{32}^2 > 0$ and the $m_1 < m_2 < m_3$. This implies that the mass eigenstate ν_3 with the least electron neutrino content is the heaviest of the three. On the other hand, in the inverse ordering (IO) we have $\Delta m_{32}^2 < 0$ and $m_3 < m_1 < m_2$, which indicates that ν_3 is the lightest neutrino mass eigenstate.
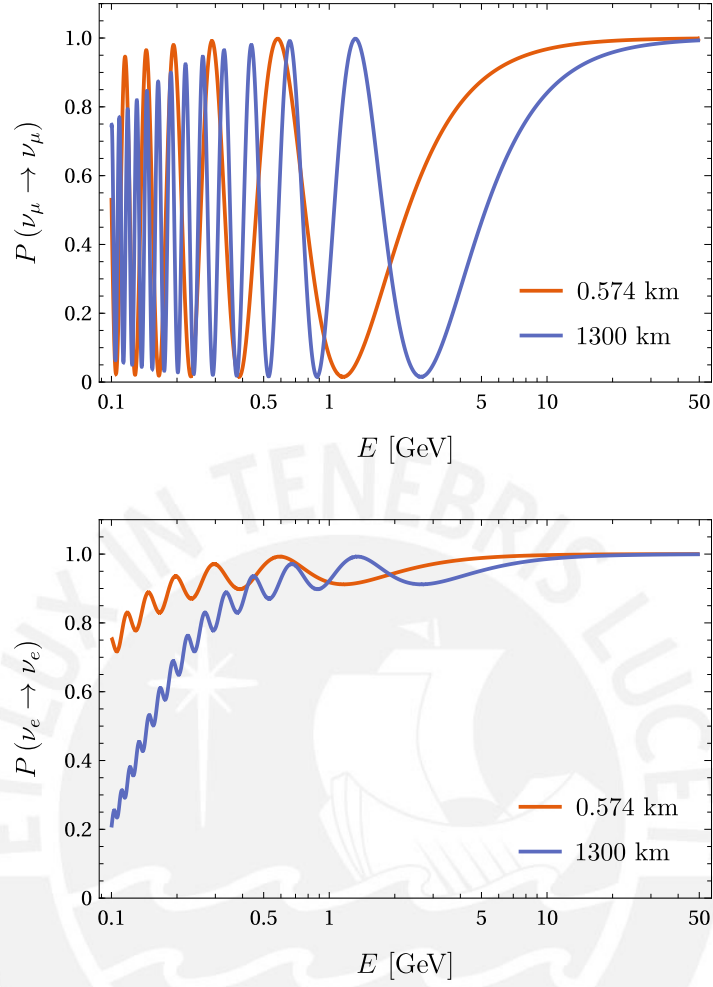
Fig. 1.2 Muon (top) and electron (bottom) neutrino survival probabilities as a function of the neutrino energy for $L = 574$ m and $L = 1300$ km.

Global analyses of neutrino experiments have constrained the values of the main parameters of the neutrino sector [61]. Current constraints at 1 sigma uncertainty are

$$\Delta m_{21}^2 = \left(7.53^{+0.20}_{-0.16}\right) \times 10^{-5} \text{ eV}^2,$$

$$\left|\Delta m_{32}^2\right| = \begin{cases} \left(2.449^{+0.032}_{-0.030}\right) \times 10^{-3} \text{ eV}^2 & \text{(NO)} \\ \left(2.509^{+0.032}_{-0.032}\right) \times 10^{-3} \text{ eV}^2 & \text{(IO)} \end{cases},$$

$$\sin^2\theta_{12} = 3.10^{+0.13}_{-0.12} \times 10^{-1},$$

$$\sin^2\theta_{23} = \begin{cases} 5.58^{+0.20}_{-0.33} \times 10^{-1} & \text{(NO)} \\ 5.63^{+0.19}_{-0.26} \times 10^{-1} & \text{(IO)} \end{cases}, \qquad (1.61)$$

$$\sin^2\theta_{13} = \begin{cases} 2.241^{+0.066}_{-0.065} \times 10^{-2} & \text{(NO)} \\ 2.261^{+0.067}_{-0.064} \times 10^{-2} & \text{(IO)} \end{cases},$$

$$\delta_{CP} = \begin{cases} 222^{\circ\,+38^\circ}_{-28^\circ} & \text{(NO)} \\ 285^{\circ\,+24^\circ}_{-26^\circ} & \text{(IO)} \end{cases}.$$
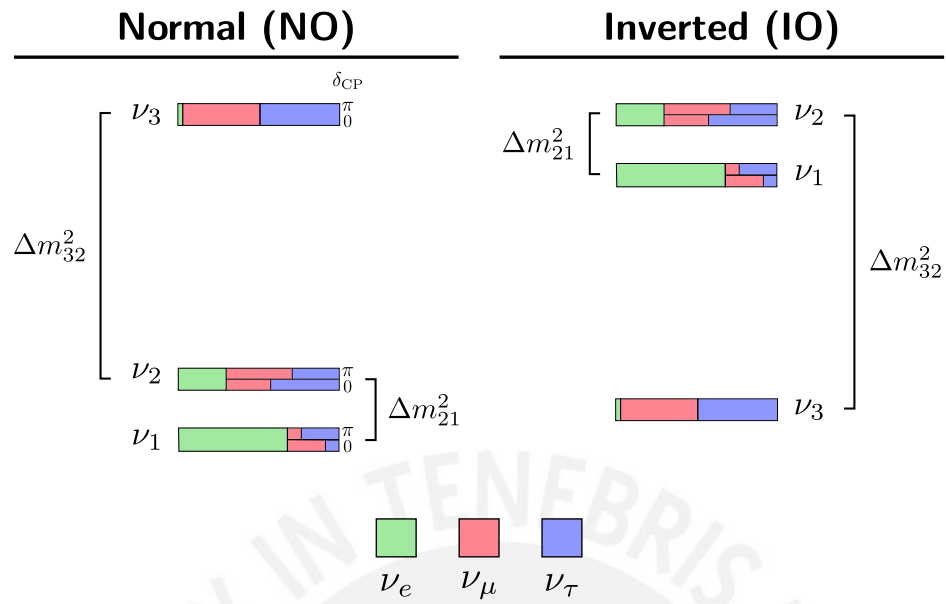
Fig. 1.3 Representation of the two mass ordering of neutrinos. The figure was adapted from [55].

It is interesting to note that for neutrinos the mixing angles θ_{12} and θ_{23} are quite large while θ_{23} is very small, a situation which is very different to the mixing in the quark sector. Additionally, there is still a large uncertainty in the CP-violating phase.

Chapter 2

Heavy neutral leptons

Neutrinos are fundamental particles in the Standard Model (SM) that are charged only under weak interactions. Since only left-handed chiral neutrinos have been detected so far, right-handed chiral neutrinos are not included in the SM. This implies that neutrinos do not interact with the Higgs field and a neutrino mass term is not necessary. For this reason, neutrinos are considered massless in the Standard Model. However, in chapter 1 we discussed that there are several ways to give mass to SM neutrinos, such as the seesaw mechanism. Furthermore, we discussed the phenomenon of neutrino oscillations, which require that neutrinos have mass. The existence of the neutrino mass can be explained by adding several right-handed neutrinos to the SM, as is explained in chapter 1. If the right-handed neutrino mass m_N satisfies $m_M \gg$ eV, we refer to this neutrino as a Heavy Neutral Lepton (HNL). Even if they exist, the mass scale of HNLs is yet unknown. However, it is possible that these sterile states might be observed in current and near-future experiments, which makes the study of these particles an important subject of current theoretical and phenomenological physics.

2.1   Mass scale of HNLs

In the context of the seesaw mechanism, the phenomenology of HNLs depends crucially on the mass scale of the new physics. As we explained in chapter 1, the mass of the light neutrinos m_ν in type-I seesaw has the form

$$m_\nu = \frac{v^2}{2\Lambda_{\mathrm{NP}}} c,$$

(2.1)

where v represents the vacuum expectation value of the Higgs, Λ_{NP} the scale of the new physics and c a coupling constant from the Weinberg operator.

If the coupling constant is of order 1, then we need large values of $\Lambda_{NP} \sim 10^{14}$ GeV to reproduce the small scale of m_v. This approach, known as high scale seesaw, is interesting because it can be embedded into GUT theories and leptogenesis. However, high scale seesaw seems to give rise to destabilization of the Higgs mass and, more crucially, is not testable at current and near-future experiments, except for some indirect hits such as proton decay and gravitational waves due to cosmis strings [53, 52, 38]. If we let the coupling constant c in Eq. (2.1) to be small with $c \ll 1$, then the value of Δ_{NP} can be sufficiently small so that the new particles can in principle be detected at current experiment as long as their coupling to the SM is sufficiently large. This particular scenario corresponds to low-scale seesaw models where, depending on the values of the coupling constants, HNLs can have masses ranging from eV to TeV. Finally, it is also possible to generate light neutrino masses even when the coupling $c \sim 1$ and Λ_{NP} is not very large. The existence of Majorana masses would be evidence that lepton symmetry is broken. Hence, it is possible to argue that the breaking of lepton symmetry might be responsible for the smallness of the neutrino mass, which is produced by the systematic cancellation of the contributions of several HNLs. This principle is present in the inverse, linear and extended seesaw models [41, 14]. In these theories, it is possible to have HNLs with masses in the MeV-TeV range and large mixings, which opens the possibility for detection in current or near future experiments.

In chapter 1 we studied some possible mechanisms for neutrino mass generation. In particular, we concluded that it is possible to add a right-handed neutrino field to the SM lagrangian since it transforms as a singlet under $SU(2)_L$. From now on, we will label as N this new sterile neutrino field which will represent a HNL. In terms of the field N, it is possible to write down an expression for the sterile neutrino sector similar to Eq. 1.31

$$\mathcal{L}_{\mathrm{HNL}} = i\bar{N}\not{\partial}N + M_\alpha^D \bar{v}_\alpha N - \frac{M_N}{2}\bar{N}^c N + \text{h.c.} \,. \tag{2.2}$$

Although the HNL cannot participate directly in the weak interaction, due to the mixing of N with the active neutrinos it couples to the SM fields with the interaction lagrangian

$$\mathcal{L}_{\mathrm{int}}^{\mathrm{HNL}} = \frac{g}{\sqrt{2}} W_\mu^+ \overline{N^c} \sum_\alpha U_{\alpha 4}^* \gamma^\mu \left(1 - \gamma_5\right) \ell_\alpha^- + \frac{g}{2\cos\theta_W} Z_\mu \overline{N^c} \sum_\alpha U_{\alpha 4}^* \gamma^\mu \left(1 - \gamma_5\right) v_\alpha + \text{h.c.} \,, \tag{2.3}$$

where the couplings are suppressed by the mixing angles $U_{\alpha 4}$ between the HNL and the active neutrinos, which are expected to be small, and ℓ_α represents the charged SM leptons.

It is important to note that, in principle, the number of HNLs is not defined. However, if the masses of the HNLs are all different, they are produced and decay independently and do not oscillate between themselves and therefore, at least from a phenomenological point of view, it is reasonable to consider only 1 sterile neutrino. Moreover, we will be mainly interested in HNLs produced in collider experiments, which are only sensitive to the HNL mass m_N and mixing squared $|U_{\alpha 4}|^2$. For these reasons, our study of HNLs in beam dump experiments will focus mainly on the analysis of the values of the HNL mass and the mixing parameter of the HNL to active neutrinos.

2.2   Production of HNLs

The production of HNLs at beam dump experiments such as DUNE or SHiP [19] depends on the decay rates of mesons into HNLs. These decays are possible because HNLs mix with active neutrinos. However, the decay rates depend on the value of the HNL mass and the mixing parameter to active neutrinos. In this section, we summarize the formulas for calculating the decay rates of charged leptons and mesons into HNL. For more details about the formulas, we refer the reader to Refs. [30, 25, 24, 43].

2.2.1   Charged lepton three-body decay

HNLs can be produced in charged lepton decays through mixing with the acting neutrinos. In the context of the DUNE experiment, this production will be mostly linked to decays of a charged lepton ℓ_α^+ into a HNL given by [24]

$$\Gamma_\pm\left(\ell_\alpha^+ \to \ell_\beta^+ \nu N\right) = \frac{G_F^2 m_\alpha^5}{192\pi^3}\left[|U_{\alpha 4}|^2 I_\ell^\pm\left(y_N^2, y_{\ell_\beta}^2, 0\right) + |U_{\beta 4}|^2 I_\ell^\pm\left(0, y_{\ell_\beta}^2, y_N^2\right)\right], \quad (2.4)$$

where m_α represents the mass of the parent charged lepton, $y_N = m_N/m_\alpha$, $y_{\ell_\beta} = m_{\ell_\beta}/m_N$, $|U_{\alpha 4}|^2$ and $|U_{\beta 4}|^2$ are the mixing parameters squared with neutrinos of flavour α and β, respectively, and

$$I_\ell^\pm(x,y,z) = 12\int_{(\sqrt{x}+\sqrt{y})^2}^{(1-\sqrt{z})^2} \frac{\mathrm{d}s}{s}(1+z-s)\left[s-x-y \mp \lambda^{\frac{1}{2}}(s,x,y)\right] \times \lambda^{\frac{1}{2}}(s,x,y)\lambda^{\frac{1}{2}}(1,s,z),$$

$$I_\ell^\pm(x,y,z) = 12\int_{(\sqrt{x}+\sqrt{y})^2}^{(1-\sqrt{z})^2} \frac{\mathrm{d}s}{s}\left[1+z-s \mp \lambda^{\frac{1}{2}}(1,s,z)\right](s-x-y) \times \lambda^{\frac{1}{2}}(s,y,z)\lambda^{\frac{1}{2}}(1,s,z).$$

$$(2.5)$$

2.2.2 Leptonic decay of pseudoscalar meson

Pseudoscalar mesons such as $\pi^{\pm}$, $K^{\pm}$, K^0 are the main sources of HNL production via mixing with electron and muon neutrinos at DUNE. Additionally, the decays of the heavy pseudoscalar mesons $D^{\pm}$, D^0 and $D_S^{\pm}$ are important for HNL production via tau mixing. The decay rate of a pseudoscalar meson h into a charged lepton ℓ_α and a HNL N is given by [30]

$$\Gamma(h \to \ell_\alpha N) = \frac{G_F^2 f_h^2 m_h^3}{8\pi} |V_{UD}|^2 |U_{\alpha 4}|^2 \left[y_N^2 + y_\ell^2 - \left(y_N^2 - y_\ell^2 \right)^2 \right] \sqrt{\lambda\left(1, y_N^2, y_\ell^2\right)}, \quad (2.6)$$

where f_H is the decay constant of the parent meson, m_h is the mass of the parent meson, $y_N = m_N/m_h$, $y_\ell = m_\ell/m_h$, V_{UD} the corresponding entry on the CKM matrix (which depends on the internal structure of the meson) and the function $\lambda(a,b,c)$ is the Källén function

$$\lambda(a,b,c) = a^2 + b^2 + c^2 - 2ab - 2ac - 2bc. \quad (2.7)$$

2.2.3 Semileptonic decay of pseudoscalar meson

At DUNE, semileptonic decays of kaons and D mesons play an important role in the production of HNLs via electron and muon mixing for the kaon and tau mixing for the D meson. The equations for the decay rates depend on the nature of the parent pseudoscalar meson and on the final state meson.

Pseudoscalar meson in final state

The simplest case is the decay of the form $h \to h' + \ell + N$, where a pseudoscalar meson h decays into another pseudoscalar meson h', a charged lepton ℓ and a heavy neutral lepton N. In this case, the decay rate of the semileptonic decay of the pseudoscalar meson into HNLs is given by [30]

$$\Gamma\left(h \to h'_P \ell_\alpha N\right) = \frac{G_F^2 m_h^5}{64\pi^3} C_K^2 |V_{UD}|^2 |U_{\alpha 4}|^2 \left(I_{P,1} + I_{P,2} + I_{P,3} + I_{P,4}\right), \quad (2.8)$$

where m_h is the mass of the parent meson, $C_K = 1/\sqrt{2}$ for decays into π^0 and $C_K = 1$ for all other cases, V_{UD} is the relevant CMK matrix element that depends on the meson structure.

The integrals $I_{P,i}$ are given by

$$
\begin{aligned}
I_{P,1} &= \int_{(y_\ell + y_N)^2}^{(1-y_{h'})^2} \frac{d\xi}{3\xi^3} \left| f_+ \left(q^2 \right) \right|^2 \Lambda^3(\xi), \\
I_{P,2} &= \int_{(1-y_{h'})^2}^{(y_\ell + y_N)^2} \frac{d\xi}{2\xi^3} \left| f_+ \left(q^2 \right) \right|^2 \Lambda(\xi) G_-(\xi) \lambda \left(1, y_{h'}^2, \xi \right), \\
I_{P,3} &= \int_{(y_\ell + y_N)^2}^{(1-y_{h'})^2} \frac{d\xi}{2\xi^3} \left| f_0 \left(q^2 \right) \right|^2 \Lambda(\xi) G_-(\xi) \left(1 - y_{h'}^2 \right)^2, \\
I_{P,4} &= 0,
\end{aligned}
\tag{2.9}
$$

where

$$
\begin{aligned}
\Lambda(\xi) &= \lambda^{1/2} \left(1, y_{h'}^2, \xi \right) \lambda^{1/2} \left(\xi, y_N^2, y_\ell^2 \right) \\
G_-(\xi) &= \xi \left(y_N^2 + y_\ell^2 \right) - \left(y_N^2 - y_\ell^2 \right)^2,
\end{aligned}
\tag{2.10}
$$

$y_i = \dfrac{m_i}{m_h}$, $\xi = \dfrac{q^2}{m_h^2}$ and the function $\lambda(a,b,c)$ is defined by Eq. (2.7). The functions $f(q^2)$ depend on the type of parent and daughter mesons. All the values of the parameters for these functions that are used in this work were taken from [30].

1. For $K \to \pi$ decays, we have

$$
f_{+,0}^{K\pi} \left(q^2 \right) = f_{+,0}^{K\pi}(0) \left(1 + \lambda_{+,0} \frac{q^2}{m_{\pi^+}^2} \right),
\tag{2.11}
$$

where

h, h'	$f_{+,0}(0)$	λ_+	λ_0
K^0, π^+	0.970	0.0267	0.0117
K^+, π^0	0.970	0.0277	0.0183

2. In the case of $D \to K$ and $D \to \pi$ decays, we have

$$
f \left(q^2 \right) = \frac{f(0) - c \left(z \left(q^2 \right) - z_0 \right) \left(1 + \frac{z(q^2) + z_0}{2} \right)}{1 - P q^2},
\tag{2.12}
$$

where

$$z\left(q^2\right) = \frac{\sqrt{t_+ - q^2} - \sqrt{t_+ - t_0}}{\sqrt{t_+ - q^2} + \sqrt{t_+ - t_0}}$$
$$t_+ = (m_h + m_{h'})^2$$
$$t_0 = (m_h + m_{h'})\left(\sqrt{m_h} - \sqrt{m_{h'}}\right)^2$$

(2.13)

and

f	$f(0)$	c	$P\left(\text{GeV}^{-2}\right)$
f_+^{DK}	0.7647	0.066	0.224
f_0^{DK}	0.7647	2.084	0
$f_+^{D\pi}$	0.6117	1.985	0.1314
$f_0^{D\pi}$	0.6117	1.188	0.0342

.

3. Finally, for $D \to \eta$ decays, we have

$$f_+^{D_s \eta}\left(q^2\right) = \frac{f_+^{D_s \eta}(0)}{\left(1 - q^2/m_{D_s^*}^2\right)\left(1 - \alpha_+^{D_s \eta} q^2/m_{D_s^*}^2\right)},$$
$$f_0^{D_s \eta}\left(q^2\right) = \frac{f_0^{D_s \eta}(0)}{1 - \alpha_0^{D_s \eta} q^2/m_{D_s^*}^2},$$

(2.14)

where $f_+^{D_s \eta}(0) = 0.495$, $\alpha_+^{D_s \eta} = 0.198$, $m_{D_S^*} = 2.112$ GeV, $f_0^{D_s \eta}(0) = f_+^{D_s \eta}(0)$ and $\alpha_0^{D_s \eta} = 0$.

Vector meson in final state

A more complicated case is given by $h \to h_V' + \ell + N$, where a pseudoscalar meson h decays into a vector meson h_V', a charged lepton ℓ and a heavy neutral lepton N. In this case, the decay rate of the semileptonic decay of the pseudoscalar meson into HNLs is given by [30]

$$\Gamma\left(h \to h_V' \ell_\alpha N\right) = \frac{G_F^2 m_h^7}{64\pi^3 m_{h'}^2} C_K^2 \left|V_{UD}\right|^2 \left|U_\alpha\right|^2 \left(I_{V,g^2} + I_{V,f^2} + I_{V,a_+^2} + I_{V,a_-^2} + \right.$$
$$\left. + I_{V,gf} + I_{V,ga_+} + I_{V,ga_-} + I_{V,fa_+} + I_{V,fa_-} + I_{V,a_+a_-}\right),$$

(2.15)

where $C_K = 1/\sqrt{2}$ for $h_V = \rho^0$ and $C_K = 0$ otherwise in this work. Although there are several integrals $I_{V,i}$, it turns out that the only nonvanishing integrals are:

$$I_{V,g^2} = \frac{m_h^2 y_{h'}^2}{3} \int_{(y_\ell + y_N)^2}^{(1-y_{h'})^2} \frac{d\xi}{\xi^2} g^2\left(q^2\right) \Lambda(\xi) F(\xi) \left(2\xi^2 - G_+(\xi)\right),$$

$$I_{V,f^2} = \frac{1}{24 m_h^2} \int_{(y_\ell + y_N)^2}^{(1-y_{h'})^2} \frac{d\xi}{\xi^3} f^2\left(q^2\right) \Lambda(\xi) \times$$
$$\times \left(3F(\xi)\left[\xi^2 - \left(y_\ell^2 - y_N^2\right)^2\right] - \Lambda^2(\xi) + 12 y_{h'}^2 \xi \left[2\xi^2 - G_+(\xi)\right]\right),$$

$$I_{V,a_+^2} = \frac{m_h^2}{24} \int_{(y_\ell + y_N)^2}^{(1-y_{h'})^2} \frac{d\xi}{\xi^3} a_+^2\left(q^2\right) \Lambda(\xi) F(\xi) \left(F(\xi)\left[2\xi^2 - G_+(\xi)\right] + 3G_-(\xi)\left[1 - y_{h'}^2\right]^2\right),$$

$$I_{V,a_-^2} = \frac{m_h^2}{8} \int_{(y_\ell + y_N)^2}^{(1-y_{h'})^2} \frac{d\xi}{\xi} a_-^2\left(q^2\right) \Lambda(\xi) F(\xi) G_-(\xi),$$

$$I_{V,fa_+} = \frac{1}{12} \int_{(y_\ell + y_N)^2}^{(1-y_{h'})^2} \frac{d\xi}{\xi^3} f\left(q^2\right) a_+\left(q^2\right) \Lambda(\xi) \times$$
$$\times \left(3\xi F(\xi) G_-(\xi) + \left(1 - \xi - y_{h'}^2\right)\left[3F(\xi)\left(\xi^2 - \left(y_l^2 - y_N^2\right)^2\right) - \Lambda^2(\xi)\right]\right),$$

$$I_{V,fa_-} = \frac{1}{4} \int_{(y_\ell + y_N)^2}^{(1-y_{h'})^2} \frac{d\xi}{\xi^2} f\left(q^2\right) a_-\left(q^2\right) \Lambda(\xi) F(\xi) G_-(\xi),$$

$$I_{V,a_+a_-} = \frac{m_h^2}{4} \int_{(y_\ell + y_N)^2}^{(1-y_{h'})^2} \frac{d\xi}{\xi^2} a_+\left(q^2\right) a_-\left(q^2\right) \Lambda(\xi) F(\xi) G_-(\xi) \left(1 - y_{h'}^2\right),$$

$$\tag{2.16}$$

where the notations are similar to the previous cases and

$$F(\xi) = (1-\xi)^2 - 2y_{h'}^2(1+\xi) + y_{h'}^4,$$
$$G_+(\xi) = \xi\left(y_N^2 + y_\ell^2\right) + \left(y_N^2 - y_\ell^2\right)^2. \tag{2.17}$$

2.2.4 Tau decays

Although at experiments such as DUNE the main contribution to the HNL productions will come from electron and muon mixing, it is important to implement HNL production from tau decays. In general, the tau leptons can be created directly at the target or as the decay of a heavy meson, such as D_s. In both cases, the tau lepton decay into HNLs represents a probe to the value of the mixing $U_{\tau 4}$.

Tau lepton two-body decays

The tau lepton can decay via $\tau \to h_{P/V}N$, where h_P represents a pseudoscalar meson and h_V a vector meson. The expressions for the decay rates of the tau for each case are given by [30]

$$\Gamma(\tau \to h_P N) = \frac{G_F^2 f_h^2 m_\tau^3}{16\pi} |V_{UD}|^2 |U_{\tau 4}|^2 \left[(1 - y_N^2)^2 - y_h^2 (1 + y_N^2) \right] \sqrt{\lambda(1, y_N^2, y_h^2)},$$

$$\Gamma(\tau \to h_V N) = \frac{G_F^2 g_h^2 m_\tau^3}{16\pi m_h^2} |V_{UD}|^2 |U_{\tau 4}|^2 \left[(1 - y_N^2)^2 - y_h^2 (1 + y_N^2 - 2y_h^2) \right] \sqrt{\lambda(1, y_N^2, y_h^2)},$$

(2.18)

where $y_i = \dfrac{m_i}{m_\tau}$, λ is defined in (2.7) and f_h is the decay constant of the meson.

Tau lepton three-body decays

Due to its large mass, the tau lepton can also have three body decays.

The first decay has the form $\tau \to N\ell_\alpha \bar{\nu}_\alpha$. In this case, the tau lepton decays into a HNL and a W boson via tau mixing and then the W boson decays into a lepton pair. The decay rate for this process is

$$\begin{aligned}
\Gamma(\tau \to N\ell_\alpha \bar{\nu}_\alpha) &= \frac{G_F^2 m_\tau^5}{96\pi^3} |U_{\tau 4}|^2 \int_{y_\ell^2}^{(1-y_N)^2} \frac{d\xi}{\xi^3} (\xi - y_\ell^2)^2 \sqrt{\lambda(1, \xi, y_N^2)} \times \\
&\quad \times \left((\xi + 2y_\ell^2) [1 - y_N^2]^2 + \xi(\xi - y_\ell^2)[1 + y_N^2 - y_\ell^2] - \xi y_\ell^4 - 2\xi^3 \right) \\
&\approx \frac{G_F^2 m_\tau^5}{192\pi^3} |U_{\tau 4}|^2 \left[1 - 8y_N^2 + 8y_N^6 - y_N^8 - 12y_N^4 \log(y_N^2) \right], \quad \text{for } y_l \to 0
\end{aligned}$$

(2.19)

The tau lepton can also decay via $\tau \to \nu_\tau \ell_\alpha N$, where the tau decays into a tau neutrino and a W boson and then the W boson decays into a charged lepton and a HNL. The decay rate for this process is

$$\begin{aligned}
\Gamma(\tau \to \nu_\tau \ell_\alpha N) &= \frac{G_F^2 m_\tau^5}{96\pi^3} |U_{\alpha 4}|^2 \int_{(y_\ell + y_N)^2}^{1} \frac{d\xi}{\xi^3} (1 - \xi)^2 \sqrt{\lambda(\xi, y_N^2, y_\ell^2)} \times \\
&\quad \times \left(2\xi^3 + \xi - \xi(1 - \xi)[1 - y_N^2 - y_\ell^2] - (2 + \xi)[y_N^2 - y_\ell^2]^2 \right) \\
&\approx \frac{G_F^2 m_\tau^5}{192\pi^3} |U_{\alpha 4}|^2 \left[1 - 8y_N^2 + 8y_N^6 - y_N^8 - 12y_N^4 \log(y_N^2) \right], \quad \text{for } y_l \to 0
\end{aligned}$$

(2.20)

Finally, the tau lepton can also decay to pions via $\tau^+ \to \pi^+ \pi^0 N$. In this work, we treat this decay only at the phase space level. The decay rate of this process is:

$$
\Gamma(\tau^+ \to \pi^+ \pi^0 N) = \Gamma(\tau^+ \to \pi^+ \pi^0 \bar{\nu}_\tau) \tau_\tau |U_{\tau 4}|^2 \int_{(m_\pi + m_N)^2}^{(m_\tau - m_\pi)^2} dx \left[\sqrt{1 - \frac{2(m_{\pi^+}^2 + x)}{m_\tau^2} + \frac{(m_{\pi^+}^2 - x)^2}{m_\tau^4}} \right.
$$
$$
\left. \times \sqrt{1 - \frac{2(m_{\pi^0}^2 + m_N^2)}{x} + \frac{(m_{\pi^0}^2 - m_N^2)^2}{x^2}} \right] ,
\tag{2.21}
$$

where τ_τ is the lifetime of the tau lepton. The integral in Eq. (2.21) represents a rescaling of the decay rate of tau into pions due to the mass of the heavy neutral lepton.

2.3   Decay of HNLs

Heavy neutral leptons can decay via mixing with the active neutrinos of the SM. There are several HNL decay channels with rates that depend on the final states of the process, the value of the HNL mass and the mixing parameters. In this section, we summarize the formulas for calculating the decay rates of HNLs into several final states and we label them for convenience. For more details about the formulas, we refer the reader to Refs. [30, 25, 24, 43].

2.3.1   Decays into three leptons

A heavy neutral lepton can decay into a neutrino and two charged leptons. The decay rate will depend on the nature of the charged leptons.

Decay 1: $N \to \ell_\alpha^- \nu_\beta \ell_\beta^+$

These decays are defined by $N \to \ell_\alpha^- \nu_\beta \ell_\beta^+$ with $\alpha \neq \beta$. In this case, the HNL decays into a charged lepton and a W boson, which decays into a lepton pair. This process is mediated only by charged currents. The decay rate for this process is

$$
\Gamma_1 \left(N \to \ell_\alpha^- \nu_\beta \ell_\beta^+ \right) = \frac{G_F^2 m_N^5}{192\pi^3} |U_{\alpha 4}|^2 I \left(x_{\nu_\beta}, x_{\ell_\beta}, x_{\ell_\alpha} \right) ,
\tag{2.22}
$$

where $x_i = \dfrac{m_i}{m_N}$,

$$I(a,b,c) \equiv 12 \int_{(b+c)^2}^{(1-a)^2} \frac{dx}{x} \left(x - c^2 - b^2\right)\left(1 + a^2 - x\right)\sqrt{\lambda\left(x, c^2, b^2\right)\lambda\left(1, x, a^2\right)} \quad (2.23)$$

and $\lambda(a,b,c)$ is defined by (2.7).

Decay 2a: $N \to \nu_\alpha \ell_\beta^+ \ell_\beta^-$

These decays are defined by $N \to \nu_\alpha \ell_\beta^+ \ell_\beta^-$. In this case, the HNL decays into a light neutrino and a Z boson, which decays into a charged lepton pair. This decay is mediated by the neutral weak current and its rate is given by

$$\Gamma_{2a}\left(N \to \nu_\alpha \ell_\beta^+ \ell_\beta^-\right) = N_Z \frac{G_F^2 M_N^5}{192\pi^3} \cdot |U_\alpha|^2 \cdot \left[C_1^f \left(\left(1 - 14x^2 - 2x^4 - 12x^6\right)\sqrt{1 - 4x^2} + \right. \right.$$
$$+ 12x^4\left(x^4 - 1\right)L(x)\right) + 4C_2^f\left(x^2\left(2 + 10x^2 - 12x^4\right)\sqrt{1 - 4x^2} + $$
$$+ 6x^4\left(1 - 2x^2 + 2x^4\right)L(x)\right)\Big]$$

$$(2.24)$$

where $x = \dfrac{m_{\ell_\beta}}{m_N}$, $L(x) = \log\left[\dfrac{1 - 3x^2 - \left(1 - x^2\right)\sqrt{1 - 4x^2}}{x^2\left(1 + \sqrt{1 - 4x^2}\right)}\right]$, $C_1^f = \dfrac{1}{4}\left(1 - 4\sin^2\theta_W + 8\sin^4\theta_W\right)$

and $C_2^f = \dfrac{1}{2}\sin^2\theta_W\left(2\sin^2\theta_W - 1\right)$ and θ_W represents the Weinberg angle. Equation (2.24)is valid for Dirac HNLs. However, for Majorana HNLs, the presence of the neutral current adds a factor of 2 to the decay rate.

Decay 2b: $N \to \nu_\alpha \ell_\alpha^+ \ell_\alpha^-$

These decays are identified by the process $N \to \nu_\alpha \ell_\alpha^+ \ell_\alpha^-$. In this case, the HNL decays into a light neutrino and a Z boson, which decays into a charged lepton pair of the same flavor of the neutrino. Since all the leptons have the same flavor, this decay has diagrams that involve neutral and charged weak currents. The rate of this process is given by

$$\Gamma_{2b}\left(N \to \nu_\alpha f \bar{f}\right) = N_Z \frac{G_F^2 M_N^5}{192\pi^3} \cdot |U_\alpha|^2 \cdot \left[C_1^f \left(\left(1 - 14x^2 - 2x^4 - 12x^6\right)\sqrt{1 - 4x^2} + \right. \right.$$
$$+ 12x^4\left(x^4 - 1\right)L(x)\right) + 4C_2^f\left(x^2\left(2 + 10x^2 - 12x^4\right)\sqrt{1 - 4x^2} + \quad (2.25)$$
$$+ 6x^4\left(1 - 2x^2 + 2x^4\right)L(x)\right)\Big]$$

where $x = \dfrac{m_{\ell_\beta}}{m_N}$, $L(x) = \log \left[\dfrac{1 - 3x^2 - (1 - x^2)\sqrt{1 - 4x^2}}{x^2 \left(1 + \sqrt{1 - 4x^2}\right)} \right]$, $C_1^f = \dfrac{1}{4}\left(1 + 4\sin^2\theta_W + 8\sin^4\theta_W\right)$

and $C_2^f = \dfrac{1}{2}\sin^2\theta_W \left(2\sin^2\theta_W + 1\right)$ and θ_W represents the Weinberg angle. Equation (2.25) is valid for Dirac HNLs. However, for Majorana HNLs, the presence of the neutral current adds a factor of 2 to the decay rate.

Decay 3a: $N \to \nu_\alpha \bar{\nu}_\beta \nu_\beta$

The HNL decays into one neutrino and a Z boson, which decays into a neutrino-antineutrino pair with a flavor that is different from the first neutrino. The rate of this process is given by

$$\Gamma_{3a}\left(N \to \nu_\alpha \nu_\beta \bar{\nu}_\beta\right) = \frac{G_F^2 M_N^5}{768\pi^3} |U_\alpha|^2 \tag{2.26}$$

Equation (2.26) is valid for Dirac HNLs. However, for Majorana HNLs, the presence of the neutral current adds a factor of 2 to the decay rate.

Decay 3b: $N \to \nu_\alpha \bar{\nu}_\alpha \nu_\alpha$

The HNL decays into one neutrino and a Z boson, which decays into a neutrino-antineutrino pair with the same as the first neutrino. The rate of this process is given by

$$\Gamma_{3b}\left(N \to \nu_\alpha \nu_\beta \bar{\nu}_\beta\right) = \frac{G_F^2 M_N^5}{384\pi^3} |U_\alpha|^2 \tag{2.27}$$

Equation (2.27) is valid for Dirac HNLs. However, for Majorana HNLs, the presence of the neutral current adds a factor of 2 to the decay rate.

2.3.2 Charged pseudoscalar meson and charged lepton

If the neutrino is heavy enough, it can decay into mesons and charged leptons. This decay is important because it can provide a signature of HNL at collider experiments.

Decay 4: $N \to l_\alpha^- h_P^+$

The HNL decays into one lepton and a W boson, which decays into a quark pair that hadronizes into a charged pseudoscalar meson. The decay rate is given by

$$\Gamma_4\left(N \to \ell_\alpha^- h_P^+\right) = \frac{G_F^2 f_h^2 |V_{UD}|^2 |U_\alpha|^2 m_N^3}{16\pi} \left[\left(1 - x_\ell^2\right)^2 - x_h^2\left(1 + x_\ell^2\right)\right]\sqrt{\lambda\left(1, x_h^2, x_\ell^2\right)}, \tag{2.28}$$

where f_h is the decay constant of the meson, V_{UD} the respective element of the CKM matrix, $x_i = \dfrac{m_i}{m_N}$ and $\lambda(a,b,c)$ is given by Eq. (2.7).

2.3.3 Neutral pseudoscalar meson and neutrino

Decay 5: $N \to \nu_\alpha h_P^0$

The HNL decays into one neutrino and a Z boson, which decays into a quark-antiquark pair that hadronizes into a neutral pseudoscalar meson. The decay rate is given by

$$\Gamma_5 \left(N \to \nu_\alpha h_P^0\right) = \frac{G_F^2 f_h^2 m_N^3}{32\pi} \left|U_\alpha\right|^2 \left(1 - x_h^2\right)^2, \tag{2.29}$$

where f_h is the decay constant of the meson and $x_h = \dfrac{m_h}{m_N}$.

2.3.4 Charged vector meson and charged lepton

Decay 6: $N \to \ell_\alpha^- h_V^+$

The HNL decays into one charged lepton and a W boson, which decays into a quark pair that hadronizes into a charged vector meson. The decay rate is given by

$$\Gamma_6 \left(N \to \ell_\alpha^- h_V^+\right) = \frac{G_F^2 g_h^2 \left|V_{UD}\right|^2 \left|U_\alpha\right|^2 m_N^3}{16\pi m_h^2} \left(\left(1 - x_\ell^2\right)^2 + x_h^2 \left(1 + x_\ell^2\right) - 2x_h^4\right) \sqrt{\lambda\left(1, x_h^2, x_\ell^2\right)}, \tag{2.30}$$

where g_h is the decay constant of the vector meson, $x_h = \dfrac{m_h}{m_N}$ and $\lambda(a,b,c)$ is defined by Eq. (2.7).

2.3.5 Neutral vector meson and neutrino

Decay 7: $N \to \nu_\alpha V^0$

The HNL decays into one neutrino and a Z boson, which decays into a quark-antiquark pair that hadronizes into a neutral vector meson. The decay rate is given by

$$\Gamma_7 \left(N \to \nu_\alpha h_V^0\right) = \frac{G_F^2 \kappa_h^2 g_\rho^2 \left|U_\alpha\right|^2 m_N^3}{32\pi m_h^2} \left(1 + 2x_h^2\right) \left(1 - x_h^2\right)^2 \tag{2.31}$$

where g_ρ is the decay constant of the ρ^0 meson, $x_h = \dfrac{m_h}{m_N}$ and the parameter κ_h depends on the meson. For the ρ^0 and ϕ mesons we have:

$$\kappa_{\rho^0} = 1 - 2\sin^2\theta_W, \tag{2.32}$$

$$\kappa_\phi = \frac{4}{3}\sin^2\theta_W - 1. \tag{2.33}$$

2.4 HNL total decay rate and lifetime

In Section 2.3 we discussed the decay channels of the HNL. In this section, we will find expressions for the total width and lifetime of the HNL. For a Dirac HNL, the total decay rate is given by

$$\Gamma_{\text{Total}}^{\text{Dirac}} = \Gamma_1 + \Gamma_{2a} + \Gamma_{2b} + \Gamma_{3a} + \Gamma_{3b} + \Gamma_4 + \Gamma_5 + \Gamma_6 + \Gamma_7 \tag{2.34}$$

and its lifetime is

$$\tau_N = \frac{1}{\Gamma_{\text{Total}}}, \tag{2.35}$$

where the decay rates Γ_i represent the decays presented in Section 2.3.

Since, in general, neutrinos can be Dirac or Majorana in nature, the available decay channels of a heavy neutral lepton will depend on its Dirac or Majorana nature. For instance, a Dirac HNL can decay via $N \to e^- \pi^+$, but a Majorana HNL can decay via both $N \to e^- \pi^+$ and $N \to e^+ \pi^-$ since it is its own antiparticle. This extends to all the charged current HNL decays, which implies that the total charged current decay rate of Majorana is twice the charged current decay rate of Dirac HNLs. Additionally, the decay rates that involve neutral currents for Majorana HNLs are also twice the corresponding decay rates of Dirac HNLs. Therefore, we can conclude that the total decay rate of Majorana HNLs is twice the total decay rate of Dirac HNLs:

$$\Gamma_{\text{Total}}^{\text{Majorana}} = 2\Gamma_{\text{Total}}^{\text{Dirac}}. \tag{2.36}$$

Additionally, the lifetimes are related by

$$\tau_{\text{Majorana}} = \frac{1}{2}\tau_{\text{Dirac}}, \tag{2.37}$$

which implies that Majorana HNLs decay faster than Dirac ones.

2.5 Oscillations into HNLs

Heavy neutral leptons mix with the active neutrinos of the standard model. Therefore, it is possible for HNLs to oscillate into active neutrinos. In general, the structure of the survival probability of a neutrino ν_α can be expressed as [40]:

$$P_{\nu_\alpha \to \nu_\alpha} = P^{\text{inv}}_{\nu_\alpha \to \nu_\alpha} + P^{\text{app}}_{\nu_\alpha \to \nu_\alpha}, \tag{2.38}$$

The first term $P^{\text{inv}}_{\nu_\alpha \to \nu_\alpha}$ in Eq. (2.38) is called invisible and takes into account the oscillation of ν_α into unobservable states such as a HNL. The second term $P^{\text{app}}_{\nu_\alpha \to \nu_\alpha}$ is called appearance and represents the case when ν_α oscillates into other states and then oscillates back to its original flavor α.

We are mainly interested in the case where the active neutrino ν_α disappears due to oscillations to HNLs; therefore, we will focus on the invisible term of the survival probability. Considering $m_N \gg m_{\nu_\alpha}$, the general formula for the invisible term is

$$
\begin{aligned}
P^{\text{inv}}_{\nu_\alpha \to \nu_\alpha} = &-4\left(1 - |U_{\alpha 4}|^2\right)|U_{\alpha 4}|^2 \sin^2\left(1.27 m_N^2 L / E_{\nu_\alpha}\right) \exp\left(-\Gamma_N L/2\right) \\
&+ 2\left(1 - |U_{\alpha 4}|^2\right)|U_{\alpha 4}|^2 \exp\left(-\Gamma_N L/2\right) \\
&+ \left(1 - |U_{\alpha 4}|^2\right)^2 + |U_{\alpha 4}|^4 \exp\left(-\Gamma_N L\right),
\end{aligned}
\tag{2.39}
$$

where Γ_N represent the total decay rate of the HNL, L the distance traveled by the active neutrino and E_{ν_α} its energy. Note that we are considering the possibility that the active neutrino oscillates into a sterile neutrino. If we set in $\Gamma_N = 0$ or $\Gamma_N L \to 0$ in Eq. (2.39), we get:

$$P^{\text{inv}}_{\nu_\alpha \to \nu_\alpha} = 1 - 4\left(1 - |U_{\alpha 4}|^2\right)|U_{\alpha 4}|^2 \sin^2\left(1.27 m_N^2 L / E_{\nu_\alpha}\right) \tag{2.40}$$

and for $\Gamma_N L \gg 1$ we obtain:

$$P^{\text{inv}}_{\nu_\alpha \to \nu_\alpha} = \left(1 - |U_{\alpha 4}|^2\right)^2. \tag{2.41}$$

In this work, we are considering HNL masses starting from 1 eV, but we are mainly interested in heavy neutral leptons where $m_N \gg 1$ eV. In this mass range, it is not possible to directly observe the behavior of the oscillations of active neutrinos into HNLs at collider experiments, but the average out of the oscillation will still have an effect on the active neutrino flux, effectively decreasing the number of active neutrinos that reach the detector. If we take the

average out in Eq. (2.39) we get:

$$P_{\nu_\alpha \to \nu_\alpha}^{\text{inv}} = \left(1 - |U_{\alpha 4}|^2\right)^2 + |U_{\alpha 4}|^4 \exp\left(-\Gamma_N L\right), \tag{2.42}$$

which, in the limit $\Gamma_4 L \ll 1$, becomes

$$P_{\nu_\alpha \to \nu_\alpha}^{\text{inv}} = 1 - 2\left(1 - |U_{\alpha 4}|^2\right)|U_{\alpha 4}|^2. \tag{2.43}$$
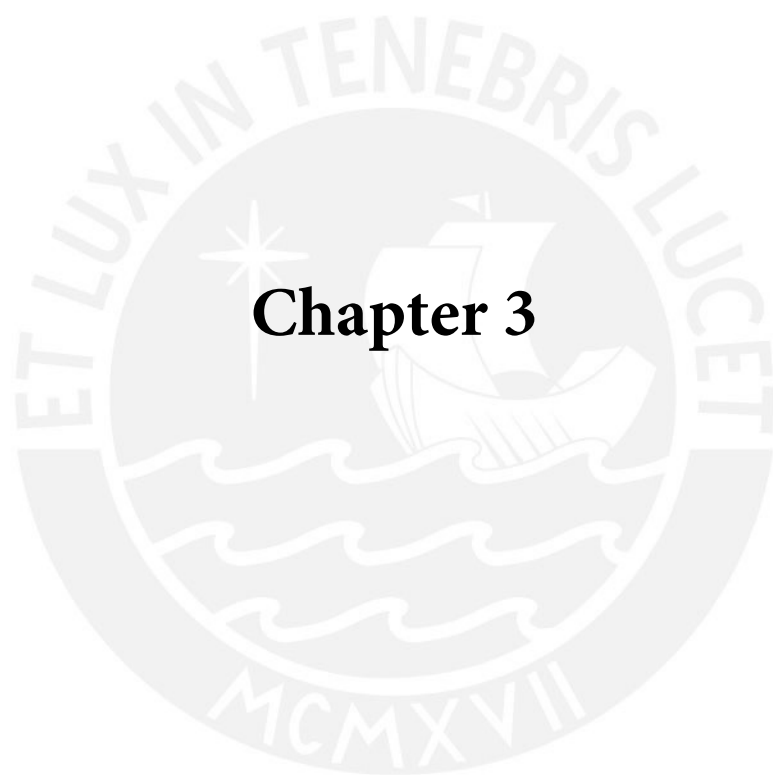
Chapter 3

Chapter 3

Experimental and simulation framework

3.1 The DUNE Experiment

Neutrino physics is currently one of the most important research fields of high energy physics. One of the main reasons for this interest in neutrinos is that several of their properties such as their mass scale, mixing angles, CP violation phase and Dirac/Majorana nature are still partially or totally unknown. Current and future neutrino experiments aim to measure these and other neutrino parameters with enough precision to determine exactly how the current Standard Model of particle physics must be extended to incorporate the neutrino properties discovered in the last decades. One of these is the Deep Underground Neutrino Experiment (DUNE) [4, 6–9], which will make use of the world's most intense neutrino beam to conduct a high precision study of neutrino oscillations and also look for beyond standard model signals in its detectors. In this section, we will describe the main features of DUNE, with particular interest in its Near Detector Complex.

3.1.1 DUNE Facilities

The DUNE experiment will consist of three main facilities: the Long-Baseline Neutrino Facility (LBNF), the DUNE Near Detector (DUNEND), and the DUNE Far Detector (DUNEFD).

1. **Long-Baseline Neutrino Facility**

   The Long-Baseline Neutrino Facility (LNBF) will be located at Fermilab and will produce the world's most intense neutrino beam. This beam will be produced in a series of steps. First, the PIP-II linear particle accelerator [1, 23] and the rest of the Fermilab accelerator chain will provide a high luminosity proton beam with a power between 1.0 and 1.2 MW over a wide energy band of 60 GeV to 120 GeV. This proton
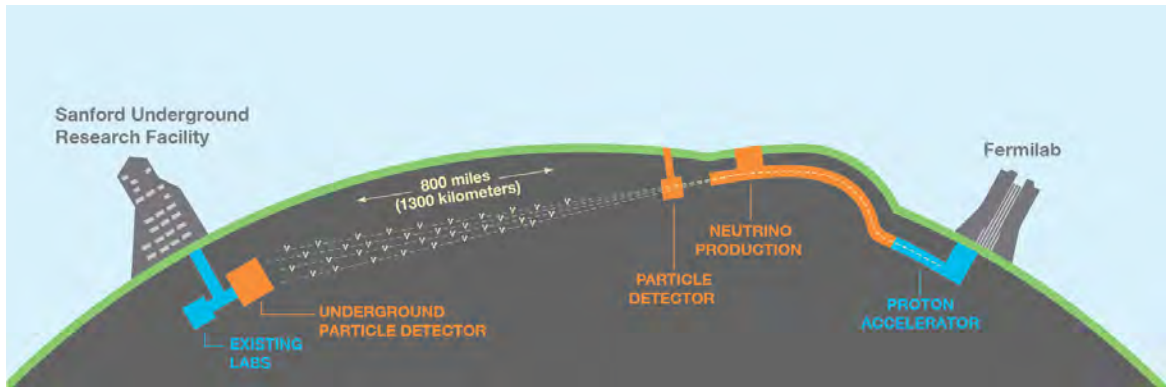
Fig. 3.1 DUNE Facilities. Image taken from [6].

beam will then collide with a graphite target located at the Target Hall Complex, with around 1.47×10^{21} POTs expected each year. Each collision will produce mesons and other particles capable of decaying into neutrinos. The charged particles produced will immediately be deflected by a set of magnetic horns, which will operate in two different configurations: one that favors the presence of neutrinos in the beam (neutrino mode) and another that favors antineutrinos (antineutrino mode). After leaving the magnetic horns, the particles will travel inside a decay pipe, where they will decay on flight. Finally, all undesired particles will be absorbed by a set of shielding facilities so that the final beam that arrives at the detectors is composed only of neutrinos.

2. **DUNE Near Detector**

The DUNE Near Detector (DUNEND) [4] complex is located at 574 m from the target and its main goal is to constraint systematic uncertainties in neutrino oscillations by precisely measuring the spectra of the neutrino beam produced by the LBNF. The DUNEND complex consists of three detectors. The first one, named ArgonCube, is a liquid argon time proyection chamber (LArTPC). It has a width of 7 m, a height of 3 m (both transverse to the beam direction), a length of 5 m in the beam direction and is filled with a fiducial mass of 50 tons of liquid argon. Its technology is very similar to the one used by the far detector, which helps to decrease systematic errors related to nuclear effects. The second detector is the multi-purpose detector (MPD), which consists of a high-pressure argon TPC surrounded by an electromagnetic calorimeter (ECAL) in a 0.5 T magnetic field. The MPD's goal is to measure the momentum and charge of the muons that exit ArgonCube. Both ArgonCube and the MPD can move horizontally from the beam axis by a distance of up to 33 m, a configuration known as DUNE PRISM. These off-axis positions make it possible to study the neutrino beam at larger angular distributions, where the beam is more monochromatic. Finally, the

DUNEND also includes the System for on-Axis Neutrino Detection (SAND) [58], which is a beam monitor that always stays on-axis and acts as a systematic crosscheck for the flux measured by ArgonCube.

3. **DUNE Far Detector** The DUNE Far Detector (DUNEFD) will be located 1300 km from the DUNEND, at the Underground Particle Detector of the Sanford Underground Research Facility, which is located 1.5 km underground. It will consist of four LArTPC detector modules with a combined total of 40 kt of liquid argon fiducial mass. Each LArTPC is located inside a cryostat of dimensions 15.1 m $\times$ 14.0 m $\times$ 62.0 m. The main goal of the DUNEFD is to measure the spectra of incoming neutrinos in order to derive neutrino oscillation parameters. The DUNEFD will be able to reconstruct neutrino interactions with unprecedented resolution and its large fiducial mass will provide high statistics capable of conducting precision measurements of neutrino oscillations. Currently, there are two LArTPC technologies being developed for the DUNEFD. In the first one, known as single-phase [9], the ionization charges drift horizontally within the liquid argon towards a vertical anode due to the action of an electric field. In this case, no signal amplification occurs inside the cryostat; hence, very low-noise electronics are needed to achieve a good signal-to-noise ratio. In the second one, known as double-phase [5], the ionization charges drift vertically upward towards a layer of argon gas above the liquid. The signal in the gas is then amplified before reaching a horizontal anode. This amplification of the signal reduces the requirements of low-noise electronics in comparison to the single-phase technology. The DUNE collaboration is currently developing both technologies to implement them in the experiment.

3.1.2 DUNE Physics

The DUNE experiment will explore several areas involving neutrino physics [7], but its main research interest will be related to the phenomenology of neutrino oscillations, a phenomenon that implies flavor-mixing in the neutrino sector as well as nonzero neutrino masses. The scale and value of these masses are still unknown and are beyond the reach of any neutrino oscillation experiment, including DUNE. However, the mass ordering of neutrinos, as well as the values of the mixing angles and the CP violating phase can and will be tested by DUNE with unprecedented precision: the mixing angles θ_{23} and θ_{13} will be measured at the few percent level and the CP violation phase δ_{CP} at the 10% level. In particular, the value of δ_{CP} is crucial in determining the matter-antimatter asymmetry in the universe; finding CP violation at DUNE would favor the leptogenesis mechanism as the origin of the baryon

asymmetry of the universe [34]. The precise values of the mixing parameters to be obtained by DUNE are also important for beyond the standard model theories, such as Gran Unified Theories, where high precision experiments are needed in order to test their predictions [21, 25].

Due to its excellent reconstruction capabilities, DUNE will also be able to look for signals that are beyond neutrino oscillations. For instance, DUNE will be sensitive to proton decays and to neutron-antineutron oscillations, two processes that involve baryon number violation, a phenomenon that is crucial for Gran Unified Theories [51, 37]. DUNE will also be able to measure the neutrino bursts produced in closeby supernovae and extract precise information about the collapses of these stars [50, 46]. Additionally, DUNE will look for evidence of beyond standard model theories such as active-sterile neutrino mixing [33], nonunitarity of the PMNS matrix [20], nonstandard interactions [2], CPT or Lorentz violation [48, 49], neutrino trident production [17], dark matter [45] and heavy neutral leptons [3].

3.2 Simulation Configuration for DUNEND

The DUNE experiment will have several facilities, each with its own particular experimental configuration. In this work, we are interested in the details that are relevant for the simulation of neutrino events at the DUNEND facility [10]. As mentioned in section 3.1, the DUNEND will consist of three detectors: ArgonCube, the MPD and SAND. Since the role of SAND is only to monitor the beam stability, we will focus on ArgonCube and the MPD. Besides, since we are only interested in the neutrino-argon CC event rates, our main interests are the masses of the detectors and their geometrical acceptance. Fig. 3.2 shows schematically the distribution of the detectors at the DUNEND. The following describes the exact parameters of the DUNEND configuration assumed in our simulations.

The LBNF will provide a 120 GeV proton beam, which will collide into a graphite target, producing 1.47×10^{21} POTs each year. At each collision, several mesons are produced, including mostly pions, kaons and charmed mesons. The muons and other long-lived charged particles (mostly pions and kaons) are deflected by magnetic horns located right after the target; as a consequence, the trajectories of some of them end up preferably oriented along the beam axis, as shown schematically in Fig. 3.2. The magnetic horns can work in two modes: a neutrino mode, which focuses positively charged particles along the beam axis and hence favors the presence of neutrinos in the beam, and an antineutrino mode, which focuses negatively charged particles and hence favors the presence of antineutrinos in the beam. On the other hand, the trajectories of neutral and short-lived are not affected by the
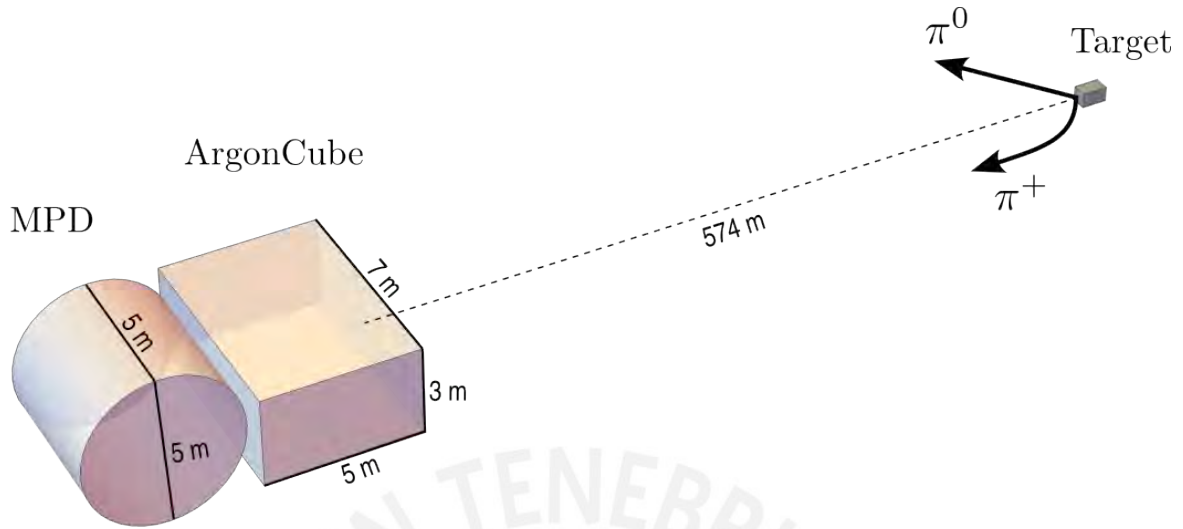
Fig. 3.2 Configuration of DUNEND used in simulations.

magnetic focusing horns. After their production at the target, most particles decay on flight inside the decay pipe, a cylinder with a length of 230 m and a diameter of 2 m. However, a small number of long-lived particles reach the end of the decay pipe and decay at rest at its surface. The decays of these particles produce a neutrino beam that is mostly focused towards the DUNEND detectors.

The first detector along the beamline is ArgonCube, a LArTPC containing a fiducial mass of 50 tons of liquid argon. It has a height of 3 m, a width of 7 m (both perpendicular to the beam axis) and a length of 5 m along the beam axis, as shown in Fig. 3.2. It is located at 574 m from the target. The second detector along the beamline is the multi-purpose detector, a high-pressure argon TPC containing 1 ton of gaseous argon. It has the shape of a cylinder, with a diameter of 5 m and a length of 5 m. The axis of the cylinder is perpendicular to the beam axis, as shown in Fig. 3.2. The MPD is positioned right after ArgonCube and at a distance of 579 m from the target. Both ArgonCube and the MPD are capable of moving horizontally to different off-axis positions, with a maximum of 30 m from the beam axis.

3.3   Meson and lepton production at DUNE

The production of the neutrino beam at DUNE will depend on the number of particles produced at the target that are capable of decaying into neutrinos, which from now on we will refer to as "parents". We will divide the possible neutrino parents into three categories: light parents (muons, pions and kaons), D mesons and tau leptons. Each kind of parent will have a different production rate and therefore will make a different contribution to the total neutrino

flux. Of course, there will be other particles produced at the target that, in principle, will also be able to decay into neutrinos; however, we will ignore them since their contributions to the neutrino flux are comparatively negligible.

3.3.1 Light parents

The DUNE neutrino beam will be produced by the decays of particles produced at the DUNE target. In each proton-on-target, several types of particles will be produced, but only some of them will have decay channels with final state neutrinos and even fewer will have branching ratios into neutrinos above a few percent. For instance, both K_L^0 and K_S^0 will be produced at the same rate at the DUNE target; however, while the former has semileptonic decays with branching ratios above 60%, the semileptonic decays of the latter have branching ratios below 0.1%. This means that the contribution of K_S^0 to the DUNE neutrino flux is small enough to be considered negligible. When one takes into account both the production rate and the branching ratios with final state neutrinos, only a handful of particles make up for almost the entire neutrino flux at DUNE. These particles are what we call light parents and are listed in Table 3.1, where we include their masses and lifetimes. One of the main properties of these particles is that they have small masses, which means that they will be sensitive to the deflections of the magnetic horns. Additionally, their large lifetimes will allow them to decay further away from the LBNF target.

Table 3.1 Light parents considered in this work.

	m [MeV]	τ [10^{-8} s]
$\mu^{\pm}$	105.66	219.70
$\pi^{\pm}$	139.57	2.60
$K^{\pm}$	493.68	1.24
K_L^0	497.61	5.12

Among these light parents, some of them will be produced more copiously than others due to the nature of the LBNF proton beam and target. In order to estimate which particles will be more relevant to the neutrino flux, we calculated an estimate of the average number of these particles to be produced at the DUNE target per POT. These estimates were obtained with a simulation in the software PYTHIA8 [57], where we used the flag `SoftQCD:all` and collided a beam of 120 GeV protons into protons and neutrons at rest. Our results are consistent with [27]. We can conclude that pions will be the most abundant light parents at DUNE, followed by kaons and finally muons.

Table 3.2 Particles that dominate the electron and muon neutrino flux at DUNE, with an estimate of the average number of these particles produced per POT when 120 GeV protons hit protons or neutrons.

	Particles per POT	
	120 GeV pp	120 GeV pn
π^+	2.8	2.4
π^-	2.2	2.5
K^+	0.23	0.23
K_L^0	0.19	0.19
K^-	0.18	0.19
μ^+	9.75×10^{-4}	2.36×10^{-4}
μ^-	8.94×10^{-4}	2.09×10^{-4}

Right after the light parents are produced at the DUNE target, they immediately enter a set of magnetic horns. The presence of these horns will affect the trajectory of the charged parents and hence will affect their contributions to the neutrino flux. The magnetic horns can act in two different configurations.

- **Neutrino mode:** In this configuration, the magnetic horns will focus the positively charged particles along the beam axis, while the negatively charged particles will be deflected away from the beam. This configuration favors the presence of electron and muon neutrinos in the flux.

- **Antineutrino mode:** The magnetic horns can also act in a second configuration that focuses the negatively charged particles along the beam axis and deflects the positively charged particles away from the beamline. This configuration favors the presence of antineutrinos in the flux.

In order to take into account the effect of the magnetic horns, we used the data provided by the DUNE Beam Interface Working Group [35], which makes use of GEANT4 [11, 16] and FLUKA [36, 28]. This data contains all the information about the energies, momenta, vertices and weights of the light parents after they exit the magnetic horns, both in neutrino and antineutrino mode. Figure 3.3 shows the spectra of light parents after they exit the magnetic horns in neutrino mode, where different bin widths have been used for different species for clarity purposes. The plot shows that muons peak around 0.2 GeV, pions around 0.3 GeV and kaons around 0.6 GeV. It is also quite clear that pions dominate over the other particles and muons are the least abundant light parents at DUNE.
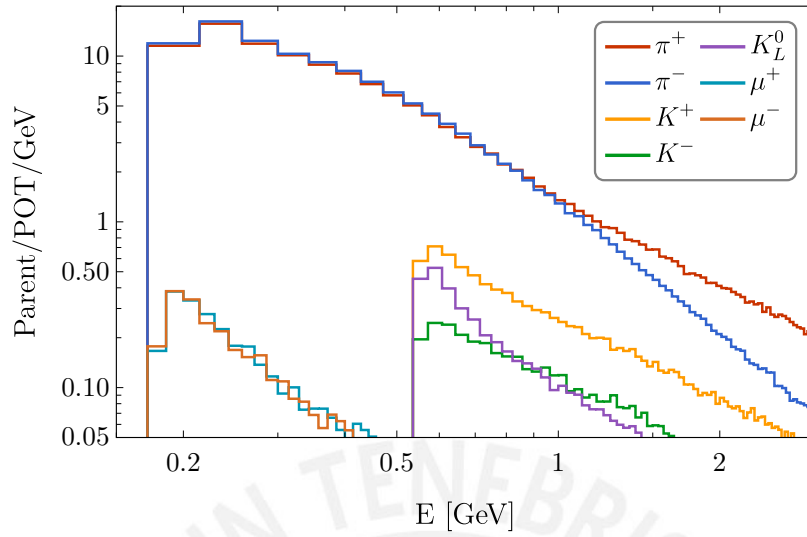
Fig. 3.3 Spectra of light parents leaving the magnetic horns at DUNE in neutrino mode.

The magnetic horns will not only affect the energy of the particles produced at DUNE but, more importantly, their propagation directions. Figure 3.4 displays the angular distribution of the charged light parents produced at the DUNE target after they exit the magnetic horns. We see that these particles are mostly oriented at very small angles. For pions and kaons, the angular distributions peak at around $0.4°$ and for muons they peak at around $0.5°$. These small angles are evidence of the focusing effect of the magnetic horns on positively charged parents when they operate in neutrino mode.
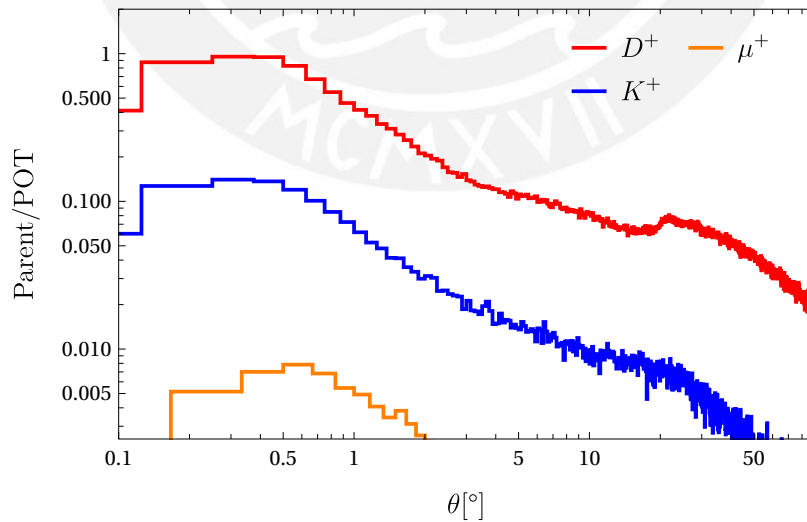
Fig. 3.4 Angular distributions of charged light parents after they exit the magnetic horns in neutrino mode.

As already mentioned, the magnetic horns can also act in antineutrino mode. In this setup, the negatively charged particles will be focused along the beam axis, favoring the production of antineutrinos. Figure 3.5 shows a comparison between the angular distributions of positively charged pions in neutrino and antineutrino mode. In antineutrino mode (blue), the positively charged pions are deflected away from the beam axis and its angular distribution peaks at around $25°$. It is also relevant to compare the different effects that the magnetic horns have on different particle species. Since the kaons are more massive than the pions, it is natural to expect that their larger inertia will tend to attenuate the amount of deflection caused by the magnetic horns. This effect is seen in Figure 3.6, where the angular distributions of both pions and kaons are shown. The distance between the peaks of the angular distributions of π^+ and π^- is larger than the one between K^+ and K^-, which indicates that the pions are more sensitive to the deflection.
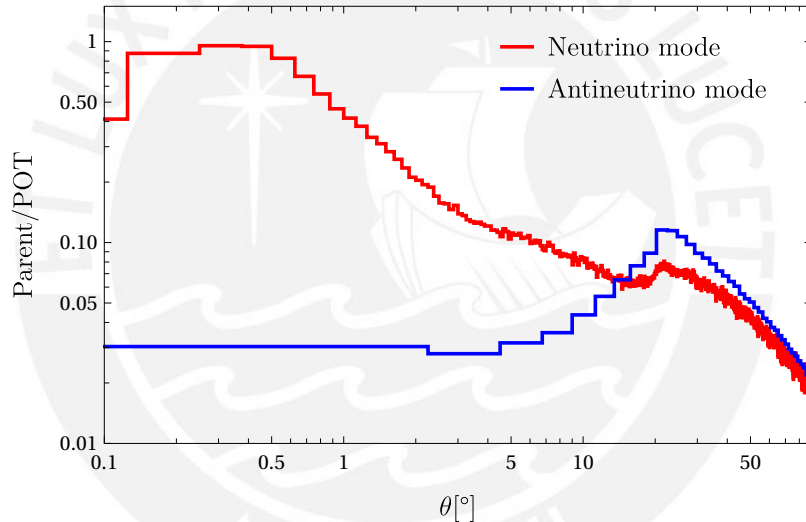
Fig. 3.5 Comparison between angular distributions of π^+ in neutrino (red) and antineutrino (blue) mode.

After leaving the magnetic horns, all these light particles will decay on flight inside the decay pipe. The decay vertices of these particles will be determined by their energies and their lifetimes. Table 3.1 lists the lifetimes of the light particles considered in this work. Muons will have the largest lifetimes and hence will propagate a larger distance before decaying into neutrinos.

Depending on the decay channels available for each specimen, some will dominate the electron or the muon neutrino flux. Table 3.3 shows the main branching ratios to neutrinos of the light parents considered in this work. We see that the charged pions will dominate the muon neutrino production at DUNE, followed by kaons. On the other hand, kaons and
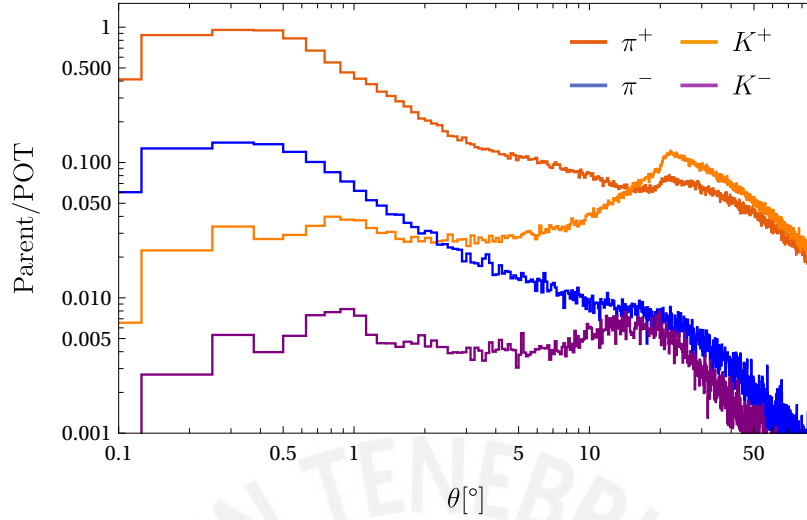
Fig. 3.6 Comparison between angular distributions of pions and kaons after they exit the magnetic horns acting in neutrino mode.

muons will dominate the electron neutrino production. A similar reasoning can be made for the antineutrinos. We have to consider that the exact contribution of each parent to the neutrino flux will also depend on the particle's direction of propagation, boost and decay vertex.

Table 3.3 Dominant branching ratios to neutrinos of light parents considered in this work.

	Channel	BR (%)
$\pi^+ \to$	$\mu^+ \nu_\mu$	99.987
	$e^+ \nu_e$	0.012
$K^+ \to$	$\mu^+ \nu_\mu$	63.56
	$\pi^0 e^+ \nu_e$	5.07
	$\pi^0 \mu^+ \nu_\mu$	3.35
	$e^+ \nu_e$	0.002
$K^0_L \to$	$\pi^\pm e^\mp \nu_e$	40.55
	$\pi^\pm \mu^\mp \nu_\mu$	27.04
$\mu^+ \to$	$e^+ \nu_e \bar{\nu}_\mu$	100.00

3.3.2 Heavy mesons

Besides light mesons such as pions and kaons, other heavier mesons capable of decaying into neutrinos will also be produced at DUNE. The creation of these heavier mesons will involve the production of heavy quarks, which is heavily suppressed due to the low $c\bar{c}$ and

$b\bar{b}$ production cross sections at DUNE energies. Still, the $c\bar{c}$ production rate is high enough to take into consideration the contribution of D mesons, especially because their decays will make up for virtually all the tau neutrino flux at DUNE. The heavy parents considered in this work are shown in Table 3.4. These mesons have short lifetimes, so they will not propagate large distances in the decay pipe. On the other hand, their large masses will be relevant when we consider the possibility of heavy neutral lepton production from their decays.

Table 3.4 Lifetimes of heavy mesons considered in this work.

	m [MeV]	τ [10^{-15} s]
D^0	1864.83	410
$D^\pm$	1869.65	1040
$D_s^\pm$	1968.27	500

In order to test how relevant these mesons will be for neutrino production at DUNE, we calculated their production rates at DUNE energies. Table 3.5 shows an estimate of the number of heavy mesons produced at DUNE per POT. These estimates were calculated with a simulation in PYTHIA8, in which we collided 120 GeV protons into protons and neutrons at rest with the flag `SoftQCD:all`. Our results are consistent with [27]. We note that neutral mesons are more abundant, followed by the charged mesons and finally the charged strange mesons. If we compare tables 3.2 and 3.5, we can conclude that the production rates of heavy mesons are several orders of magnitude smaller than that of the lighter parents, which will then dominate the electron and neutrino flux. Still, the heavy parents are important because they will be the only ones capable of producing tau neutrinos and also because they can produce heavy neutral leptons with masses larger than the kaon mass.

Table 3.5 Most abundant heavy particles at DUNE that can decay into neutrinos, with an estimate of the average number of these particles produced per POT when 120 GeV protons hit protons or neutrons.

	Particles per POT	
	120 GeV pp	120 GeV pn
$\bar{D}^0$	1.1×10^{-5}	1.2×10^{-5}
D^0	6.8×10^{-6}	6.7×10^{-6}
D^-	5.7×10^{-6}	6.1×10^{-6}
D^+	3.6×10^{-6}	3.6×10^{-6}
D_s^-	1.5×10^{-6}	1.7×10^{-6}
D_s^+	1.1×10^{-6}	1.1×10^{-6}

Although some of the D mesons produced at the DUNE target are charged, the magnetic horns will not have any effect on their trajectories because, according to Table 3.4, their lifetimes are so small that they decay almost instantaneously after being produced. This also implies that the momenta of these particles is the same when the horns operate in neutrino and antineutrino mode. Due to their small production rate, the simulation of the production of heavy mesons in PYTHIA8 can be quite computationally expensive. In order to obtain good statistics for the momentum distributions of these particles, we decided to obtain the energy and momenta of these particles from parametrization formulas. The production cross-section of charmed mesons in proton-proton collisions at beam energies of 400 GeV can be parametrized in the center of mass frame by the empirical form

$$\frac{d^2\sigma}{dx_F dp_T^2} \propto (1 - |x_F|) e^{-b p_T^2},\tag{3.1}$$

where $x_F = 2p_z\sqrt{s}$, p_z is the longitudinal momentum of the particle, p_T the transverse momentum, $n = 6.1 \pm 0.7$ and $b = 1.08 \pm 0.09$ [18]. The values of these parameters were fitted from the E769 experiment, which operated at beam energies of 400 GeV, greater than those typical of DUNE. In order to study the effects of this energy difference, we simulated fixed-target proton on proton collisions at beam energies of 400 GeV and 120 GeV in PYTHIA8 with the flag `SoftQCD:all`. As expected, Eq. 3.1 works well for beam energies of 400 GeV. However, we found that the simulated data at 120 GeV is not properly represented by 3.1. This discrepancy arises from the charmed meson production cross-section dependence on x_F, which is no longer accurately described by the function $(1 - |x_F|)^n$. On the other hand, the exponential dependence on p_T^2 was corroborated, albeit with a different value for the parameter b. In order to obtain a more reliable parametrization for charmed meson production at DUNE energies, we fitted the simulated data provided by PYTHIA8 to the parametrization formula

$$\frac{d^2\sigma}{dx_F dp_T^2} \propto \sqrt{\frac{a}{\pi}} e^{-a x_F^2} e^{-b p_T^2},\tag{3.2}$$

where the x_F dependence is now modeled by a Gaussian distribution. The values obtained for the parameters a and b for each meson flavor are shown in Table 3.6.

Figure 3.7 compares the data produced by PYTHIA8 with the best fits of the parametrization formulas 3.1 and 3.1. We note that the equation 3.2 is a much better representation of the data produced by PYTHIA8. In this work, we generated all the charmed meson energy and momenta by making use of the parametrization formula of Eq. 3.2 and the values of Table 3.6.

Table 3.6 Values of the parameters a and b of parametrization formula (3.2) obtained by fitting to simulated data produced with PYTHIA8.

	a	b
D^+	15.282 ± 0.113	0.721 ± 0.015
D^-	12.959 ± 0.163	0.923 ± 0.021
D_s^+	16.886 ± 0.166	0.627 ± 0.009
D_s^-	15.176 ± 0.228	0.784 ± 0.017
D^0	16.203 ± 0.107	0.744 ± 0.014
$\bar{D}^0$	13.013 ± 0.160	0.957 ± 0.022

(a) caption

(b) caption
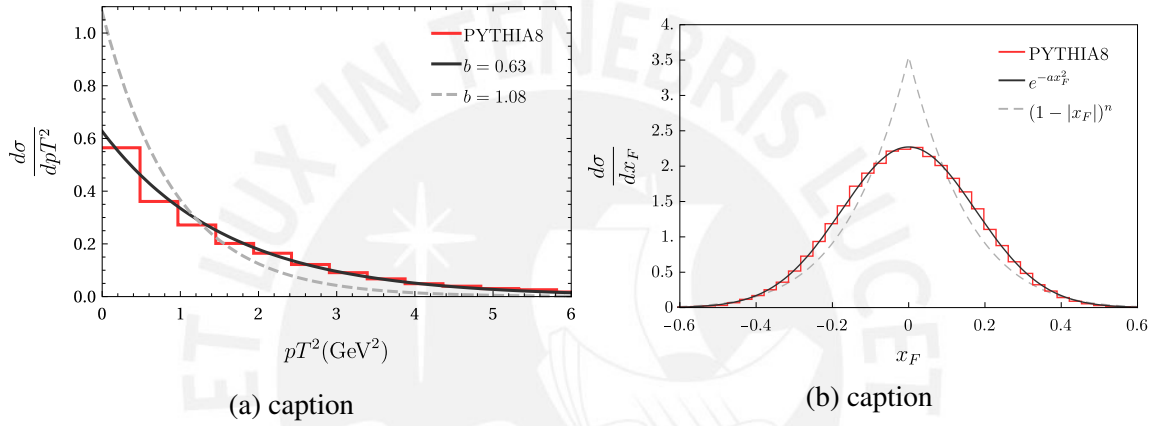
Fig. 3.7 Differential cross sections for D meson production at DUNE energies in PYTHIA8 (red) and parametrizations (3.2) (solid black) and (3.1) (dashed black).

With the help of the parametrization formulas, we produced a large dataset of D mesons that provided sufficiently high statistics to test their contributions to the DUNE neutrino flux. Figure 3.8 shows the spectra of D mesons produced at the DUNE target. Since all the heavy parents are D mesons, their spectra are quite similar, although with differences in their abundances and peak energies. For instance, $\bar{D}^0$ is the most abundant heavy parent and D_s^+ is the most energetic. It is important to remember that these particles will not be affected by the magnetic horns and, therefore, they are not sensitive to the neutrino or antineutrino configurations.

In this work, we will assume that, after being produced at the DUNE target, these heavy mesons will decay promptly right after the target. This approach is motivated by the small lifetime of D mesons, which is shown in Table 3.4. The largest lifetime is on the order of $\mathcal{O}(10^{-15})$ s, which is much smaller than the lifetimes of lighter particles, which are around $\mathcal{O}(10^{-8})$ s, seven order of magnitudes larger.
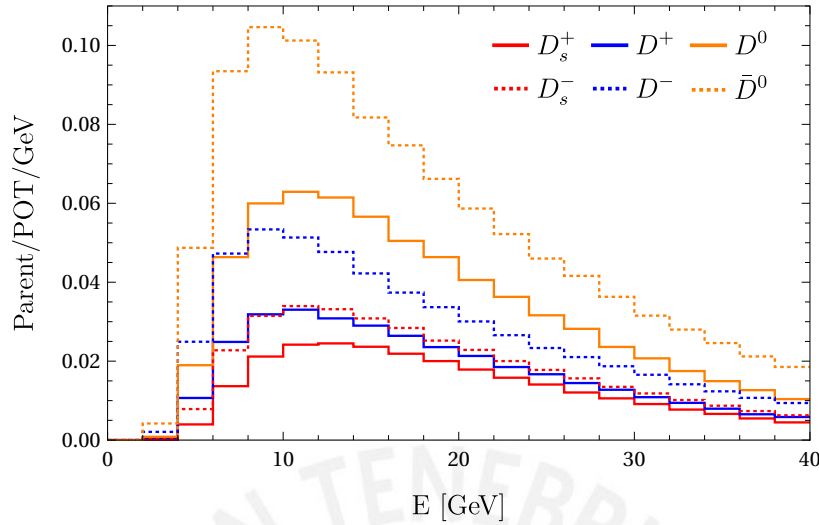
Fig. 3.8 Spectra of heavy parents at DUNE.

Finally, we will list the decay channels we considered for the heavy mesons. Since they don't have dominant channels into neutrinos, we decided to include a large variety of possible decays. Table 3.7 shows the branching ratios of these decay channels. Almost all of them are below 10% and most of them are on the order of a few percent. The largest branching ratio belongs to the decay $D_s^+ \to \phi e^+ \nu_e$, which is around 24%. We have also included some branching ratios that are very small because they might still be relevant if these mesons decay into HNLs.

3.4   Active neutrino flux at DUNE

In the last section, we discussed the production of the particles at the DUNE target that are responsible for the largest contributions to the neutrino flux. These particles will travel through the magnetic horns and then will decay on flight inside the decay pipe into neutrinos and other particles. The contribution of each particle species to the neutrino flux will depend on its lifetime, which determines its decay vertex, and decay channels. In order to calculate the neutrino flux at the DUNEND, we used a simulation in PYTHIA8. We gave PYTHIA all the relevant information about the parents (masses, lifetimes, decay channels, branching ratios, energies, momenta and production vertices) and then let it handle all the decay kinematics. In this way, we obtained a dataset that contains information about all the neutrinos produced at DUNE. Finally, we used a custom script to store the kinematic information of the active neutrinos that lie within the geometrical acceptance of the detectors at DUNEND. This script takes into account the tridimensional shapes of the detectors,

Table 3.7 Dominant branching ratios to neutrinos of light parents considered in this work.

	Channel	BR (%)		Channel	BR (%)
$D_s^+ \rightarrow$	$e^+ \nu_e$	8.3×10^{-3}	$D^+ \rightarrow$	$e^+ \nu_e$	8.8×10^{-4}
	$\mu^+ \nu_\mu$	0.55		$\mu^+ \nu_\mu$	3.7×10^{-4}
	$\tau^+ \nu_\tau$	5.48		$\tau^+ \nu_\tau$	0.12
	$\eta e^+ \nu_e$	2.32		$K^0 e^+ \nu_e$	8.73
	$\eta \mu^+ \nu_\mu$	2.40		$K^0 \mu^+ \nu_\mu$	8.74
	$\eta' e^+ \nu_e$	0.80		$\bar{K}^{*0} e^+ \nu_e$	5.40
	$\eta' \mu^+ \nu_\mu$	1.10		$\bar{K}^{*0} \mu^+ \nu_\mu$	5.25
	$\phi e^+ \nu_e$	23.9			
	$\phi \mu^+ \nu_\mu$	1.90			
$D^0 \rightarrow$	$K^- e^+ \nu_e$	3.53			
	$K^- \mu^+ \nu_\mu$	3.31			
	$K^{*-} e^+ \nu_e$	2.15			
	$K^{*-} \mu^+ \nu_\mu$	1.86			

including the fact that the multi-purpose detector has the shape of a cylinder with its axis perpendicular to the beamline. Figure 3.9 shows our results for the ν_μ flux at ArgonCube produced by the decays of π^+ when the horns are working in neutrino mode. The flux has a peak around 2.3 MeV which, as we will see, represents the peak of the muon neutrino flux at DUNE. Due to their larger abundancy and better orientation along the beamline, the contribution of the positive pions dominates the ν_μ flux at DUNE, producing a total flux at ArgonCube of around 9.4×10^{-8} $\nu_\mu/POT/cm^2$, which, assuming 1.47×10^{21} POTs per year, translates into 29×10^{18} muon neutrinos hitting ArgonCube each year. The other light parents will also contribute to the muon neutrino flux, albeit with much lower intensity. Figure 3.10 displays our results for the ν_μ flux at ArgonCube produced by several light parents when the horns operate in neutrino mode. It is clear from the plot that the charged pions dominate the ν_μ flux below 5 MeV, which is the region where the peak is located. Above 10 MeV, the contribution of charged kaons becomes dominant and they account for virtually all the muon neutrino flux at higher energies. In comparison, the flux produced by muons and neutral kaons is completely overshadowed by pions over the entire energy range.

Although DUNE is optimized for muon neutrino production, a large amount of electron neutrinos will also be produced, although at a much lower rate. Figure 3.11 shows the results of our calculations of the expected electron neutrino flux at ArgonCube. First, we note that the ν_e flux is around 2 orders of magnitude smaller than the ν_μ flux. This difference is considerable, but, as we will see in the next sections, the electron neutrino flux is still high enough to provide good statistics for heavy neutral lepton searches. We also note that muons
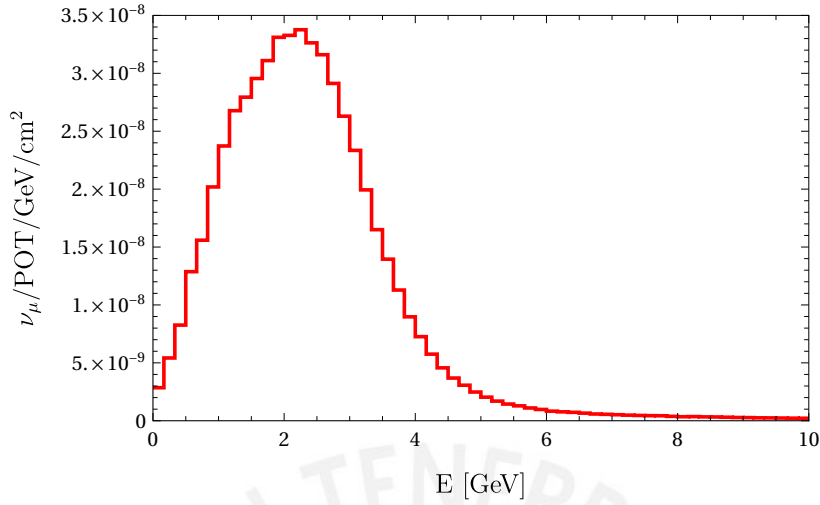
Fig. 3.9 Muon neutrino flux at ArgonCube produced by π^+ decays when the horns operate in neutrino mode. The peak is around 2.3 GeV.
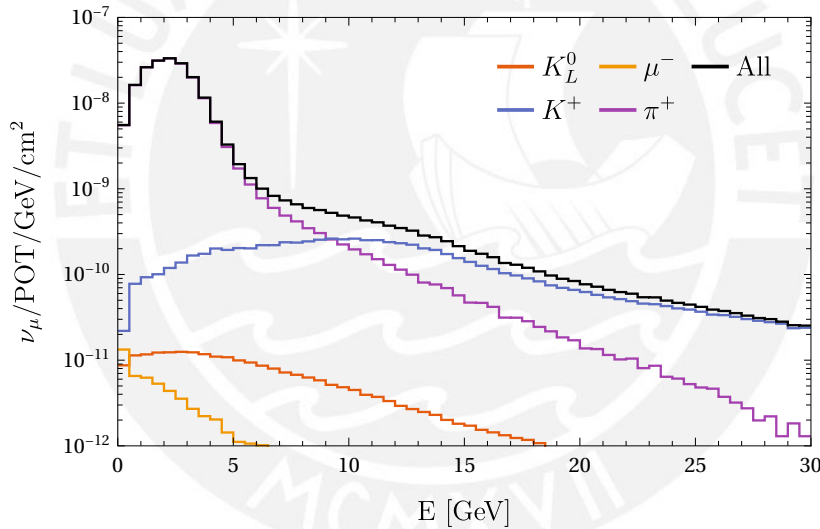
Fig. 3.10 Muon neutrino flux at ArgonCube produced by light parents when the horns operate in neutrino mode. The black line represents the total flux.

are the main source of electron neutrinos. This is in agreement with Table 3.3, where one can verify that the only particles capable of decaying into electron neutrinos are K_L^0L, K^+ and μ^+. Of these three particles, the muons, although less abundant, decay exclusively into electron neutrinos, hence dominating the electron neutrino flux.

As we saw in the last section, the heavy mesons will also have decay channels into neutrinos and, therefore, will also contribute to the neutrino flux. However, due to their much smaller production rate, their contributions are expected to be much smaller. Figure 3.12 shows the contributions of heavy parents to the muon neutrino flux at ArgonCube in neutrino
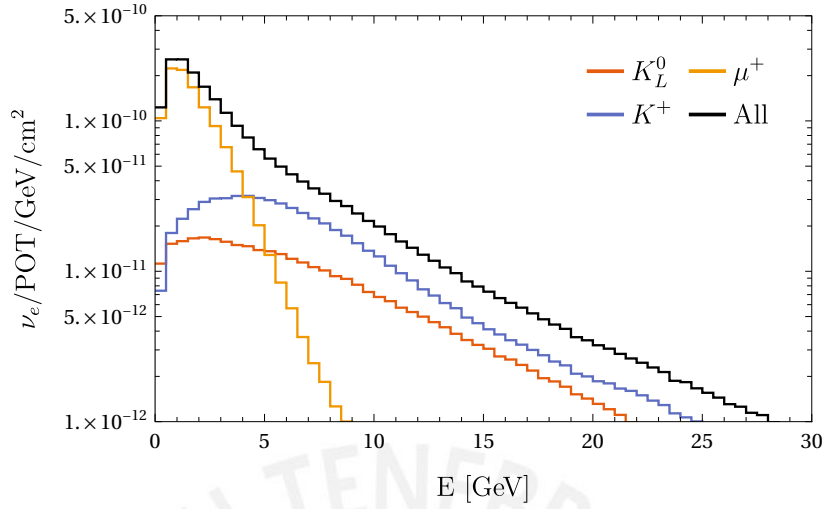
Fig. 3.11 Electron neutrino flux at ArgonCube produced by light parents when the horns operate in neutrino mode. The black line represents the total flux.

mode. Comparing Figures 3.10 and 3.12 we see that the contributions of heavy mesons are about 5 orders of magnitude smaller than the ones from light parents. For this reason, these particles will have a negligible contribution to the muon neutrino flux. The same happens for the electron neutrino flux, which is totally dominated by the decays of light particles.
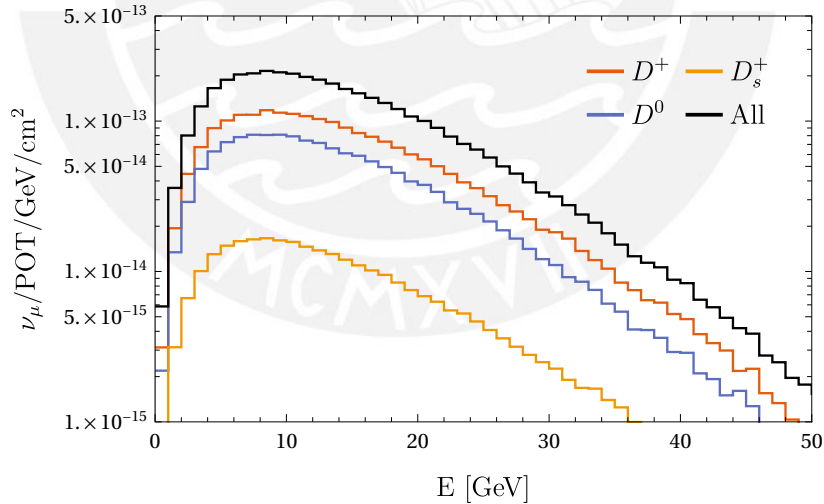
Fig. 3.12 Muon neutrino flux at ArgonCube produced by heavy parents. The black line represents the total flux.

Heavy mesons become relevant when one studies the tau neutrino flux at DUNE. From Table 3.7 we can infer there are two ways to produce tau neutrinos at DUNE: by direct decays of D^+ or D_s^+ or by tau lepton decays. In the first case, due to the larger branching ratio, more neutrinos are produced, but they are less energetic because most of the meson

energy is expended in creating the tau lepton. In the second, the production rate is lower, but the neutrinos are more energetic since a large part of the tau lepton energy goes into the tau neutrino. Figure 3.13 displays the contributions of the heavy mesons considered in this work to the ν_τ flux at AgonCube. The tau neutrino production peaks at energies around 3.5 GeV and then decreases slowly. We also note that the ν_τ flux is much smaller than the ν_μ and ν_e flux. This is expected because the LBNF works at energies that favor muon neutrino production, but are not high enough to produce a large amount of tau neutrinos.
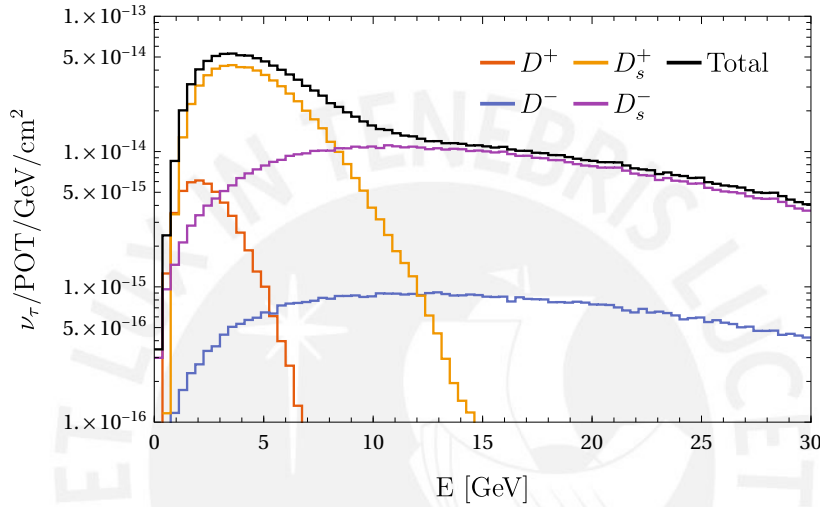
Fig. 3.13 Tau neutrino flux at ArgonCube produced by heavy parents. The black line represents the total flux.

We also included in our simulations the possibility of moving ArgonCube and the MPD horizontally up to a distance of 30 m from the beamline. This setup allows us to calculate the neutrino fluxes at different off-axis positions. Figure 3.14 shows a comparison between the muon neutrino on-axis and at an off-axis position of 30 m. The off-axis configuration has three effects on the neutrino flux. The first and more obvious one is that the neutrino flux will be smaller at off-axis positions since most of the neutrinos will be focused along the beamline. The second one is that the flux peaks at lower energies, around 1 GeV. The final one is that the neutrino peak is much more focused; in this sense, we say that the neutrino flux is more monochromatic at off-axis positions.

3.5 Neutrino charged current events

The neutrino flux at ArgonCube will interact with the liquid argon at the time projection chamber and will generate several neutrino interactions. In this work, we will focus on the
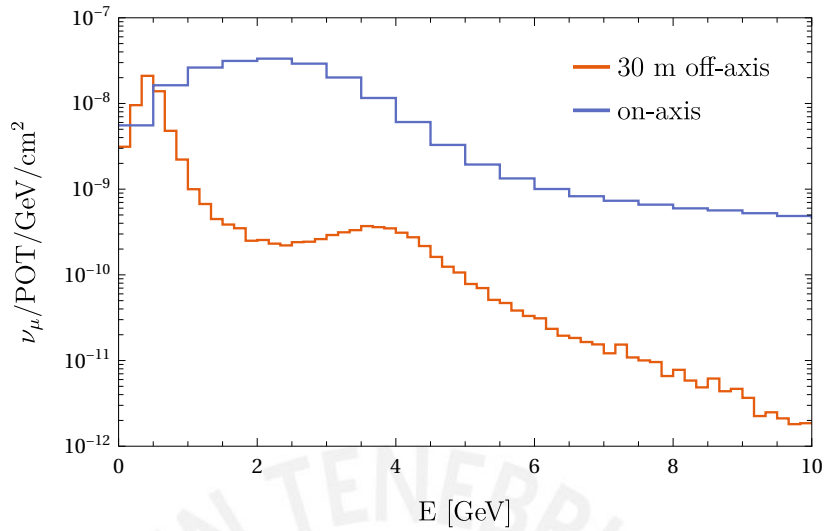
Fig. 3.14 Comparison between the muon neutrino fluxes at ArgonCube in on-axis (red) and 30 m off-axis (blue) configurations.

neutrino-argon charged-current (CC) events that occur in the ArgonCube detector of the DUNEND. In order to calculate these CC event rates, we extracted the inclusive neutrino-Argon cross-section data from Ref. [10]. Figure 3.15 shows the dependence of the neutrino-argon cross-section on the energy of the incident neutrino. The plot shows that the electron and muon neutrinos have the largest cross sections while the tau neutrino cross sections are the smallest.
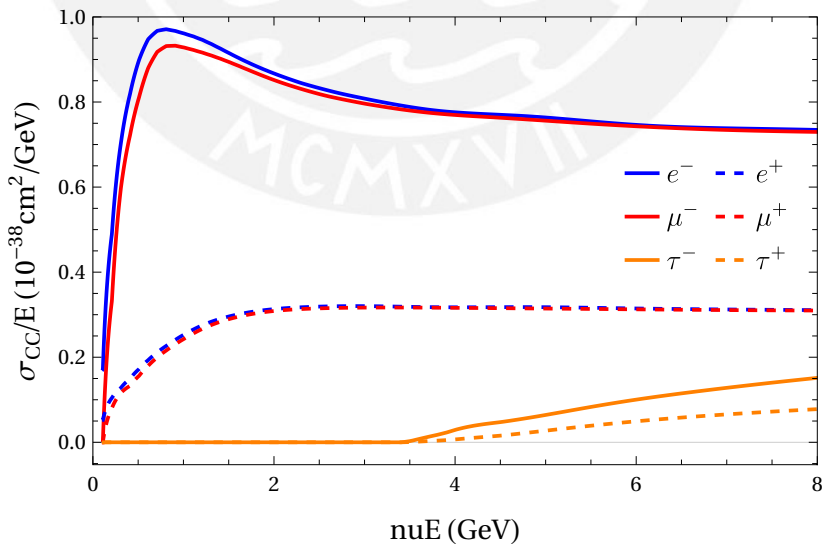
Fig. 3.15 Neutrino-argon inclusive charged current cross sections per nucleon.

In order to calculate the total neutrino CC event rates at DUNEND, we convoluted the neutrino-argon cross sections with the neutrino fluxes calculated previously. Figure 3.16 shows the inclusive neutrino CC event rates at ArgonCube in one year of operation in neutrino mode. The muon neutrino cross sections are by far the dominant events. In total, around 8×10^8 ν_μ CC events and 9×10^6 ν_e CC events are expected at DUNE assuming 10 years of operation in neutrino mode. For the tau neutrinos, one must keep in mind that both their production rate and their cross sections with argon are very low at DUNE energies. This translates into a very small number of ν_τ CC events at ArgonCube, around 3 in 10 years of operation in neutrino mode.
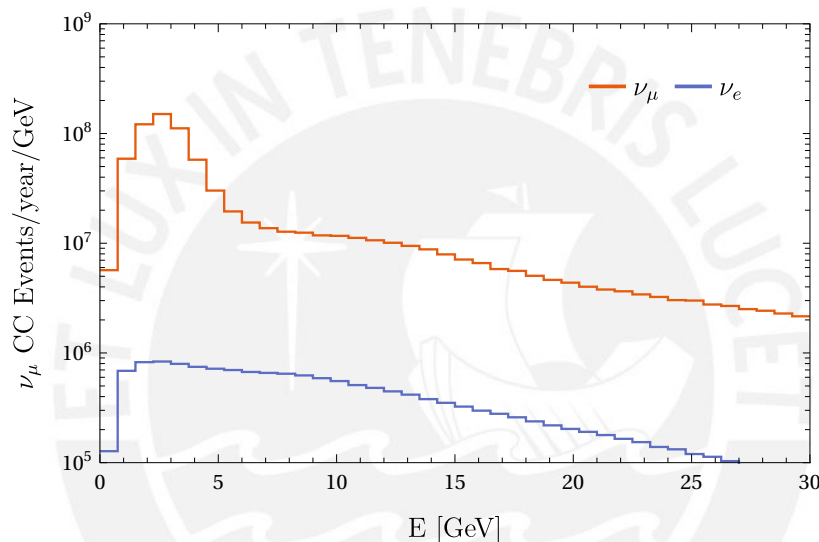
Fig. 3.16 Muon neutrino charged current events at ArgonCube in one year of operation in neutrino mode and on-axis position.

3.6 Heavy neutral lepton production at DUNE

In the last section, we discussed the production, flux and CC event rates of neutrinos at DUNE. In this section, we will explain how heavy neutral leptons can be produced at DUNE and the signals that they might leave in the near detector. In general, heavy neutral leptons can be produced in any decay that involves the production of an active neutrino. We will be interested in heavy neutral leptons produced in the decays of light and heaver parents discussed in previous sections. Table 3.8 shows the HNL production channels considered in this work, where we have included channels where the HNL is produced in a tau lepton decay. At DUNE energies, the direct production of tau leptons at the target is heavily suppressed, so we are only considering tau leptons that are produced in D meson decays. We also display

the maximum value allowed for the HNL mass in each channel. As we discussed in previous sections, the light mesons will dominate active neutrino production at DUNE; hence, they will also dominate HNL production for masses below the kaon mass, which is around 493 MeV. Above the kaon mass, only heavy particles such as D mesons and tau leptons will be kinematically allowed to decay into HNLs. However, due to the low production rate of the heavy parents, the production of HNLs with masses above the kaon mass will be heavily suppressed.

Table 3.8 Channels considered for the production of heavy neutral leptons. The maximum mass allowed for the heavy neutral lepton for each channel is shown. Charged conjugate channels were also considered.

	Channel	m_N [MeV]		Channel	m_N [MeV]
	Light parents				
$\mu^+ \to$	$e^+ \nu_e \bar{\nu}_\mu$	105.14	$K^+ \to$	$\mu^+ \nu_\mu$	387.81
$\pi^+ \to$	$\mu^+ \nu_\mu$	33.91		$\pi^0 e^+ \nu_e$	358.19
	$e^+ \nu_e$	139.06		$\pi^0 \mu^+ \nu_\mu$	253.04
$K_L^0 \to$	$\pi^\pm e^\mp \nu_e$	357.12		$e^+ \nu_e$	493.17
	$\pi^\pm \mu^\mp \nu_\mu$	252.38			
	Heavy parents				
$D_s^+ \to$	$e^+ \nu_e$	1967.83	$D^+ \to$	$e^+ \nu_e$	1869.07
	$\mu^+ \nu_\mu$	1862.68		$\mu^+ \nu_\mu$	1763.92
	$\tau^+ \nu_\tau$	191.48		$\tau^+ \nu_\tau$	92.72
	$\eta e^+ \nu_e$	1419.97		$K^0 e^+ \nu_e$	1371.46
	$\eta \mu^+ \nu_\mu$	1314.82		$K^0 \mu^+ \nu_\mu$	1266.31
	$\eta' e^+ \nu_e$	1010.05		$\bar{K}^{*0} e^+ \nu_e$	973.52
	$\eta' \mu^+ \nu_\mu$	904.90		$\bar{K}^{*0} \mu^+ \nu_\mu$	868.37
	$\phi e^+ \nu_e$	948.37	$\tau^+ \to$	$\pi^+ \bar{\nu}_\tau$	1637.29
	$\phi \mu^+ \nu_\mu$	843.22		$K^+ \bar{\nu}_\tau$	1283.16
$D^0 \to$	$K^- e^+ \nu_e$	1370.64		$K^{*+} \bar{\nu}_\tau$	881.31
	$K^- \mu^+ \nu_\mu$	1265.49		$\rho^+ \bar{\nu}_\tau$	1001.6
	$K^{*-} e^+ \nu_e$	968.77		$\pi^+ \pi^0 \bar{\nu}_\tau$	1502.31
	$K^{*-} \mu^+ \nu_\mu$	863.62		$\bar{\nu}_\tau e^- \bar{\nu}_e$	1776.35

In order to calculate the branching ratios for HNL production, we made use of the equations presented in Ref. [30] to calculate the rates of all the channels of Table 3.8. The production of HNLs via semileptonic decays involves hadronic currents that cannot be

calculated from first principles due to the non-perturbative nature of QCD at low energies. Therefore, the dynamics of these decays are modeled by form factors that represent the momentum distribution of the quarks inside the mesons and parametrize the momentum transfer between the hadronic current and the lepton pair [56]. For most of the semileptonic decays in Table 3.8, we used the form factors presented in [30]. The only exception was the decay $D_s^+ \to \phi l_\alpha^+ \nu_\alpha$, where we used the parametrizations of the form factors from [15].

All the decay rates were calculated in the software Wolfram Mathematica [47] with a script that takes as arguments the mass of the HNL and its mixing parameters and returns the corresponding decay rate. For simplicity, we have assumed that only one mixing parameter to active neutrinos $|U_{\alpha 4}|^2$ is non-zero at a time, although our scripts are capable of calculating the HNL production rates in the more complicated case in which two or three mixing parameters are different than zero.

We used the decay rates of the parents into heavy neutral leptons to calculate the branching ratios of the decay channels in Table 3.8. As a rule of thumb, the branching ratios of the HNL production channels will decrease with their mass and increase with their mixings to active neutrinos. However, this is not always true, since the mass dependence of the branching ratios is sometimes nontrivial. Figure 3.17 branching ratios of HNL production from light parents when $|U_{\mu 4}|^2 = 1$ and the other mixing are set to zero. We see that HNL production from pion decays peaks at low energies but then decays rapidly because it becomes kinematically suppressed. The same happens for the semileptonic decays of charged and neutral kaons, although the kinematic suppressions are less pronounced. An interesting scenario occurs for the leptonic decays of charged kaons, where there is a peak at around 260 MeV and then the branching ratio decreases due to kinematic effects.

Another aspect that one has to take into account in order to simulate the HNL flux at DUNE is the Dirac or Majorana nature of neutrinos. For Dirac neutrinos, there will be additional restrictions on the possible production channels of heavy neutral leptons. For instance, the decay $\pi^+ \to N \mu^+$ will produce heavy neutral leptons states N, but the charge conjugate decay $\pi^- \to \bar{N} \mu^-$ will produce the corresponding antiparticle, $\bar{N}$. In both cases, the decay rates of the pions are the same; therefore, if we have an equal amount of π^+ and π^- at DUNE, we will obtain the same number of N and $\bar{N}$. However, as we have seen in previous sections, this is not the case: at DUNE, more π^+ will be produced at the target in comparison to π^-, and the magnetic horns might add an extra effect that will favor even more the presence of π^+ in the beamline. Therefore, if the HNLs are Dirac, it is expected to have more N than $\bar{N}$ traveling along the decay pipe. This effect is important because these HNLs will have very different decay channels: the N states will decay into active neutrinos
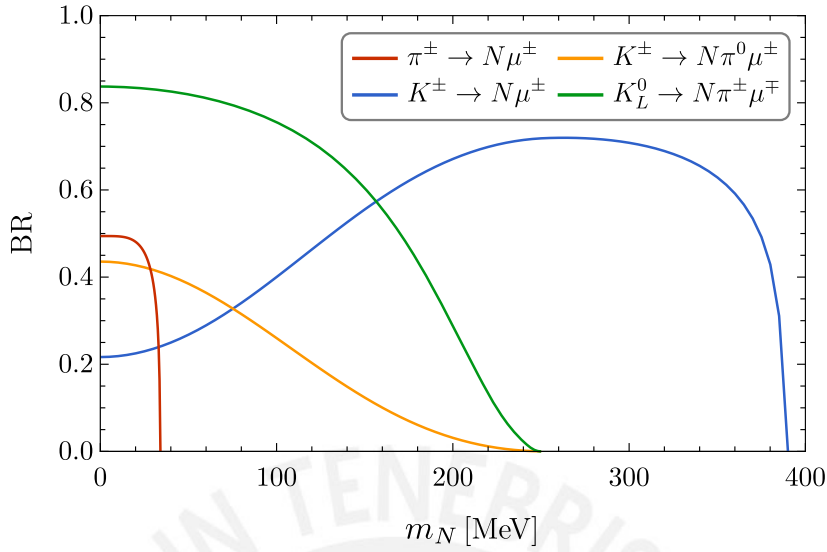
Fig. 3.17 Mass dependence of the branching ratios of HNL production from light parents for $|U_{\mu 4}|^2 = 1$.

and charged antileptons, while the $\bar{N}$ states will decay into active antineutrinos and charged leptons; hence if neutrinos are Dirac, more charged antileptons will be produced from the HNL decays in neutrino mode. On the other hand, if the neutrinos are Majorana, both decays $\pi^+ \to N\mu^+$ and $\pi^- \to N\mu^-$ are possible and have the same rate. Even if the number of π^+ and π^- mesons are different, both will produce the same N states, which will decay into charged leptons or antileptos with the same rate. Hence, if neutrinos are Majorana, the same amount of charged leptons and antileptons will be produced from HNL decays in neutrino mode. This distinction in the decay rates will be relevant when discussing the decays of HNLs inside one of the detectors of the DUNEND.

3.7   Heavy neutral lepton decay

After their production, the HNLs will decay into states that involve active neutrinos and other particles such as leptons and mesons. Table 3.9 shows the HNL decay channels considered in this work, where we also include the minimum mass of the HNL. Since we are only considering the case where only one mixing is nonzero at a time, one must keep in mind that, in practice, not all the decay channels displayed will be active at the same time. For instance, if only the muon mixing $|U|_{\mu 4}$ is nonzero, then only decays involving final muons or muon neutrinos are possible.

The Dirac or Majorana nature of the HNL is also important when one wants to simulate the decay of these particles. For instance, a Dirac HNL can decay via $N \to \mu^- \pi^+$, but a

Table 3.9 Heavy neutral lepton decay channels considered in this work. The minimum mass of the heavy neutral lepton for each channel is shown.

Channel	m_N [MeV]	Channel	m_N [MeV]
$\nu\nu\nu$	10^{-9}	$e^{\mp}\rho^{\pm}$	775.77
$\nu e^+ e^-$	1.02	$\nu\omega$	782.65
$\nu e^{\pm}\mu^{\mp}$	106.17	$\mu^{\mp}\rho^{\pm}$	880.92
$\nu\pi^0$	134.98	$e^{\mp}K^{*\pm}$	892.27
$e^{\mp}\pi^{\pm}$	140.08	$\nu\eta'$	957.78
$\nu\mu^+\mu^-$	211.32	$\mu^{\mp}K^{*\pm}$	997.42
$\mu^{\mp}\pi^{\pm}$	245.23	$\nu\phi$	1019.46
$e^{\mp}K^{\pm}$	494.19	$\nu e^{\pm}\tau^{\mp}$	1777.37
$\nu\eta$	547.86	$e^{\mp}D^{\pm}$	1870.09
$\mu^{\mp}K^{\pm}$	599.34	$\nu\mu^{\pm}\tau^{\mp}$	1882.52
$\nu\rho^0$	775.26	$\tau^{\mp}\pi^{\pm}$	1916.43

Majorana HNL can decay via both $N \to \mu^-\pi^+$ and $N \to \mu^+\pi^-$. Additionally, the decay rates of charged current mediated channels are the same for Dirac and Majorana, but rates of the neutral current mediated channels of Majorana HNls are twice as big as the rates of Dirac neutrinos. We took this distinction into account when calculating the rates of all the decays displayed in Table 3.9.

In order to simulate the decays of heavy neutral leptons, we made use of the formulas presented in [30] to design a script in the software Wolfram Mathematica that takes as an input the value of the HNL mass, its Dirac or Majorana nature and the value of the mixing parameter and returned the decay rates of all its channels. Figure 3.18 shows our results for the branching ratios of the decay channels considered in this work as a function of the HNL mass m_N for $|U_{\alpha 4}|^2 = 1$. In the plot of the charged current decays (top), we have added the rates of charged conjugate channels, so that the branching ratios are valid for Dirac and Majorana neutrinos. For masses below the electron mass, the dominant and only available decay for the HNLs is the NC-mediated channel $N \to \nu\nu\nu$. This channel is important because it is present along the entire mass range and also because it is the only direct way in which a HNL can decay into more than one neutrino, a phenomenon that might in principle increase by two the number of active neutrinos at DUNE. It is also important to note that a HNL can produce active neutrinos if it directly decays into active neutrinos, but it can also do it in an indirect way if its decay products eventually decay into active neutrinos.

After calculating the rates and branching ratios of all the aforementioned HNL decay channels, we designed a script in Wolfram Mathematica that creates a PYTHIA8 configu-
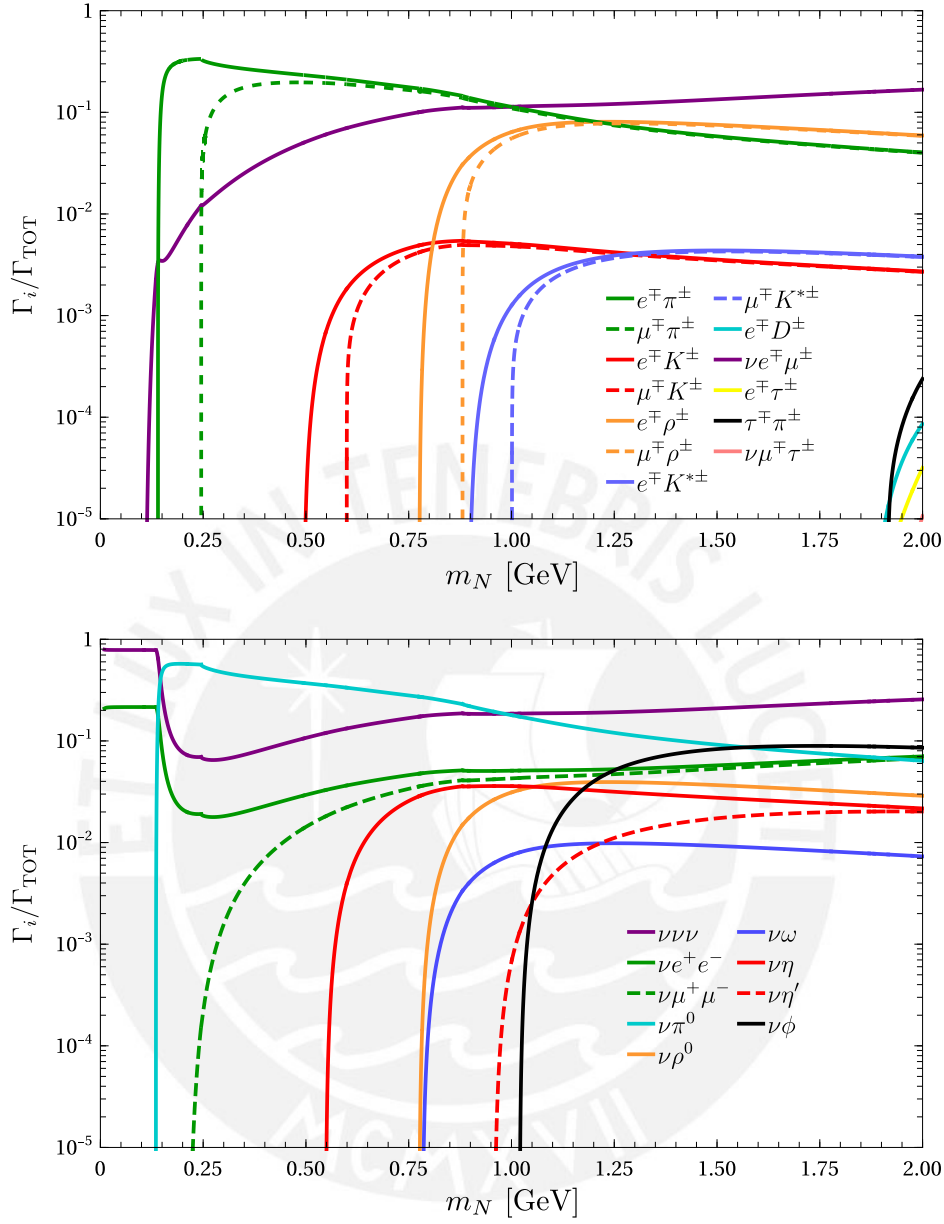
Fig. 3.18 Branching ratios of charged current (top) and neutral current (bottom) mediated decays of HNLs for $|U_{\alpha 4}|^2 = 1$.

ration file that contains all the information that PYTHIA needs to handle the kinematics of the HNL decay. This information includes the heavy neutral lepton mass, possible decay channels with their respective branching ratios and also a flag that tells PYTHIA that all the HNL decay products are also allowed to decay. We also set the HNL lifetime to zero in PYTHIA so that the HNL production and decay vertices are the same. We do this because, as we will see in the next sections, we are interested in handling the kinematics of the HNL propagation ourselves. We then let PYTHIA handle the HNL decay chain kinematics and

stored, on a event by event basis, what we considered the most relevant information of the HNL decay chain:

1. The mass, energy, momentum and production/decay vertex of the HNL.
2. The flavor, energy, momentum and production vertex of the active neutrinos directly produced in the HNL decay.
3. The flavor, energy, momentum and production vertex of the active neutrinos indirectly produced in the HNL decay, that is, neutrinos that are produced when the HNL decay products decay themselves into active neutrinos.

We used this information to calculate two different probabilities that are necessary to estimate the signals of the presence of heavy neutral leptons at DUNE.

3.7.1 Active neutrino flux from HNLs

All heavy neutral leptons produced at DUNE will be able to decay into active neutrinos. These neutrinos will be part of the DUNE neutrino flux and hence can, in principle, increase or decrease the number of CC event rates at the detectors of the DUNEND complex. In order to simulate the production and detection of these active neutrinos, we separated them into two categories. The first category contains all the active neutrinos that are produced directly in a HNL decay. Among these neutrinos, we are interested only in the ones that traverse one of the detectors of the DUNEND because they can produce CC interactions with the argon present inside them. Figure 3.19 shows schematically how an active neutrino produced directly in the HNL decay may hit ArgonCube and hence produce a CC event signal. If the HNL decays in position A, the active neutrino's trajectory will not cross ArgonCube. On the other hand, if the HNL decays between points B and C, the active neutrino will hit the detector. The points B and C can also be identified by the distances d_1 and d_2 along the HNL propagation line. We designed two functions in `C++` (one for ArgonCube and one for the MPD) that take as input the production vertex of the HNL, its momentum, the momentum of the active neutrino and the off-axis position of the detector and returns the distances d_1 and d_2. Again, we took into account all the possible ways in which the active neutrino might cross the detectors, which also include cases where the HNL traverses the detectors. With these distances at hand, we calculated the probability for the HNL to decay within the distances d_1 and d_2 with the formula

$$w(d_1, d_2) = \exp\left(-\frac{d_1}{v\gamma\tau_0}\right) - \exp\left(-\frac{d_2}{v\gamma\tau_0}\right), \qquad (3.3)$$

where v is the HNL's velocity, γ its Lorentz factor and τ_0 its proper lifetime. This probability was used to add an extra weight to the active neutrino when we calculated its contribution to the CC event rates at DUNEND.
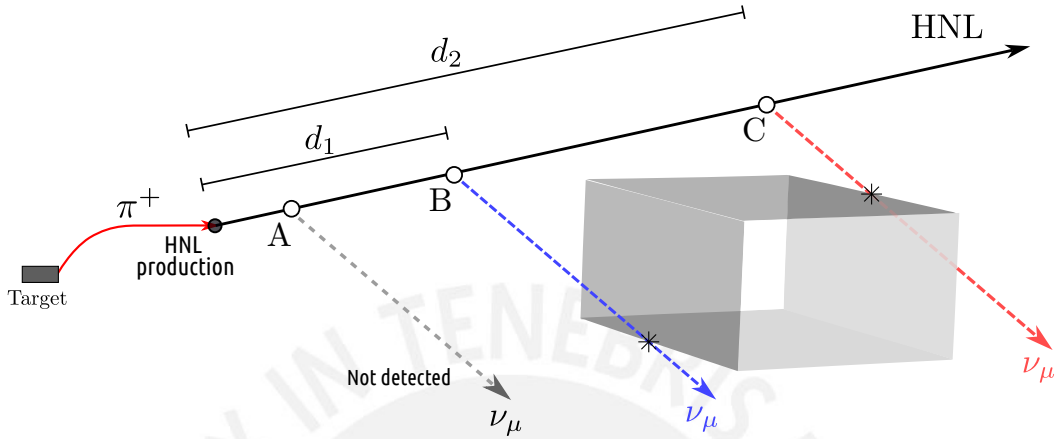
Fig. 3.19 Schematic representation of the distances d_1 and d_2 that a HNL must travel so that an active neutrino produced directly in its decay may hit ArgonCube.

The second category contains the active neutrinos that are produced indirectly in a HNL decay, that is, neutrinos that are produced by decays of other particles along the decay chain of the HNL. Figure 3.20 displays schematically how an active neutrino can be indirectly produced in a HNL decay for the case when a HNL decays into a charged pion. Here, we are assuming that the momentum and propagation distance of the pion and the momentum of the muon neutrino are fixed, so that the only free variable is the distance that the HNL propagates before decaying. The final trajectory of the muon neutrino depends on the decay position of the heavy neutral lepton. If the HNL decays at position A the muon neutrino cannot be detected. On the other hand, if the HNL decays between points B and C, then the final muon neutrino hits ArgonCube. We designed two a custom function, one for ArgonCube and one for the MPD, that take as inputs the production vertex of the HNL, the momentum and propagation distance of the active neutrino's parent, the momentum of the active neutrino and the off-axis position of the detector and returns the distances d_1 and d_2. Again, we considered all the possible ways in which these indirect neutrinos can be detected and tested our function against a randomly generated one. Finally, we used Eq. 3.3 to calculate the probability that the HNL decays between the distances d_1 and d_2 and used this to add an extra weight to all the active neutrinos produced indirectly in HNL decays.
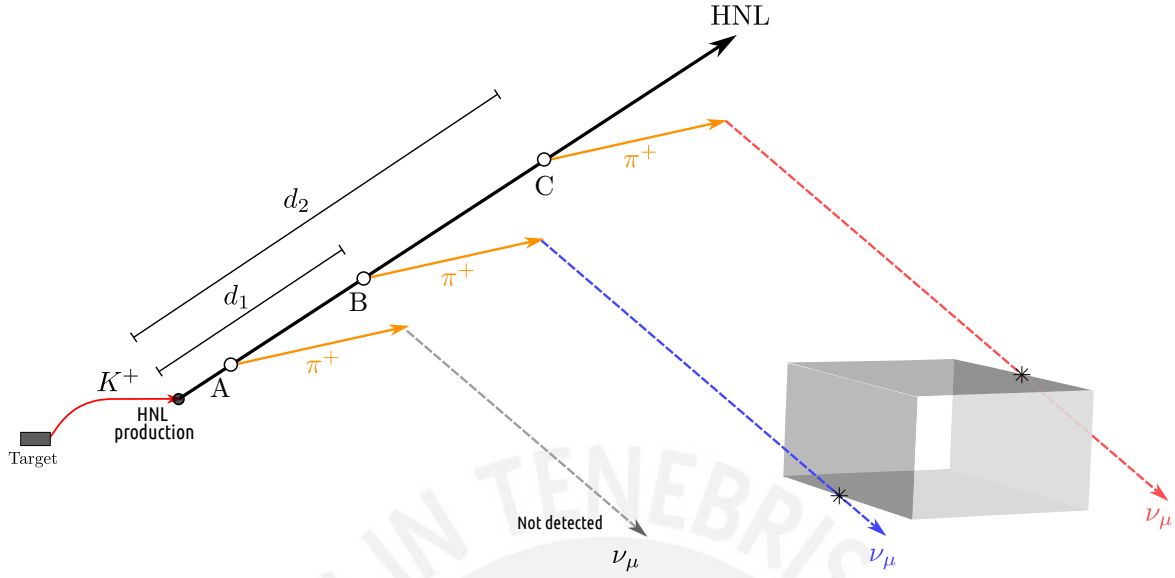
Fig. 3.20 Schematic representation of the distances d_1 and d_2 that a HNL must travel to leave an indirect neutrino signal at ArgonCube.

3.8 Neutrino flux in the presence of HNLs

In the previous sections, we discussed the production and decay of HNLs at DUNE. Since our work is mainly interested in charged-current neutrino events at DUNEND, we will discuss how the total active neutrino flux at DUNE is formed when HNLs are present.

Standard model active neutrinos These are the neutrinos that are produced in decay chains that do not involve the production of a HNL in any step. Examples of these neutrinos are the ones produced by decays of light and heavy parents produced at the target, such as $\pi^+ \to \mu^+ \nu_\mu$. When we turn off the production of heavy neutral leptons, these neutrinos compose the entirety of the DUNE neutrino flux. On the other hand, if we activate the production of HNLs at DUNE, their parents will have additional decay channels. For instance, if $|U_{\alpha 4}|^2 \neq 0$, the charged pions will have the additional decay channel $\pi^+ \to \mu^+ N$. This means that the branching ratio of the standard model decay $\pi^+ \to \mu^+ \nu_\mu$ will decrease, which will, in turn, decrease the number of standard model active neutrinos produced in pion decays. In general, whenever a HNL is produced, it is replacing the production of a standard model active neutrino. For this reason, the production of HNLs tends to decrease the number of standard model active neutrinos at DUNE. As we will discuss in the next sections, this effect can be quite relevant and directly affect the number of neutrino charged current events at the DUNEND complex.

Beyond standard model active neutrinos These are the neutrinos produced along the decay chain of a HNL. They can be produced directly in the HNL decay or indirectly when one of the decay products of the HNL decays on flight. Since each HNL produced is replacing the production of an otherwise active neutrino, these neutrinos coming from HNL decays can, in principle, make up for the initial loss of the active neutrino. However, since these BSM active neutrinos are produced later in the decay chain of the light and heavy parents, their angular distributions might be heavily affected, to the point that their trajectories do not intersect the detectors at the DUNEND complex. Still, some BSM neutrinos are expected to hit the detectors at the DUNEND, particularly when the HNL decays near the detector. Also, since, according to Table 3.9, the HNLs can decay into three neutrinos via $N \to \nu\nu\nu$, it might even be possible for these BSM neutrinos to increase the number of active neutrinos at DUNE. All the effects discussed in this section were included and our simulations and will be discussed in the next sections.
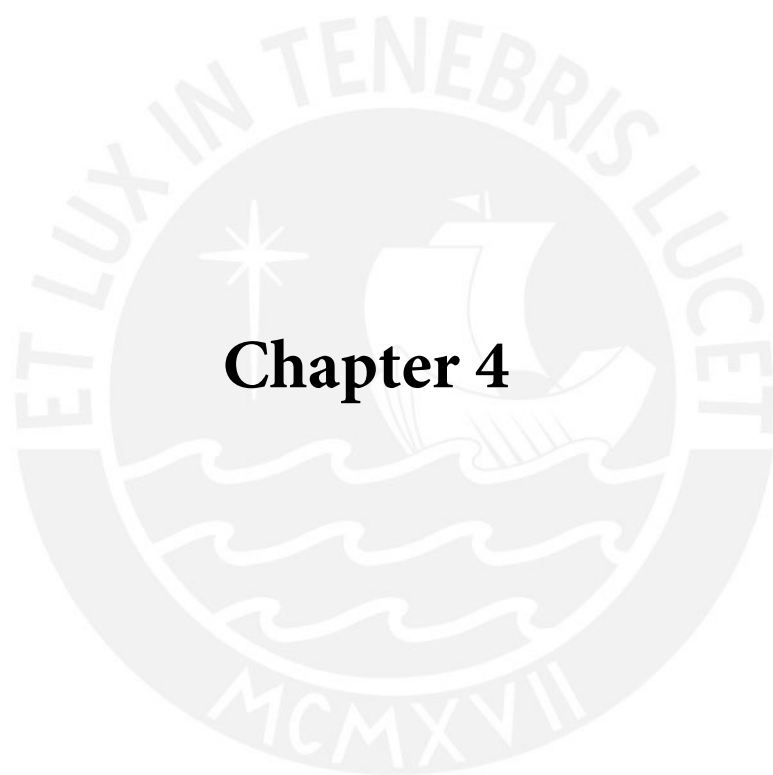
Chapter 4

Chapter 4

Results and discussion

4.1 HNL production and propagation

The rates at which heavy neutral leptons will be produced at DUNE will depend on several factors: the abundance of the HNL parents, the branching ratios of the decay channels of these parents into heavy neutral leptons, the HNL mass m_N and the value of the mixing parameter involved $|U_{\alpha 4}|^2$. Figure 4.1 illustrates our results for the total number of HNLs that will be produced each year at DUNE from each parent as a function of m_N when $|U_{\mu 4}|^2 = 10^{-4}$ and the other mixings are set to zero. The plot is valid for both Dirac and Majorana neutrinos. We see that pions have the largest contribution to the HNL flux at DUNE. After production from pions is kinematically forbidden, HNL production from kaons dominates up until the charged kaon mass. We also note that HNL production from heavy mesons is completely overshadowed by production from light parents and only becomes relevant above the kaon mass, where the only possible contribution comes from charmed mesons.

The HNLs produced at DUNE will propagate and then decay on flight. The position of the decay vertex of a particular HNL will depend on the momentum of its parent and the kinematics of its decay. There are three possible scenarios for the decay of a heavy neutral lepton at DUNE:

1. The HNL decays before DUNEND. In this case, the HNL will decay into active neutrinos and other particles, such as mesons or charged leptons. The active neutrinos produced by these HNLs might, in principle, hit the detectors at DUNEND, especially if the HNL decays close to ArgonCube. On the other hand, the charged particles or mesons produced in the HNL decay will not leave any sensible trace and, for all purposes, their information will be completely lost.
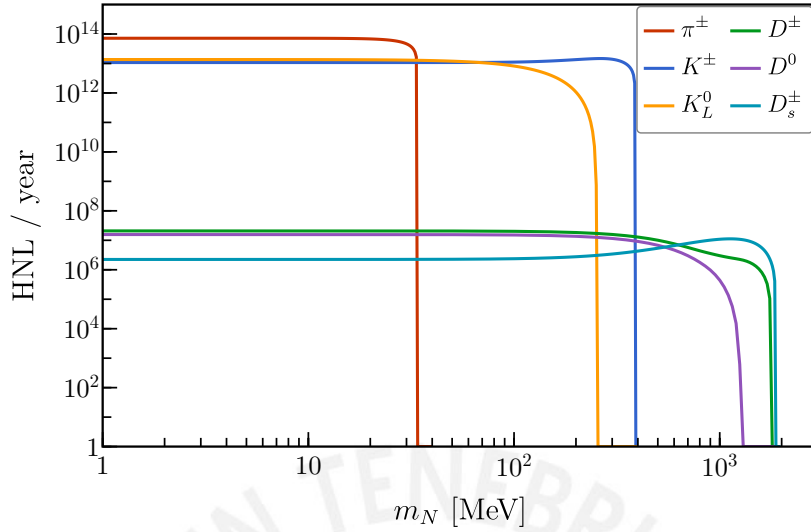
Fig. 4.1 Heavy Neutral leptons produced from mesons in one year in neutrino mode for $|U_{\mu 4}|^2 = 10^{-4}$.

2. The HNL decays inside DUNEND. In this second scenario, all the products of the HNL decay will propagate inside a detector of DUNEND. In particular, the charged particles will leave traces inside the time projection chambers of ArgonCube and the MPD, which will count as signals that might allow us to identify the energy and momentum of the HNL. This scenario has already been studied in Refs. [24, 27, 31] and used to estimate the future limits that DUNE will be able to set on the values of m_N and $|U_{\alpha 4}|^2$.

3. The HNL decays behind DUNEND. In this last scenario, all the HNL decay products are completely lost since none of them will propagate inside ArgonCube or the MPD. Since each HNL produced at DUNE is replacing the production of an active neutrino, when a HNL decays behind DUNEND and all its decay products are lost the DUNE flux at DUNEND is effectively losing one active neutrino. As we will discuss in the next sections, this effect can be used to indirectly study the production of HNLs at DUNE.

Figure 4.2 shows the average z position of the decay vertex of the HNLs produced at DUNE as a function of m_N for $|U_{\mu 4}|^2 = 10^{-4}$ and $|U_{\mu 4}|^2 = 10^{-1}$, where the position of the LArTPC of Argoncube is represented by a dotted line. We see that for very small masses, the HNLs decay on average behind the DUNEND complex, which means that each HNL counts as one less active neutrino in the DUNE flux. As the HNL mass increases, the average HNL decays closer to the detectors. For HNL masses around 255 MeV the HNLs decay near the DUNEND complex,
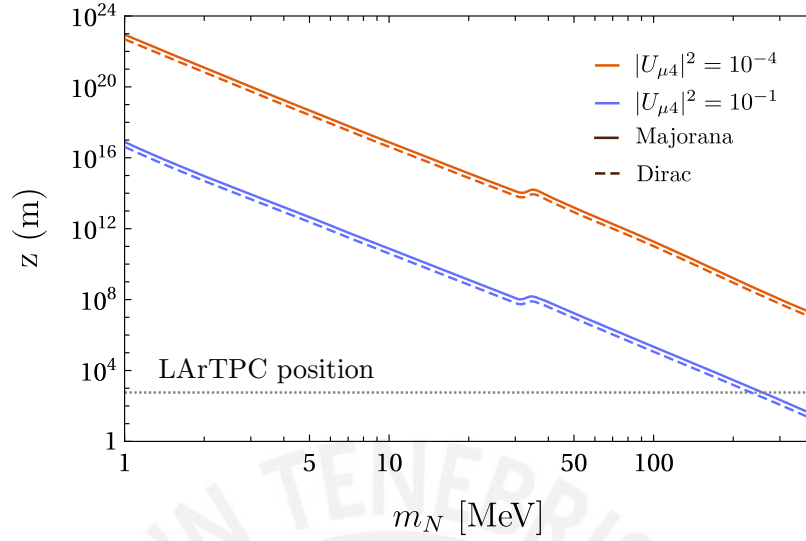
Fig. 4.2 Average HNL's decay positions projected along the Z axis for $|U_{\mu4}|^2 = 10^{-4}$ and $|U_{\mu4}|^2 = 10^{-1}$. The dotted line represents the position of the LArTPC.

4.2 Active neutrino flux

As seen in the previous chapter, the DUNE active neutrino flux will be affected by the presence of HNLs. In this section, we will study exactly how the active neutrino flux will change when HNLs are produced at DUNE. In the following, we will use a set of conventions to differentiate between different contributions to the total active neutrino flux at DUNE.

1. We will use the label $\Phi_{\nu_\alpha}^{\mathrm{SM}}$ for the neutrino flux of flavor α produced at DUNE when only Standard Model processes are allowed in the DUNE neutrino production chain. In other words, $\Phi_{\nu_\alpha}^{\mathrm{SM}}$ represents the neutrino flux prediction when there is no HNL production, which is equivalent to setting $|U_{\alpha4}|^2 = 0$. This is also the neutrino flux predicted by the DUNE collaboration.

2. If we activate the HNL production at DUNE, not every single parent decay will produce HNLs. Most parent decays will involve only SM processes with final-state active neutrinos. We will use the label $\phi_{\nu_\alpha}'^{\mathrm{SM}}$ for the neutrino flux of flavor α produced by the standard model decays of light or heavy parents when HNLs production is possible at DUNE. From this definition follows that if one deactivates the HNL production, the flux $\phi_{\nu_\alpha}'^{\mathrm{SM}}$ becomes $\Phi_{\nu_\alpha}^{\mathrm{SM}}$. It is important to note that, although the neutrinos in $\phi_{\nu_\alpha}'^{\mathrm{SM}}$ are produced only in SM processes, their production rates might still be indirectly affected by the existence of HNLs at DUNE. In particular, we will prove that, if HNLs are produced at DUNE, we have $\phi_{\nu_\alpha}'^{\mathrm{SM}} < \Phi_{\nu_\alpha}^{\mathrm{SM}}$.

3. Finally, whenever a HNL is produced at DUNE, it will propagate and decay on flight into several particles that might include active neutrinos. Additionally, the HNL decay products might also decay on flight and produce additional active neutrinos. We will use the label $\phi_{\nu_\alpha}'^{\text{BSM}}$ for the flux composed by all the active neutrinos produced along HNL decay chains. This flux will increase with the HNL production rate and will also depend heavily on the average decay vertex of the HNLs.

4.2.1 Standard Model neutrino Flux

In the previous chapter, we discussed how all the active neutrinos produced at DUNE will come from decays of particles that we have categorized into light or heavy parents. These parents have different branching ratios into neutrinos and hence each will produce active neutrinos at a different rate. These active neutrinos will always be produced at DUNE, independently of whether HNLs are produced or not. If we activate the HNL production at DUNE, then all these parents will gain some extra decay channels into HNLs, each with its corresponding branching ratio. Since the sum of all the branching ratios must be equal to 1, this implies that the branching ratios of these parents into SM active neutrinos must necessarily be reduced. This suppression in the production of SM active neutrinos due to HNLs will have an important effect on the active neutrino flux. In order to understand exactly how this process occurs, we will show how the SM parent meson's branching ratios are modified when HNLs are produced.

Let us start by defining the SM total decay rate of the pion (Γ_π^{SM})

$$\Gamma_\pi^{\text{SM}} = \Gamma^{\text{SM}}(\pi \to e\nu_e) + \Gamma^{\text{SM}}(\pi \to \mu\nu_\mu), \tag{4.1}$$

and the BSM decay rate of the pion with heavy neutral leptons (Γ_π^{BSM})

$$\Gamma_\pi^{\text{BSM}} = \Gamma^{\text{BSM}}(\pi \to e\nu_e) + \Gamma^{\text{BSM}}(\pi \to \mu\nu_\mu) + \Gamma(\pi \to NX). \tag{4.2}$$

If we use the approximation [44]

$$\nu_\alpha \approx \nu_\alpha^{\text{SM}} \left(1 - \frac{|U_{\alpha4}|^2}{2}\right) + U_{\alpha4}N. \tag{4.3}$$

we can rewrite the partial BSM decay rates of the pion as

$$\Gamma^{\text{BSM}}(\pi \to e\nu_e) \approx \Gamma^{\text{SM}}(\pi \to e\nu_e) \left(1 - \frac{|U_{e4}|^2}{2} \right), \tag{4.4}$$

$$\Gamma^{\text{BSM}}(\pi \to \mu\nu_\mu) \approx \Gamma^{\text{SM}}(\pi \to \mu\nu_\mu) \left(1 - \frac{|U_{\mu 4}|^2}{2} \right). \tag{4.5}$$

Therefore, the total BSM decay rate of the pion can be written as

$$\Gamma_\pi^{\text{BSM}} = \Gamma^{\text{BSM}}(\pi \to e\nu_e) + \Gamma^{\text{BSM}}(\pi \to \mu\nu_\mu) + \Gamma(\pi \to NX)$$

$$\approx \Gamma^{\text{SM}}(\pi \to e\nu_e) \left(1 - \frac{|U_{e4}|^2}{2} \right) + \Gamma^{\text{SM}}(\pi \to \mu\nu_\mu) \left(1 - \frac{|U_{\mu 4}|^2}{2} \right) + \Gamma(\pi \to NX). \tag{4.6}$$

We can see that the pion decay rates into SM neutrinos have been decreased by the presence of the HNL. This will affect the branching ratios of direct production of SM neutrinos from pion decays. For instance, the branching ratio of ν_μ production from pion decays in the presence of HNLs takes the form

$$\begin{aligned} \text{BR}^{\text{BSM}}(\pi \to \mu\nu_\mu) &= \frac{\Gamma^{\text{BSM}}(\pi \to \mu\nu_\mu)}{\Gamma_\pi^{\text{BSM}}} \\ &\approx \frac{\Gamma^{\text{SM}}(\pi \to \mu\nu_\mu) \left(1 - \frac{|U_{\mu 4}|^2}{2} \right)}{\Gamma_\pi^{\text{SM}}} \cdot \frac{\Gamma_\pi^{\text{SM}}}{\Gamma_\pi^{\text{BSM}}} \\ &\approx \frac{\Gamma^{\text{SM}}(\pi \to \mu\nu_\mu)}{\Gamma_\pi^{\text{SM}}} \cdot \frac{\Gamma_\pi^{\text{SM}}}{\Gamma_\pi^{\text{BSM}}} \left(1 - \frac{|U_{\mu 4}|^2}{2} \right) \\ &\approx \text{BR}^{\text{SM}}(\pi \to \mu\nu_\mu) \cdot \frac{\Gamma_\pi^{\text{SM}}}{\Gamma_\pi^{\text{BSM}}} \left(1 - \frac{|U_{\mu 4}|^2}{2} \right). \end{aligned} \tag{4.7}$$

A similar relation can be found for the branching ratio of ν_e production from pion decays:

$$\text{BR}^{\text{BSM}}(\pi \to e\nu_e) \approx \text{BR}^{\text{SM}}(\pi \to e\nu_e) \cdot \frac{\Gamma_\pi^{\text{SM}}}{\Gamma_\pi^{\text{BSM}}} \left(1 - \frac{|U_{e4}|^2}{2} \right), \tag{4.8}$$

where $\text{BR}^{\text{SM}}(\pi \to \mu(e)\nu_{\mu(e)})$ represents the branching ratio of $\nu_\mu(\nu_e)$ production from pion decays in the SM. We can see that the introduction of HNLs causes the production of either

muon or electron neutrinos from pions to be suppressed by the factor

$$\mathcal{K}_\pi^\alpha \left(m_N, |U_{\alpha 4}|^2 \right) = \frac{\Gamma_\pi^{\text{SM}}}{\Gamma_\pi^{\text{BSM}}} \left(1 - \frac{|U_{\alpha 4}|^2}{2} \right), \tag{4.9}$$

with $\alpha = e, \mu$. Fig. 4.3 illustrates the dependence on m_N of the factor $\mathcal{K}^\mu$ for several parents assuming $|U_{\mu 4}|^2 = 10^{-4}$. For each meson, the suppression factor acts only up to a maximum HNL mass due to kinematical constraints. The suppression factor will effectively decrease the number of SM active neutrinos produced at DUNE directly from parent decays. Although we can consider that these active neutrinos are always lost, it is still possible, at least in principle, that the HNL produced in the parent decay might itself decay into active neutrinos, hence making up for the initial neutrino loss. It could even be possible that the HNL decays into two or more active neutrinos; in this case, the number of active neutrinos at DUNE would increase. However, due to the kinematics involved in the HNL decay, most of the lost active neutrinos will not be recovered and the suppression factor will indeed decrease the active neutrino flux at DUNE. Although the effect is small, the high luminosity of DUNE makes it possible to use this effect to set limits on the heavy neutral leptons parameters.
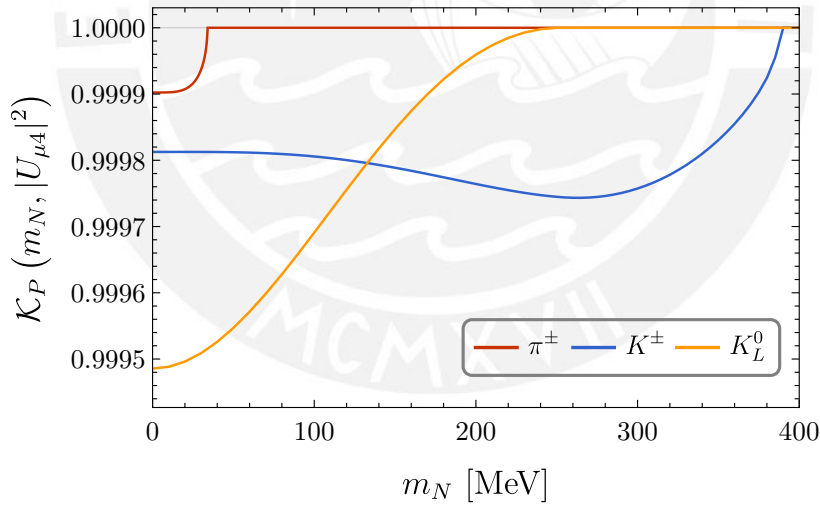
Fig. 4.3 Suppression factor $\mathcal{K}^\mu \left(m_N, |U_{\mu 4}|^2 = 10^{-4} \right)$ of muon neutrino production as a function of m_N.

Thus, each particle capable of producing active neutrinos can produce HNLs, leading to a suppression of the active neutrino flux. The latter happens even when only one mixing $|U_{\alpha 4}|^2$ is turned on. In fact, we can see from Eqs. (4.7) and (4.8) that, if we turn off either one of the mixings $|U_{\alpha 4}|^2$, the production of the active neutrinos of flavor α is still suppressed by the factor $\Gamma_\pi^{\text{SM}}/\Gamma_\pi^{\text{BSM}}$. As we will show further ahead, the reduction in the active neutrino flux

would imply the possibility that they do not reach the DUNEND, decreasing the number of expected CC events at this facility. Figure 4.4 shows the muon neutrino flux of SM neutrinos hitting ArgonCube for $|U_{\mu 4}|^2 = 10^{-4}$ and different values of m_N. We see that the number of SM active neutrinos reaching ArgonCube decreases whenever HNLs are produced. This phenomenon is produced by the suppression factor discussed above. The suppression on the SM neutrino flux is greater for lower values of m_N. In particular, we found that below around 10 MeV the SM neutrino flux is always reduced to the flux shown in Figure 4.4 for $m_N = 1$ MeV. This happens because for masses below 10 MeV the HNL production rates are virtually the same and hence the mass has no effect on the suppression factor.
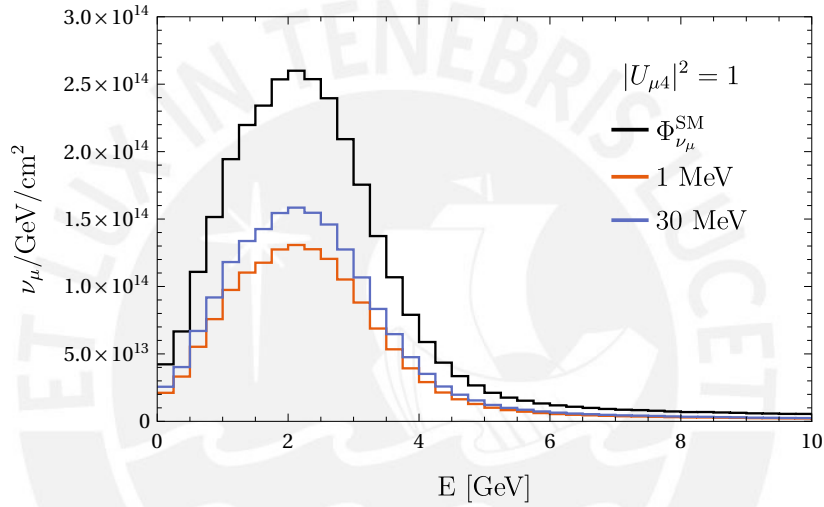
Fig. 4.4 Change in the SM muon neutrino flux at DUNE due to the presence of heavy neutral leptons for $|U_{\mu 4}|^2 = 1$ and different values of m_N.

The suppression of the production of SM active neutrinos will have a direct impact on the flux, which can in principle be measured at DUNE. We can roughly estimate the significance N_σ of the decrease of the SM muon neutrino flux as

$$N_\sigma = \frac{|\phi'^{\mathrm{SM}}_{\nu_\mu} - \Phi^{\mathrm{SM}}_{\nu_\mu}|}{\sqrt{\Phi^{\mathrm{SM}}_{\nu_\mu}}}, \tag{4.10}$$

where we are assuming the ideal case in which there are no systematic uncertainties in the flux. Figure 4.5 shows an estimate of the significance of the change in the SM neutrino flux due to the presence of HNLs for $|U_{\mu 4}|^2 = 10^{-4}$ and several values of m_N. We note that the statistical significance of the change in the SM flux is very large, reaching more than 1000σ for very small masses and energies around 3 MeV. Even for masses around 300 MeV, there

is a significant variation in SM flux at larger neutrino energies which can also be probed by DUNE.
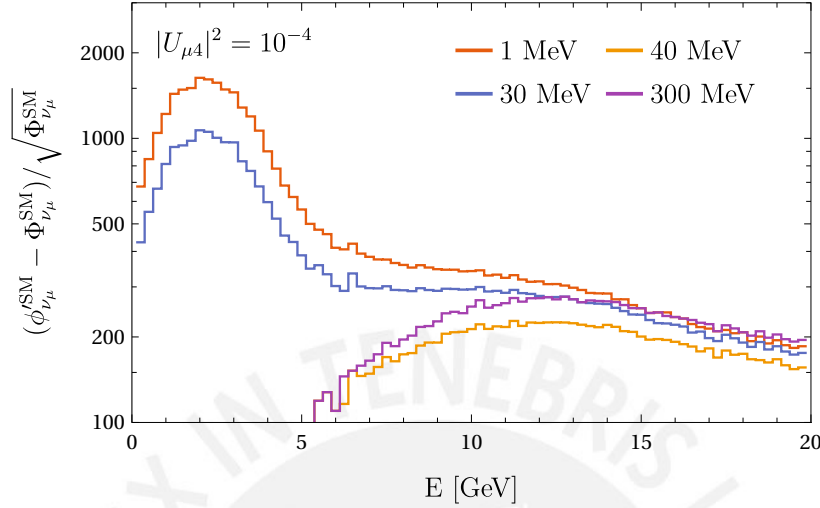
Fig. 4.5 Significance of the change of muon neutrino flux due to the presence of heavy neutral leptons for $|U_{\mu 4}|^2 = 1$ and no systematic uncertainties.

The suppression of the SM neutrinos also depends on the value of the mixing parameter involved. In principle, as the mixing increases, the change in the SM neutrino flux decreases as well. Figure 4.6 displays how the suppression of the active SM neutrino flux at DUNE changes with the value of the mixing parameter for $m_N = 1$. As expected, larger mixings produce larger suppression on the flux, which is reflected in fewer events. We will see that this dependence of the neutrino suppression on the mixing parameter can help us estimate the limits that DUNE will be able to set to the HNL parameters. We also show in Figure 4.7 the significance of the change in the SM neutrino flux for $m_N = 1$ MeV and some values of $|U_{\mu 4}|^2$ assuming the ideal case where there are no systematic uncertainties in the DUNE flux prediction. We see that for mixings close to 1 there is a very large significance in the decrease of the SM neutrino flux of more than $10^6 \sigma$. This effect implies that large mixings necessarily produce an equally large deficit of neutrinos produced from SM decays at DUNE. This deficit is of course ideal since systematic uncertainties will have an effect on it; however, it is a very strong indirect signal of the presence of heavy neutral leptons that can probe the presence of HNLs at DUNE.

Although the suppression of the SM neutrino flux is always present, there are some regions of the parameter space $(m_N, |U_{\mu 4}|^2)$ in which the effect is larger. In general, the suppression will be larger for lower masses, since this allows for a larger production of HNLs and also because the pion is the most abundant HNL parent at DUNE and it can only produce HNLs by muon mixing up to HNL masses of 33.91 MeV. In order to understand how the SM
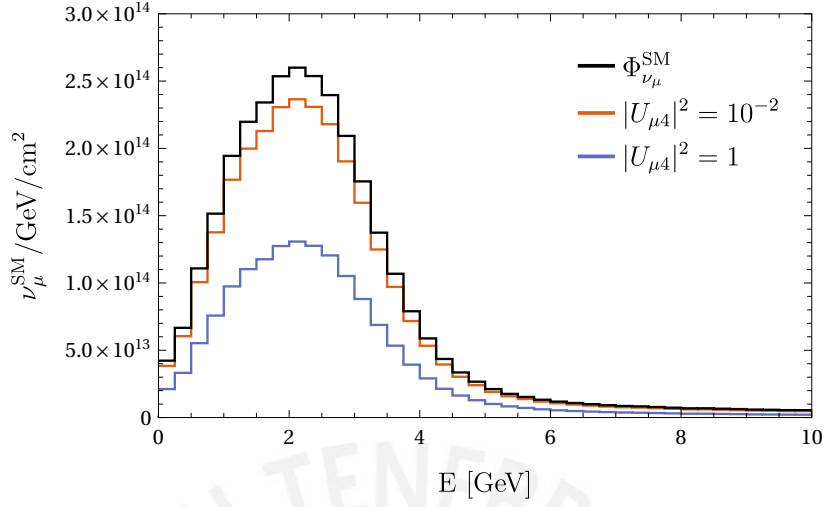
Fig. 4.6 Change in the SM muon neutrino flux at DUNE due to the presence of heavy neutral leptons for $m_N = 1$ MeV and some values of $|U_{\mu 4}|^2$.
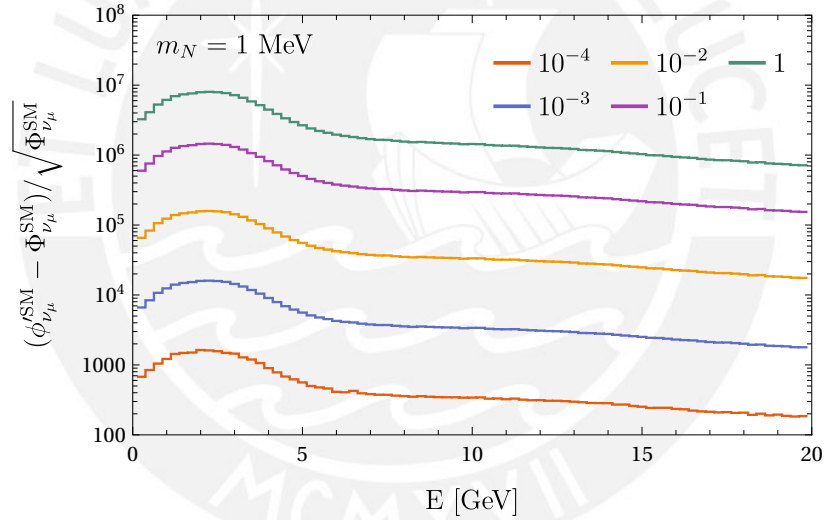
Fig. 4.7 Significance in the change of the SM muon neutrino flux due to the presence of heavy neutral leptons for $m_N = 1$ MeV and no systematic uncertainties.

neutrino suppression acts in the parameter space, we calculated the ratio between the SM muon neutrino flux with HNLs $\phi_{\nu_\mu}^{\prime\rm SM}$ and the full standard model prediction without HNLs $\Phi_{\nu_\mu}^{\rm SM}$ in two different regions. The first one contains HNL masses below 40 MeV and is shown in Figure 4.8. We see that for low masses and large mixings, the ratio $\phi_{\nu_\mu}^{\prime\rm SM}/\Phi_{\nu_\mu}^{\rm SM}$ is very small, reaching a minimum of 0.5, which means that there is a high suppression on the SM neutrino flux. This suppression decreases as the mass increases; particularly, the SM suppression almost seems to disappear above 30MeV, when HNL production from muon mixing with pions is kinematically forbidden. Figure 4.9 shows the same ratio for HNL

masses above 40 MeV. We note that the suppression of the SM neutrinos is always present, although much less pronounced since the smallest ratio is very close to 1. Finally, the deficit of SM neutrinos disappears around 400 MeV, when muon neutrino production from kaons is kinematically forbidden.
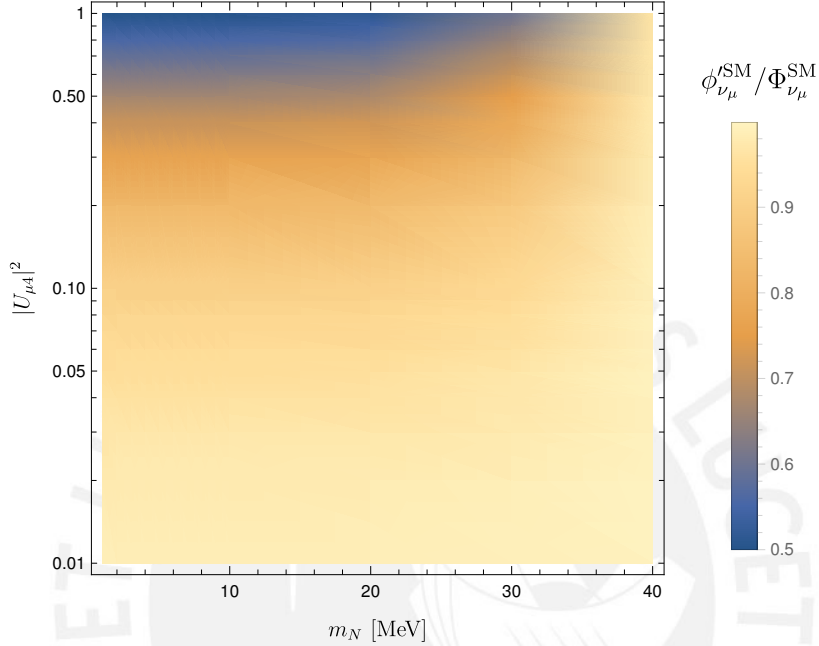
Fig. 4.8 Ratio $\phi_{\nu_\mu}'^{\mathrm{SM}}/\Phi_{\nu_\mu}^{\mathrm{SM}}$ along the parameter space for low values of m_N.

4.2.2   BSM neutrino flux at DUNE

Whenever a HNL decays it can produce leptons, mesons and also active neutrinos. These particles produced will also decay on flight and hence produce additional active neutrinos. We will refer as BSM active neutrinos to all neutrinos produced in HNL decays, whether directly in the HNL decay or indirectly in the decay of its products, and represent their flux by the label $\phi_{\nu_\alpha}'^{\mathrm{BSM}}$. These neutrinos are different from the SM neutrinos in the sense that they are only present when HNLs are produced; hence, they act as an indirect signal of the presence of HNLs in the decay chain of light and heavy parents. The BSM active neutrinos produced at DUNE will have a much lower production rate than the active neutrinos and their contribution is expected to be negligible to the total neutrino flux. Figure 4.10 shows a comparison between the full standard model neutrino flux prediction without HNLs $\Phi_{\nu_\mu}'^{\mathrm{SM}}$ and the BSM muon neutrinos flux $\phi_{\nu_\mu}'^{\mathrm{BSM}}$ for $m_N = 1$ Mev and some values of $|U_{\mu 4}|^2$. We see that the BSM neutrino flux is very small in comparison to the neutrino flux prediction of the DUNE collaboration. This implies that, if these BSM are present in the flux, they will
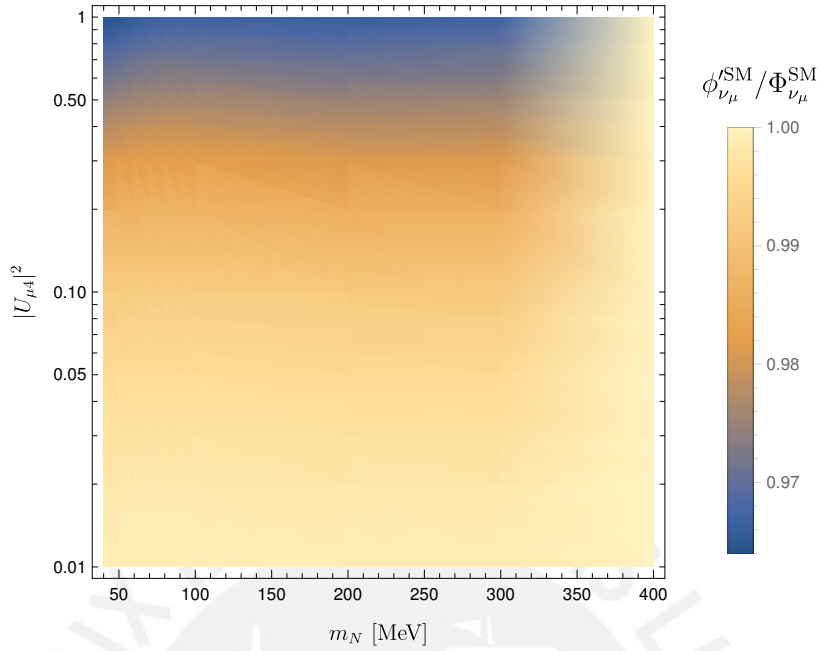
Fig. 4.9 Ratio $\phi'^{SM}_{\nu_\mu}/\Phi^{SM}_{\nu_\mu}$ along the parameter space for large values of m_N.

have a negligible contribution to the CC event rates at ArgonCube. This effect is amplified by the fact that the BSM neutrino flux decreases rapidly with energy, which in turn decreases even more the CC event rates from these neutrinos.
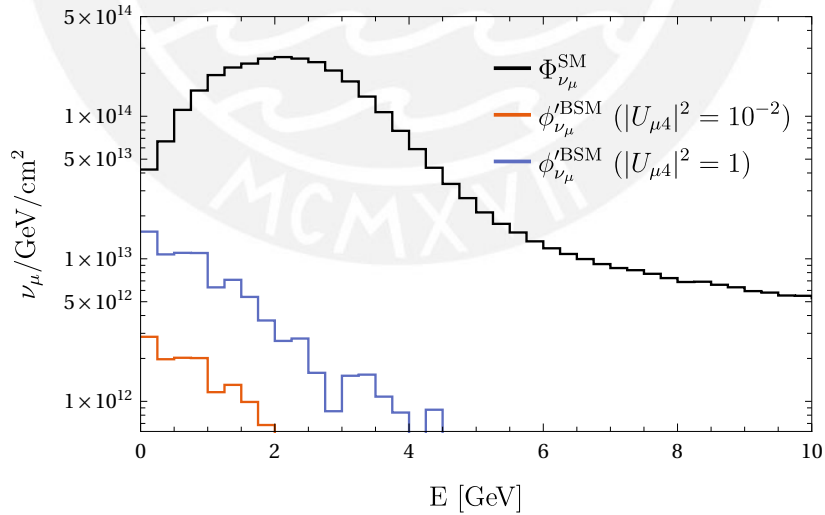
Fig. 4.10 BSM muon neutrino flux at DUNE for $m_N = 1$ MeV and some values of $|U_{\mu4}|^2$.

One can also compare the $\phi'^{BSM}_{\nu_\mu}$ neutrino flux with the $\phi'^{SM}_{\nu_\mu}$ discussed in the previous section. Figure 4.11 shows a comparison between $\Phi^{SM}_{\nu_\mu}$ and the fluxes $\phi'^{SM}_{\nu_\mu}$ and $\phi'^{BSM}_{\nu_\mu}$ for

$m_N = 1$ and $|U_{\mu 4}|^2 = 1$. We see that even in the extreme case of maximum mixing, the BSM neutrino flux is always smaller than the SM flux in the presence of HNLs when $m_N = 1$.
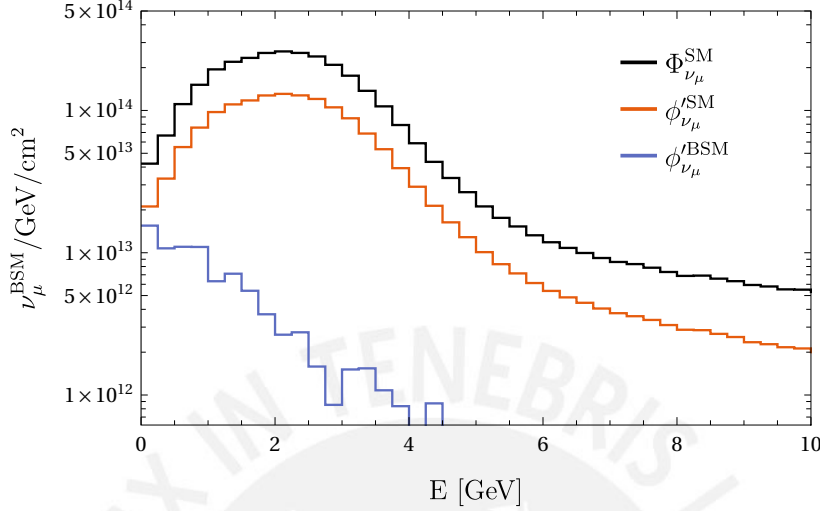
Fig. 4.11 SM and BSM muon neutrino flux at DUNE for $m_N = 1$ MeV and $|U_{\mu 4}|^2 = 1$.

The large difference between the BSM and SM fluxes when HNLs are produced is not present for all masses. There are some interesting regions of the parameter space $(m_N, |U_{\mu 4}|^2)$ where the BSM neutrino flux reaches a maximum and, although it is still smaller than the SM neutrino flux, it is not negligible. Figure 4.12 shows the ratio $\phi'^{\text{BSM}}_{\nu_\mu}/\phi'^{\text{SM}}_{\nu_\mu}$ over the parameter space $m_N, |U_{\mu 4}|^2$ for $m_N < 40$ MeV. The ratio in all cases is smaller than one and is below 0.06. This implies that, for low masses, the muon neutrino flux produced by the BSM neutrinos is less than 6% of the flux produced by the SM neutrinos. We also note that the ratio decreases rapidly with the mixing and that for $|U_{\mu 4}|^2 = 10^{-2}$ it is almost zero, meaning that contribution to the flux from BSM neutrinos is negligible. The regions of the parameter space above 40 MeV are displayed in Figure 4.13. In this case, the ratio is even smaller, always below 0.04, which means that the BSM neutrino flux is always less than 4% of the SM flux. However, we see that there is an increase in this ratio for masses between 200 and 300 MeV. Within this region, the BSM neutrino flux increases in comparison with the rest of the parameter space above 40 MeV. This sudden increase in the BSM flux at ArgonCube is produced mainly by the average decay position of the HNLs. As shown in Figure 4.2, the average z-decay positions for masses between 200 and 300 MeV are right before the position of the DUNEND. This means that most HNLs will decay close enough to ArgonCube that the BSM active neutrinos produced in their decays will have a high chance of hitting the detector. If we also take into account that, according to Figure 4.9, the SM neutrino flux is very close to the SM model prediction in this mass range, then the effect of the increase in the BSM neutrino flux becomes even more relevant, as we will see in the next sections.
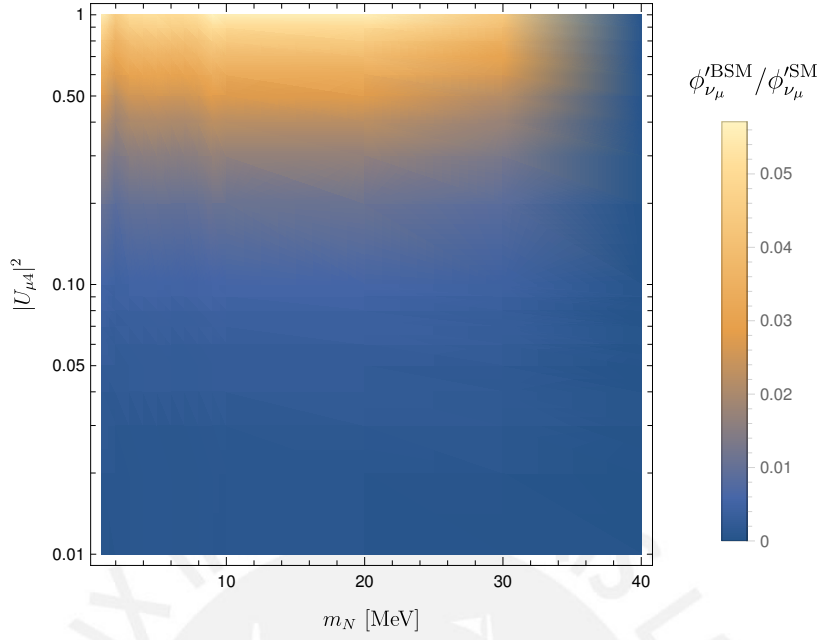
Fig. 4.12 Ratio $\phi_{\nu_\mu}'^{\text{BSM}}/\phi_{\nu_\mu}'^{\text{SM}}$ along the parameter space for $m_N < 40$ MeV.
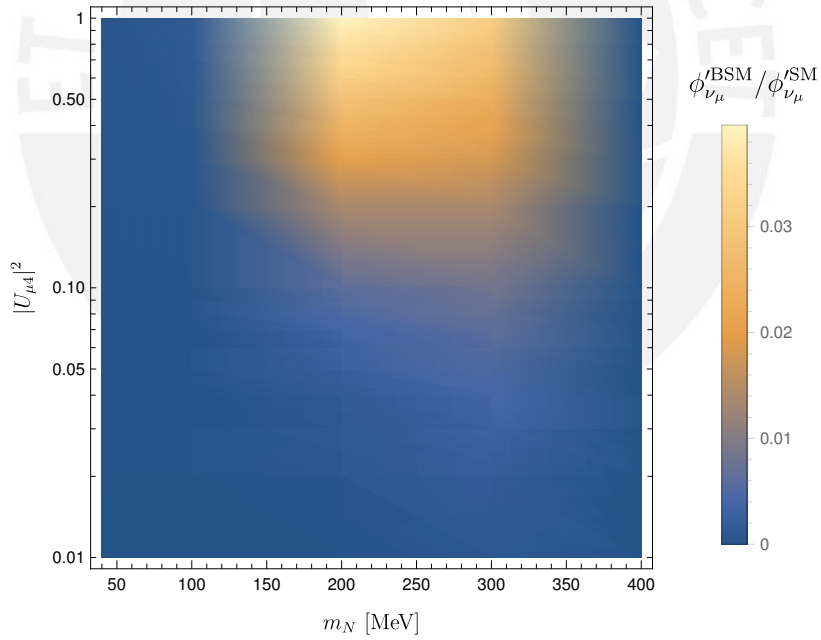
Fig. 4.13 Ratio $\phi_{\nu_\mu}'^{\text{BSM}}/\phi_{\nu_\mu}'^{\text{SM}}$ along the parameter space for $m_N > 40$ MeV.

4.2.3 Total active neutrino flux at DUNE

We have already seen that there are mainly two contributions to the total active neutrino flux at DUNE when HNLs are produced. The first contribution comes from the active neutrinos

produced in the standard model decays of light and heavy mesons, which we have referred to as SM active neutrinos. The second contribution to the active neutrino flux comes from the active neutrinos produced in decay channels that involve the production of a HNL. If we combine these two sources of active neutrinos, we get the total neutrino flux at DUNE, which we will label as ϕ'. Figure 4.14 displays the comparison between the SM, BSM and SM+BSM (Total) muon neutrino flux produced at DUNE for $m_N = 1$ MeV. We see that for low masses the total neutrino flux is completely dominated by the neutrinos that come from SM decays.
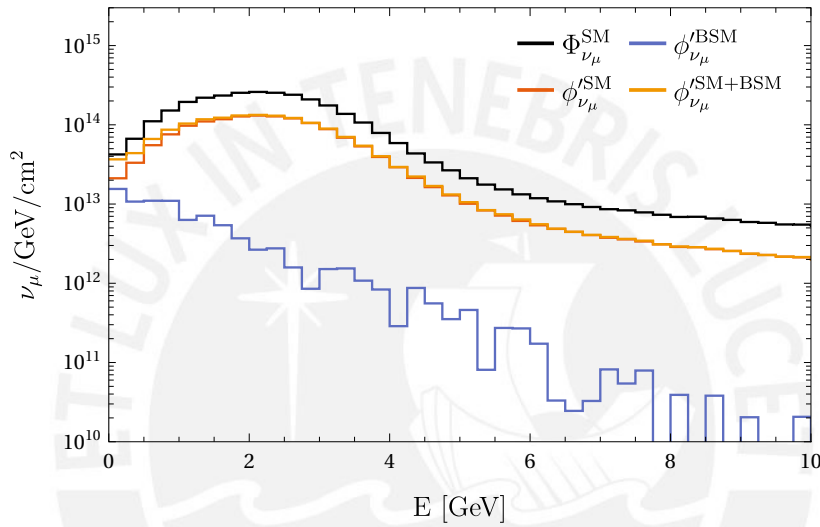
Fig. 4.14 Comparison between different contributions to the total active neutrino flux at DUNE.

As expected, the presence of HNLs will affect the total active neutrino flux at DUNE. The change in the active neutrino flux will depend on the values of the parameters $\left(m_N, |U_{\mu 4}|^2\right)$. Figure 4.15 (left) displays the estimated statistical significance of the change in the muon neutrino flux at DUNE due to the presence of HNLs form $|U_{\mu 4}|^2 = 10^{-4}$ and some HNL masses, assuming the ideal case where there are no systematic uncertainties. The most significant change in the neutrino flux happens for very low masses. As the mass increases, the effects of HNLs on the muon neutrino flux decrease, but are still relevant even for $m_N = 300$ MeV. Figure 4.15 (right) shows the ideal statistical significance of the change in the muon neutrino flux for $m_N = 1$ MeV and several values of $|U_{\mu 4}|^2$. As expected, the significance increases with the value of the mixing parameter squared.

The dependence of the statistical significance of the change in neutrino events on $\left(m_N, |U_{\mu 4}|^2\right)$ is also displayed in Figure 4.16 for a large region of the parameter space. We can see that for low masses (left) there is always a deficit in the active neutrino flux due to the suppression of the SM neutrino events. On the other hand, for masses above 40 MeV
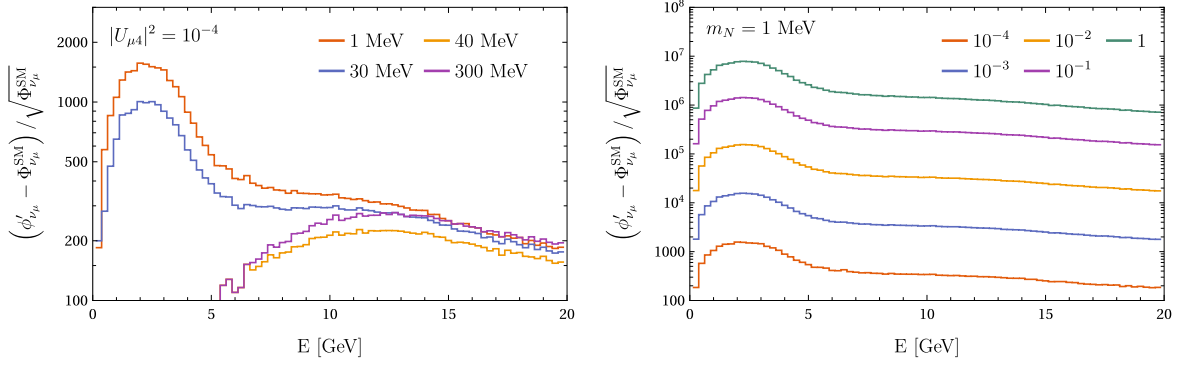
Fig. 4.15 Significance in the change of the muon neutrino flux at DUNE due to the presence of heavy neutral leptons for no systematic uncertainties.

(right), there is mostly a deficit of active neutrinos, except for a region around 200 MeV, where a clear excess of active neutrinos is present. This excess is produced by the BSM active neutrinos discussed in the previous sections and represents an indirect signal of the presence of HNLs at DUNE.
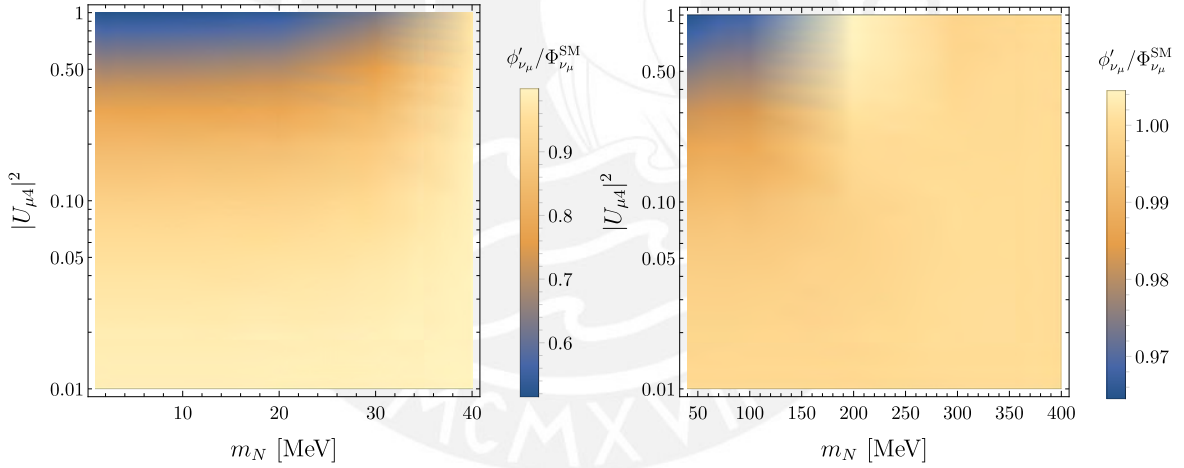
Fig. 4.16 Ideal statistical significance in the change of the muon neutrino flux due to heavy neutral leptons over the parameter space of $\left(m_N, |U_{\mu 4}|^2\right)$.

In order to better understand the excess of active neutrinos around 200 MeV, we have calculated the ratio $\left(\phi'_{\nu_\mu} - \Phi^{\mathrm{SM}}_{\nu_\mu}\right)/\Phi^{\mathrm{SM}}_{\nu_\mu}$ when $m_N = 200$ MeV for some values of $|U_{\mu 4}|^2$. The results are shown in Figure 4.17, where we can clearly see that, for high mixings, there is an excess in low-energy muon neutrinos reaching ArgonCube. This excess decreases with the mixing. In particular, for $|U_{\mu 4}|^2 = 10^{-2}$, the excess is almost negligible. This excess is produced by the HNL decays into three neutrinos that occur very close to the DUNEND Complex.
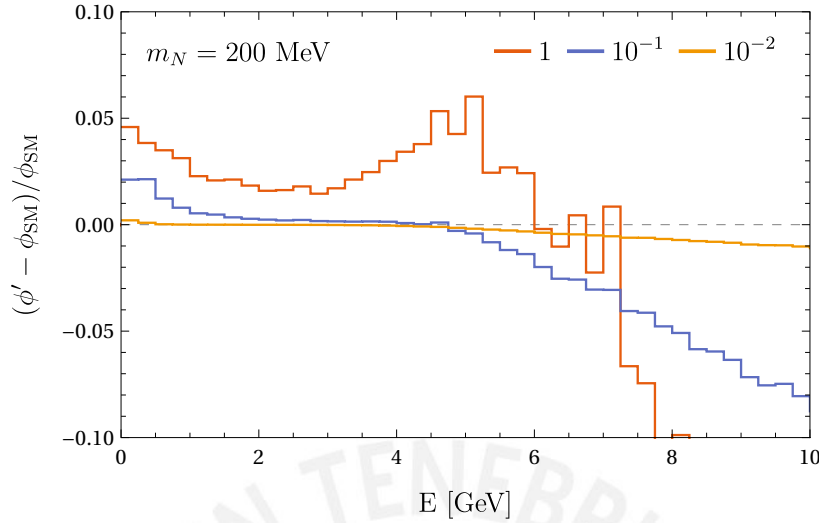
Fig. 4.17 Ideal statistical significance in the change of the muon neutrino flux at DUNE due to the presence of heavy neutral leptons for $m_N = 200$ MeV.

4.3 Neutrino Charged Current events at DUNE

The active neutrino flux studied in the previous section will hit the detectors at DUNEND and interact with the Argon atoms present in them. These interactions will be mediated by neutral current (NC) or charged current (CC) interactions. In this work, we are interested in the CC neutrino-Argon interactions since they produced charged particles that can be traced at DUNE. In order to estimate the CC neutrino event rates at DUNE, we convoluted the neutrino fluxes with GEANT4 inclusive cross sections. Figure 4.18 shows the CC event rates at ArgonCube in the presence of HNLs for some masses (left) and mixings (right). In both cases, the SM neutrino CC event rates are also shown in black. It is evident that the muon CC event rates decrease when HNLs are produced. This phenomenon is produced mainly by the decrease in the SM neutrino flux at DUNE. This deficit in CC event rates constitutes an indirect signal of the production of HNLs at DUNE.

Since the CC event rates constitute detectable signals at DUNE, we are interested in determining how significant these changes are. We will use the label $N_\alpha'^{CC}$ for the number of neutrino CC events of flavor α at ArgonCube when HNLs are produced and the label N_α^{CC} for the standard model prediction of the same rates. As a rule of thumb, we have $N_\alpha'^{CC} < N_\alpha^{CC}$, although in some particular cases this might change.
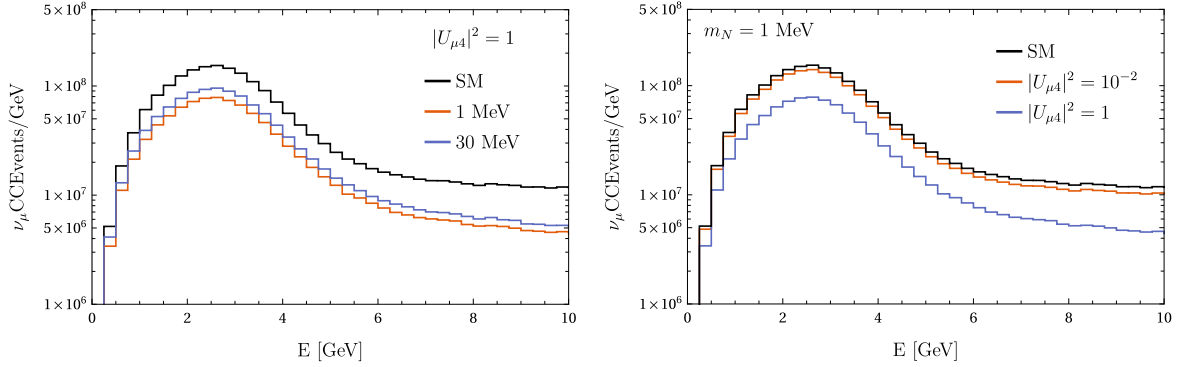
Fig. 4.18 CC muon neutrino event rates at ArgonCube when HNLs are produced for $|U_{\mu 4}|^2 = 1$ (left) and $m_N = 1$ (right).

Having defined labels for the relevant parameters, we will roughly estimate the significance of the change in the neutrino CC events of flavor α with the expression

$$N_\sigma = \frac{|N_\alpha'^{CC} - N_\alpha^{CC}|}{\sigma_{\text{tot}}} = \frac{|\Delta N_\alpha^{CC}|}{\sigma_{\text{tot}}}, \tag{4.11}$$

where σ_{tot} represents the total uncertainty in the flux. This total uncertainty can be estimated by the expression

$$\sigma_{\text{tot}} = \sqrt{\sigma_{stat}^2 + \sigma_{\text{sys}}^2}, \tag{4.12}$$

where σ_{stat} represents the statistical uncertainty in the CC event rates given by

$$\sigma_{stat} = \sqrt{N_\alpha^{CC}} \tag{4.13}$$

and σ_{sys} the total systematic uncertainty in the flux, which contains includes the uncertainties generated by the estimations of the production rates of the parents at the target and the values of the cross sections. In the ideal case where there are no systematic uncertainties, we have $\sigma_{\text{tot}} = \sigma_{\text{stat}} = \sqrt{N_\alpha^{CC}}$. Therefore, the ideal significance of the change in the CC event rates is given by

$$N_\sigma^{\text{ideal}} = \frac{|N_\alpha'^{CC} - N_\alpha^{CC}|}{\sqrt{N_\alpha^{CC}}}. \tag{4.14}$$

The ideal significance of the change in the CC event rates at DUNE is shown in Figure 4.19 for some values of m_N (left) and mixings (right), where the significance is calculated

in each bin separately. We see that the change of CC events in each bin can be very large, particularly for high values of the mixing parameter.
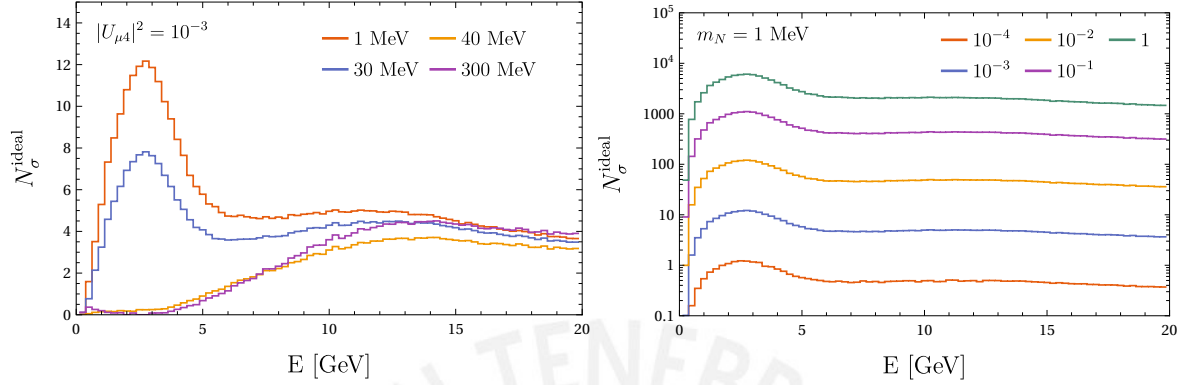
Fig. 4.19 Ideal statistical significance of the change in muon neutrino CC event rates at DUNE for fixed mixing (left) and HNL mass (right).

The significance of the change in CC events becomes more apparent when one calculates the total number of neutrino CC events at DUNE, which is obtained by integrating the neutrino CC event rates over the entire energy range. Figure 4.20 shows the ideal statistical significance of the total change in muon neutrino CC events at DUNE over a large region of the parameter space. We see that for low masses (left) the ideal statistical significance is always very large even for mixings $\mathcal{O}(10^{-2})$. Even for large masses (right), the ideal statistical significance is also large, meaning that DUNE might be sensitive to the variations in the neutrino CC events due to the presence of HNLs.
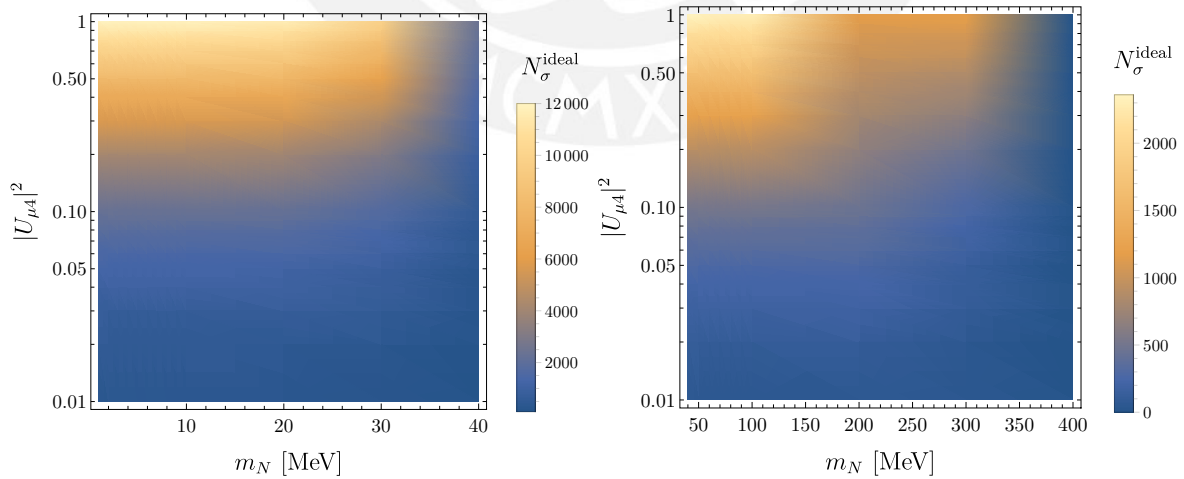
Fig. 4.20 Ideal statistical significance of the change of the total number CC muon neutrino events over a region of the parameter space $(m_N, |U_{\mu 4}|^2)$.

If one takes into account the possible systematic uncertainties in the prediction of the active neutrino flux at DUNE and the values of the neutrino cross sections, the statistical significance of the change in neutrino CC events at DUNE diminishes. As a first example, we will explore three different possibilities for the systematic error:

- $\sigma_{\text{sys}} = 0.01 \, N_\alpha^{\prime\text{CC}}$

  The systematic uncertainty is equal to 1% the neutrino CC events prediction.
- $\sigma_{\text{sys}} = 0.05 \, N_\alpha^{\prime\text{CC}}$

  The systematic uncertainty is equal to 5% of the neutrino CC events prediction.
- $\sigma_{\text{sys}} = 0.1 \, N_\alpha^{\prime\text{CC}}$

  The systematic uncertainty is equal to 10% of the neutrino CC events prediction.

The presence of statistical uncertainty will decrease the significance of the change in the neutrino CC events. This happens because the deficit produced by the presence of HNLs cannot be distinguished from a possible deficit in CC events due to systematic uncertainty. Therefore, as the systematic error increases, the significance of the change of CC events must decrease. Figure 4.21 shows how the significance of the change in total muon neutrino CC events decreases with the value of the statistical error. We note that the significance drops dramatically even for a 1% systematic uncertainty. This happens because the change in the CC events at DUNE is only an indirect consequence of the production of HNLs, making it a very subtle signal. Still, the effect is always present and we also must consider that Figure 4.21 is taking into account only the change in the muon neutrino CC events. If one also includes the change in electron neutrinos and the corresponding antiparticles in the calculation of the statistical significance, this effect grows larger, to the point that it can be used to test the presence of HNLs at DUNE, as we will see in the next sections.

Figure 4.22 shows how the dependence of the statistical significance of the total change in electron (left) and muon (right) neutrino CC events at DUNE in 10 years of operation (5 years neutrino mode and 5 years antineutrino mode) on the value of m_N for a 1% systematic error and some mixing parameters. For the electron neutrinos, the ideal statistical significance reaches a maximum at around 30 MeV and then decreases. In the case of muon neutrinos, the statistical significance always decreases, with a steep decrease at around 30 MeV. The threshold $m_N = 30$ MeV is related to the maximum HNL mass that can be produced in pion decays. The sudden increase in electron neutrino CC events significance happens because, after around 30 MeV, the neutrinos are produced mostly in kaon decays, which has decay channels into electron neutrinos with large branching ratios, as opposed to the pions, which mainly decay into muon neutrinos.

As we have already seen, the larger the systematic uncertainty, the lower the statistical significance of the change in the neutrino CC events at DUNE. Figure 4.24 shows the statisti-
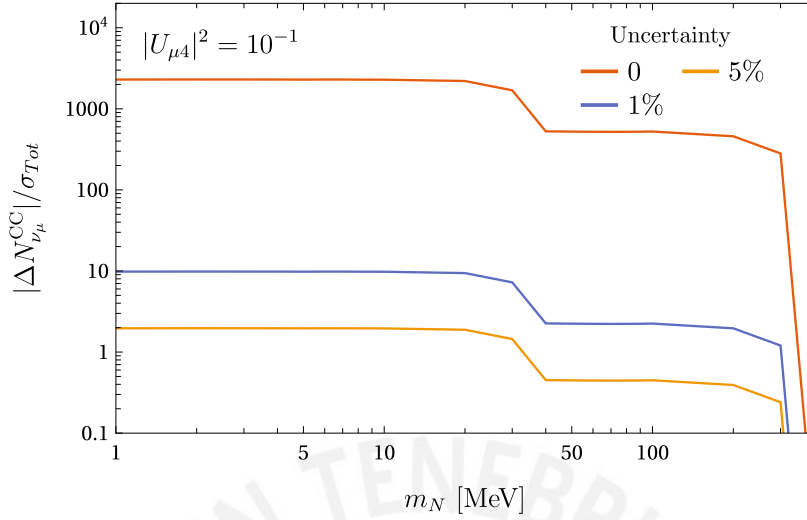
Fig. 4.21 Significance of the change in the total muon neutrino CC events for 10 years of operation for some systematic uncertainties.
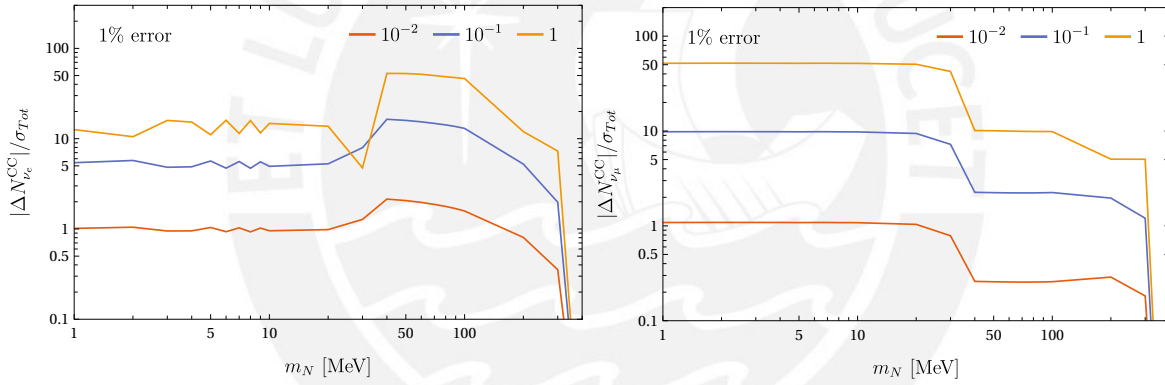
Fig. 4.22 Significance of the change in the total electron (left) and muon (right) neutrino CC events at DUNE for a 1% uncertainty and 10 years of operation.

cal significance of the change in muon neutrino CC events at DUNE for 10 years of operation for masses below 40 MeV and several systematic uncertainties. We can clearly see the effect that the systematic uncertainty has on the significance of this indirect signal of HNLs.

The ideal significance of variation of the total electron neutrino CC events at DUNE due to HNLs has a very interesting behavior for large mixings. Figure 4.23 shows the ratio $\Delta N_e^{CC}/\sigma_{\text{tot}}$ as a function of the HNL mass for mixings close to 1. Note that in this plot we are not taking the absolute value of ΔN_e^{CC}, so we can distinguish when we have an excess ($\Delta N_e^{CC} > 0$) or deficit ($\Delta N_e^{CC} < 0$) of CC events. We see that for a 0% systematic error (left) and $|U_{\mu 4}|^2 = 1$ there is actually a very significant excess of CC events for masses below 30

MeV. Even for a 1% systematic error (right) the excess of electron neutrino events is also present.
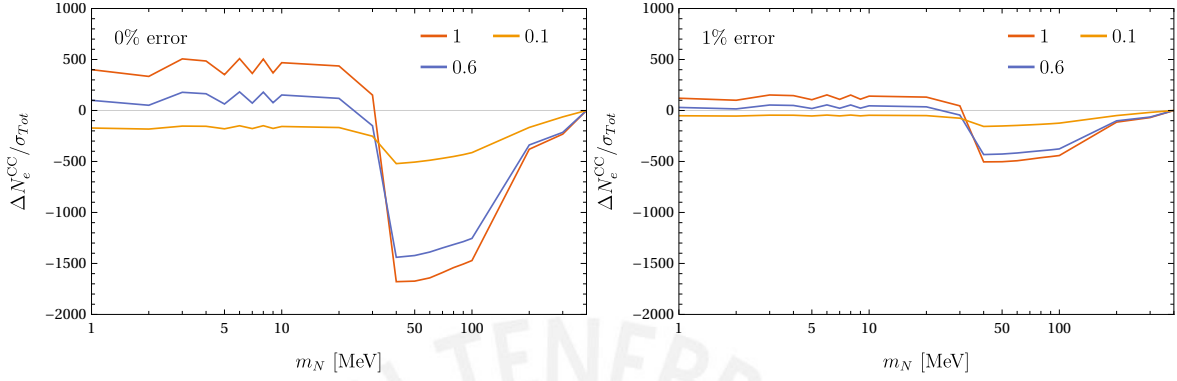
Fig. 4.23 Significance of the change in the total electron neutrino CC events at DUNE for a 0% (left) and 1% (right) uncertainty and 10 years of operation.

4.4   Sensitivity of DUNE to HNLs from CC events deficit

In the previous section, we studied how the neutrino charged current (CC) events at DUNE are affected by the production of heavy neutral leptons. In this section, we will study the significance of these event rates and use them to estimate the sensitivity of DUNE to heavy neutral leptons.

4.4.1   Statistical formulas

The experimental sensitivity for a given parameter Θ (or set of parameters) at some confidence level is computed as the following difference:

$$\Delta\chi^2 = \chi^2(\Theta) - \chi^2_{\min}, \tag{4.15}$$

where $\chi^2_{\min} = \chi^2(\Theta = 0)$ represents the null hypothesis and it is usually taken as zero. The Gaussian definition of the χ^2 is:

$$\chi^2(\Theta) = \sum_{i=1}^{nbins} \frac{\left(N^i_{\text{true}} - N^i_{exp}(\Theta)\right)^2}{N^i_{\text{true}}}. \tag{4.16}$$

Since there is no data when the sensitivity is estimated, the role of the number of observed events for the ith bin, N^i_{obs}, is taken by the so-called "true" number of events for the ith bin,
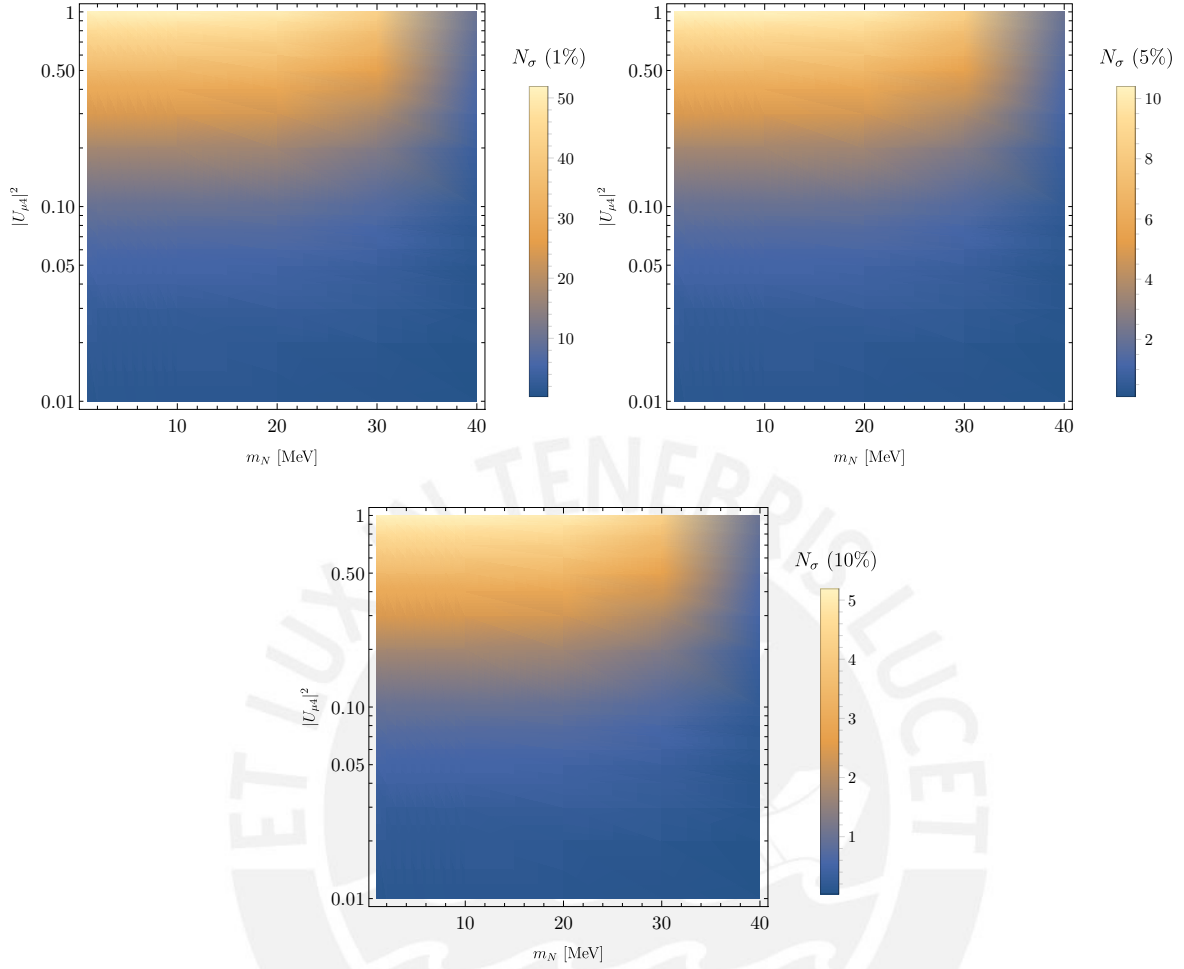
Fig. 4.24 Significance of the change of the total number muon neutrino CC events over the parameter space $(m_N, |U_{\mu 4}|^2)$ for several systematic uncertainties: 1% (top left), 5% (top right) and 10% (bottom).

N^i_{true}, which are compared with the expectation or test hypothesis $N^i_{\text{exp}}(\Theta)$. The Poissonian definition of the χ^2 is [26]:

$$\chi^2(\Theta) = 2\sum_i \left[N^i_{\text{exp}}(\Theta) - N^i_{\text{true}} + N^i_{\text{true}} \ln\left(\frac{N^i_{\text{true}}}{N^i_{\text{exp}}(\Theta)} \right) \right] \qquad (4.17)$$

In order to estimate the future sensitivity of DUNE to HNLs due to the deficit of neutrino CC events, we have to consider that the predictions of our simulations carry systematic uncertainties related to the distributions of hadron production at the DUNE target, the neutrino CC cross section uncertainties, among others. We will incorporate these uncertainties in our calculations by assuming an overall normalization uncertainty in each bin of our spectra,

which, in practice, means that the value of the event rates in each bin is not completely known and can fluctuate by a certain amount. This normalization uncertainty will be defined by the variable σ_a. We will consider the values $\sigma_a = 0.05$, 0.1 and 0.2, which are equivalent to overall normalization uncertainties of 5%, 10% and 20%, respectively, in the CC events of each bin. Also, for simplicity, we will consider that the value of σ_a in each bin is the same. This systematic uncertainty can be accounted for by introducing a set of nuisance parameters a_i that must be profiled when calculating the value of χ^2. In this context, profiling means that for each set of parameters Θ one must calculate the values of a_i that minimize the χ^2. The introduction of the non-oscillation systematical uncertainties into the χ^2, such as the modeling of either the neutrino flux or the neutrino cross sections, goes through adding nuisance parameters. If we consider that the content of each bin has an associated systematic uncertainty, this is achieved by making the substitution:

$$N_{\exp}^i (\Theta) \mapsto N_{\exp}^i (\Theta) = (1+a_i) N_{exp}^i(\Theta) \tag{4.18}$$

and adding the following term to the χ^2 :

$$\sum_{i=1}^{\text{nbins}} \frac{a_i^2}{\sigma_i^2}, \tag{4.19}$$

where the value of σ_i defines the estimated uncertainty of the i-th bin. If we combine equations (4.16), (4.18) and (4.19) we obtain

$$\chi^2(\Theta, a_i) = \sum_{i=1}^{\text{nbins}} \frac{a_i^2}{\sigma_i^2} + \sum_{i=1}^{\text{nbins}} \left(\frac{(1+a_i) N_i^{exp}(\Theta) - N_i^{\text{true}}}{\sqrt{N_i^{\text{true}} + \left(\sigma_i N_i^{\text{true}}\right)^2}} \right)^2. \tag{4.20}$$

In our case, we have $\Theta = (m_N, |U_{\alpha 4}|^2)$ because the neutrino flux will depend on the HNL mass and the value of the active mixing parameter. Also, we will compare the spectra of the neutrino CC events with and without HNLs, so that N_i^{exp} represents the CC events in the i-th bin with HNLs and N_i^{true} the CC events in the same bin without HNLs. Additionally, we are including an overall normalization uncertainty that affects all neutrino flavors equally. We estimate the sensitivity of DUNE to $(m_N, |U_{\alpha 4}|^2)$ through the following χ^2

$$\chi^2 = \frac{a^2}{\sigma_a^2} + \sum_{\nu_e, \nu_\mu, \bar{\nu}_e, \bar{\nu}_\mu} \left[\sum_{i=1}^{\text{nbin}} \frac{a_i^2}{\sigma_a^2} + \sum_{i=1}^{\text{nbin}} \left(\frac{N_i^{\text{SM}} - N_i^{\text{BSM}}(1+a+a_i)}{\sqrt{N_i^{\text{SM}}}} \right)^2 \right], \tag{4.21}$$

where N_i^{BSM} represents the neutrino CC events in the i-th bin when HNLs are produced and N_i^{SM} the DUNE prediction of CC events in i-th bin according to the Standard Model. The nuisance parameters a and a_i encompass the normalization uncertainties and allow for the values of N_i^{BSM} to fluctuate; these parameters are always profiled in the calculation of the χ^2. We must note that the fact of combining all the neutrino flavors in our definition of χ^2 is fundamental for improving the sensitivity of our results. The tau neutrinos are not considered since their contributions to the χ^2 are negligible.

The deficit of neutrino CC events at DUNE is an indirect signal of HNLs. Therefore, in the case that no significant deficit is found, the absence of this deficit can be used to set limits on the values of the parameters $(m_N, |U_{\alpha 4}|^2)$ with a particular confidence level. We calculated the value of χ^2 in the parameter space $10^{-6} \text{ MeV} < m_N < 10^7 \text{ MeV}$ and $10^{-12} < |U_{\alpha 4}|^2 < 1$ for $\alpha = e, \mu$ and $\sigma_a = 0.5, 0.1, 0.2$ and then used these values to estimate the limits that DUNE might be able to set to the parameters $(m_N, |U_{\alpha 4}|^2)$ at 90% confidence level.

4.4.2 Analysis of χ^2 in the parameter space of $\left(m_N, |U_{\alpha 4}|^2\right)$

In the previous section, we defined the formula (4.21) that we will use in our work to estimate the sensitivity of DUNE to heavy neutral leptons. In this section, we will show some results for muon mixing considering 10 years of operation (5 in neutrino and 5 in antineutrino mode). As an example, figure 4.25 shows the dependence of χ^2 on $|U_{\mu 4}|^2$ when we set $m_N = 1$ MeV and consider the ideal case of no systematic uncertainties $\sigma_a = 0$. As expected, we see that the value of χ^2 becomes very large when the value of the mixing increases. For comparison,
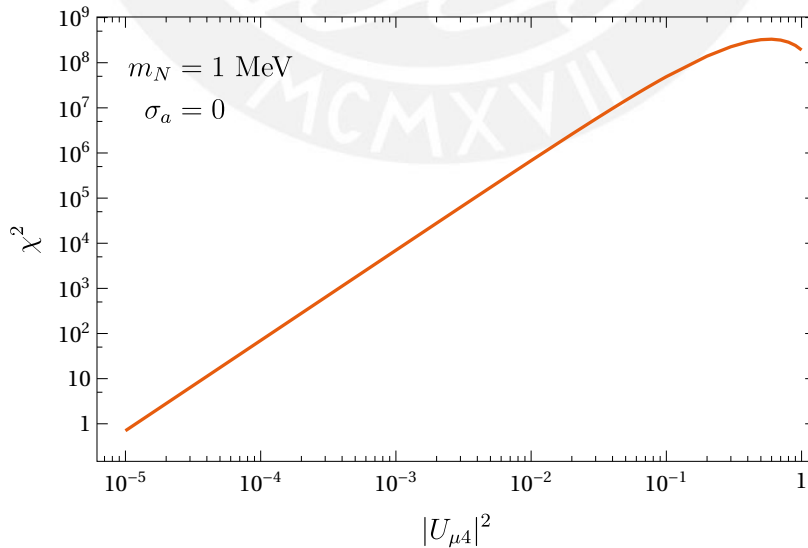
Fig. 4.25 Dependence of χ^2 on $|U_{\mu 4}|^2$ for $m_N = 1$ MeV and the ideal case $\sigma_a = 0$.

figure 4.26 shows the dependence of χ^2 on $|U_{\mu4}|^2$ when we set $m_N = 1$ MeV and consider the conservative case $\sigma_a = 0.2$, which is equivalent to a 20% uncertainty in the overall number of neutrino CC events at DUNEND. We see that the value of σ_a has a considerable effect on the values of χ^2. For instance, values of $\chi^2 > 1$ are only achievable when $|U_{\mu4}|^2 > 10^{-2}$. This implies that, for a 20% uncertainty, DUNE will only be sensitive to large values of the mixing parameter when $m_N = 1$MeV. We can conduct a similar analysis if we set the value
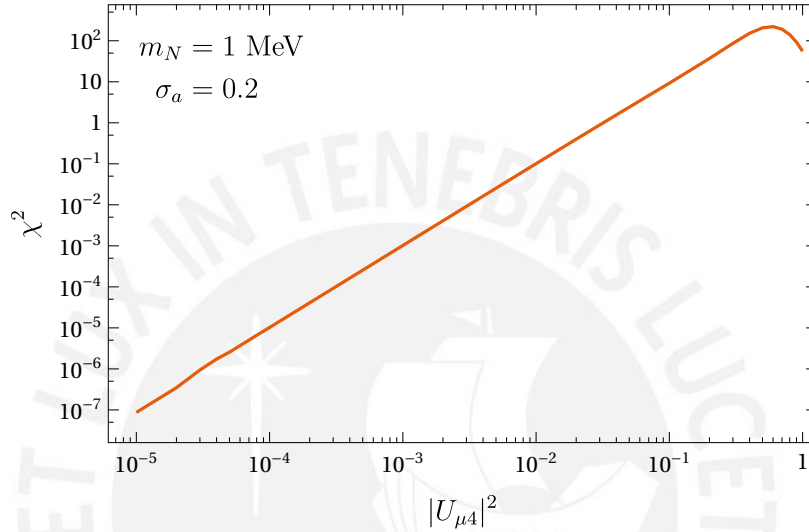
Fig. 4.26 Dependence of χ^2 on $|U_{\mu4}|^2$ for $m_N = 1$ MeV and the conservative case $\sigma_a = 0.2$.

of the mixing $|U_{\mu4}|^2$ and study how χ^2 depends on m_N. Figure 4.27 shows the dependence of χ^2 on m_N for $|U_{\mu4}|^2 = 10^{-4}$ and the ideal case $\sigma_a = 0$. We see that the value of χ^2 is greater than 1 for very low values of m_N. However, χ^2 drops for $m_N \sim 30$ MeV. The reason for this is that at this mass the decay $\pi^+ \to \mu^+ N$ becomes kinematically forbidden and this causes the sensitivity to drop. The sensitivity then drops again for $m_N \sim 380$ MeV because the decay channel $K^+ \to \mu^+ N$ becomes also kinematically forbidden. For comparison, Figure 4.28 shows the dependence of χ^2 on m_N for the conservative case $\sigma_a = 0.2$ and for $|U_{\mu4}|^2 = 10^{-4}$ (red blue) and $|U_{\mu4}|^2 = 10^{-1}$ (blue line). We see that when the systematic uncertainty is 20%, we completely lose sensitivity to mixing parameters around $|U_{\mu4}|^2 = 10^{-4}$ for all masses. However, if we increase the value of the mixing parameter, the sensitivity also increases. For instance, for $|U_{\mu4}|^2 = 10^{-1}$, we can obtain values of $\chi^2 > 1$ for most masses, although again a large drop in sensitivity occurs at $m_N \sim 30$ MeV.

In general, increasing the value of $|U_{\alpha4}|^2$ or decreasing the value of σ_a increases the values of χ^2. The value of m_N also plays an important role because it determines what channels for HNL production are kinematically allowed. Figure 4.29 shows how the value of χ^2 varies along the parameter space $\left(m_N, |U_{\mu4}|^2\right)$ for two different values of σ_a. In the ideal
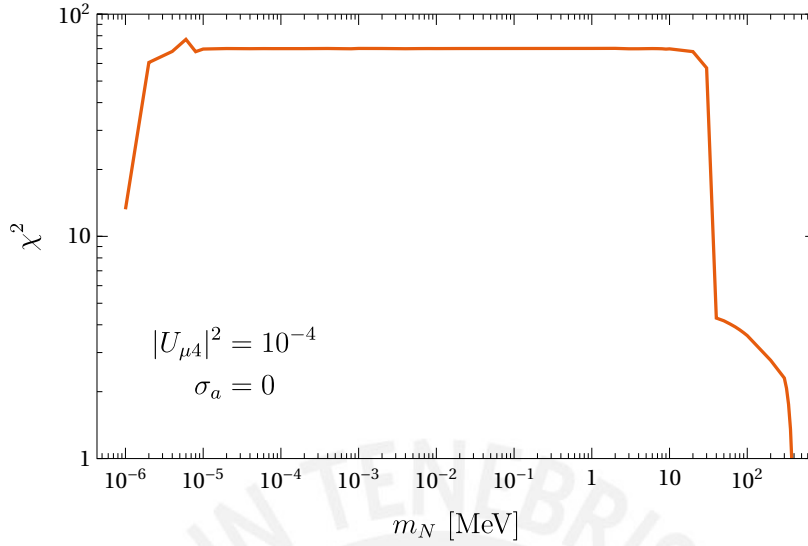
Fig. 4.27 Dependence of χ^2 on m_N for $|U_{\mu 4}|^2 = 10^{-4}$ and the ideal case $\sigma_a = 0$.

case $\sigma_a = 0$ (left) the value of χ^2 increases up to 10^8 for low masses. We also clearly see two drops of sensitivity: one at $m_N \sim 30$ MeV and another at $m_N \sim 380$ MeV. These drops were explained earlier and are produced because the HNL production channels $\pi^+ \to \mu^+ N$ and $K^+ \to \mu^+ N$ become kinematically forbidden at those values of m_N. On the other hand, in the more conservative scenario of $\sigma_a = 0.2$ (right), we see that the sensitivity drops below 1 for most of the parameter space, except when the mixing is close to 10^{-1}. In both cases, there is also an extra effect due to neutrino oscillations, although this effect is small and cannot be perceived in the plots.

4.4.3 Estimated sensitivity of DUNE to HNLs

In order to estimate the sensitivity of DUNE to HNLs from neutrino CC event deficits, we calculate the value of χ^2 according to Eq. (4.21) and then find the 90% confidence level regions. Figure 4.30 shows our results for muon (top) and electron (bottom) mixing for several values of $\sigma_a = 0.05$, 0.1 and 0.2, which correspond to an overall normalization uncertainty in of 5%, 10% and 20%, respectively.

Our results are presented in Fig. 4.30. The bottom panel of this figure shows the estimated DUNE sensitivity to $|U_{\mu 4}|^2$ at 90% confidence level on the LArTPC assuming Majorana neutrinos, ten years of operation (five in neutrino and five in antineutrino mode) and on-axis position. In our analysis, the CC event rates from all neutrino flavors are considered. For masses close to 1 eV, the limits decrease because, for the typical energies and flight distances of active neutrinos at DUNEND, the probability of neutrino oscillations into HNLs tends
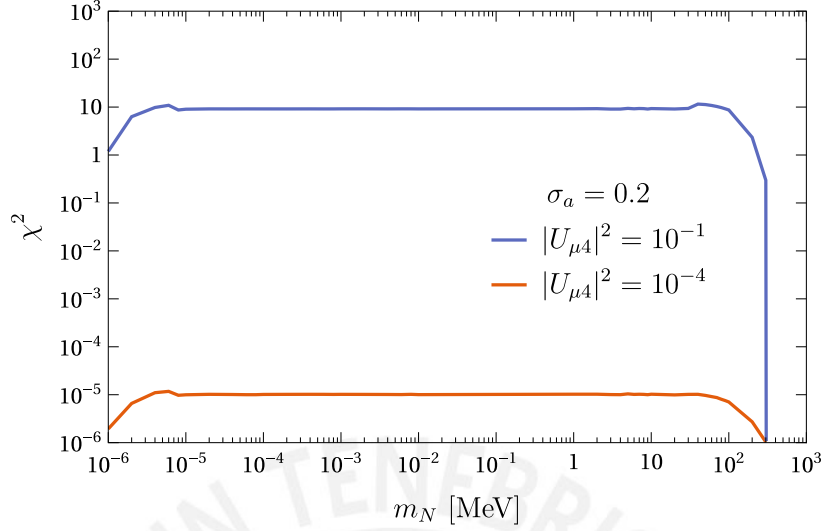
Fig. 4.28 Dependence of χ^2 on m_N for $|U_{\mu4}|^2 = 10^{-4}$ (red) and $|U_{\mu4}|^2 = 10^{-1}$ (blue) for the conservative case $\sigma_a = 0.2$.

to zero as the value of m_N approaches 1 eV. Right above 1 MeV, the limits start to oscillate since the survival probability of the active neutrinos is sensitive to m_N. For masses between 10 eV and 10 MeV, the limits are independent of m_N. The latter is because of three factors. The first one is the averaging out of the neutrino oscillations into HNLs for large values of m_N. The second one is that, for these very low masses, the total number of HNLs produced is practically independent of m_N. The other factor is that the HNL lifetime for lower masses is enormous, decaying all of them far away from the detector without the possibility of leaving a trace on it. As we already know, above $m = 33.91$ MeV, the production channel $\pi^+ \to \mu^+ N$ is kinematically forbidden, and there is a sudden loss in the sensitivity. As the mass increases, production from charged kaons starts to dominate and does so up to the end of the curve, which is at 387.81 MeV. For instance, for $\sigma_a = 0.05$ and $\sigma_a = 0.2$, the sensitivity of DUNE below 10 MeV is around $|U_{\mu4}|^2 < 2 \times 10^{-2}$ and $|U_{\mu4}|^2 < 8.5 \times 10^{-2}$, respectively. We point out that even in the conservative case of $\sigma_a = 0.2$ our limits are competitive with direct searches below 1.3 MeV.

The top q panel of Fig. 4.30 shows the expected DUNE sensitivity when we turn on $|U_{e4}|^2$ being the other ones zero. The rest of the characteristics are the same as for the left panel. In general, the sensitivity pattern is similar to the one observed for the left panel. The limits oscillate close to 1 eV and, for higher masses, they become mass-independent since most HNLs decay behind the LArTPC. Above 10 MeV, the pion decay channel $\pi^{\pm} \to e^{\pm} N$ starts to dominate because, in contrast to $\pi^{\pm} \to e^{\pm} \nu_e$, it is less suppressed by helicity due to the larger size of the HNL mass. This effect decreases the number of both ν_e and ν_{μ} CC events
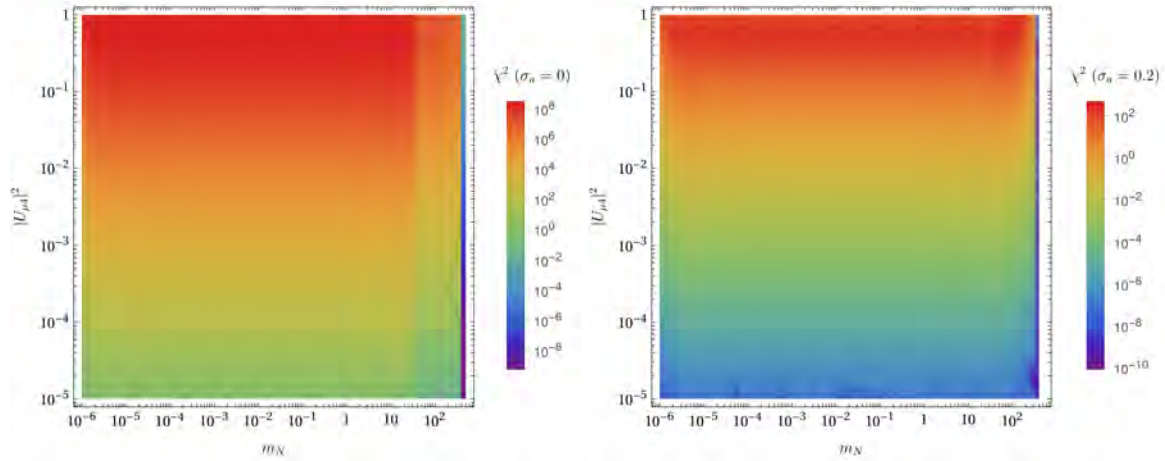
Fig. 4.29 Variation of χ^2 over the parameter space $\left(m_N, |U_{\mu4}|^2\right)$ for $\sigma_a = 0$ (left) and $\sigma_a = 0.2$ (right).

according to the suppression factor in Eq. (4.9), affecting the CC event rates of both electron and muon neutrinos. At around 139 MeV, HNL production from pion decays becomes kinematically forbidden, which translates into a decrease in sensitivity. Finally, the curve ends when production from kaons is kinematically forbidden at 493.17 MeV. For $\sigma_a = 0.05$ and $\sigma_a = 0.2$, the sensitivity of DUNE below 10 MeV is around $|U_{e4}|^2 < 1.5 \times 10^{-2}$ and $|U_{e4}|^2 < 6.5 \times 10^{-2}$, respectively. Even in the conservative case of $\sigma_a = 0.2$, our limits are competitive with direct searches below 1.3 MeV and also provide a small increase of sensitivity by a factor of 1.5 around 5 eV in comparison with experimental constraints.

Although we are making our calculations for ten years of exposure, it is important to point out that our sensitivity for $|U|^2$ increases only slightly when compared with one year of exposure. If we had not included systematic uncertainties, the limits would roughly improve as $\dfrac{|U|^2}{\sqrt{T}}$, where T represents the exposure time; in this ideal scenario, after 10 years of operation, the limits would improve by a factor of around $1/\sqrt{10} \approx 0.32$. However, introducing uncertainties in our χ^2 prescription heavily penalizes the sensitivity of our approach: in this more realistic scenario, after 10 years of operation, the limits improve by only a factor of around 0.9 in comparison with one year of exposure. Therefore, in the context of our analysis, the first year of operation of DUNE is the most important.

Another important remark must be made about the effects of neutrino oscillations in this work. Neutrino oscillations involving HNLs are only relevant when $m_N \sim 1$ eV. Since our analysis starts a 1 eV, the effects of neutrino oscillations will only be visible as a wiggle at the beginning of our sensitivity plots. For completeness, in Fig. 4.31 we show a zoom of the
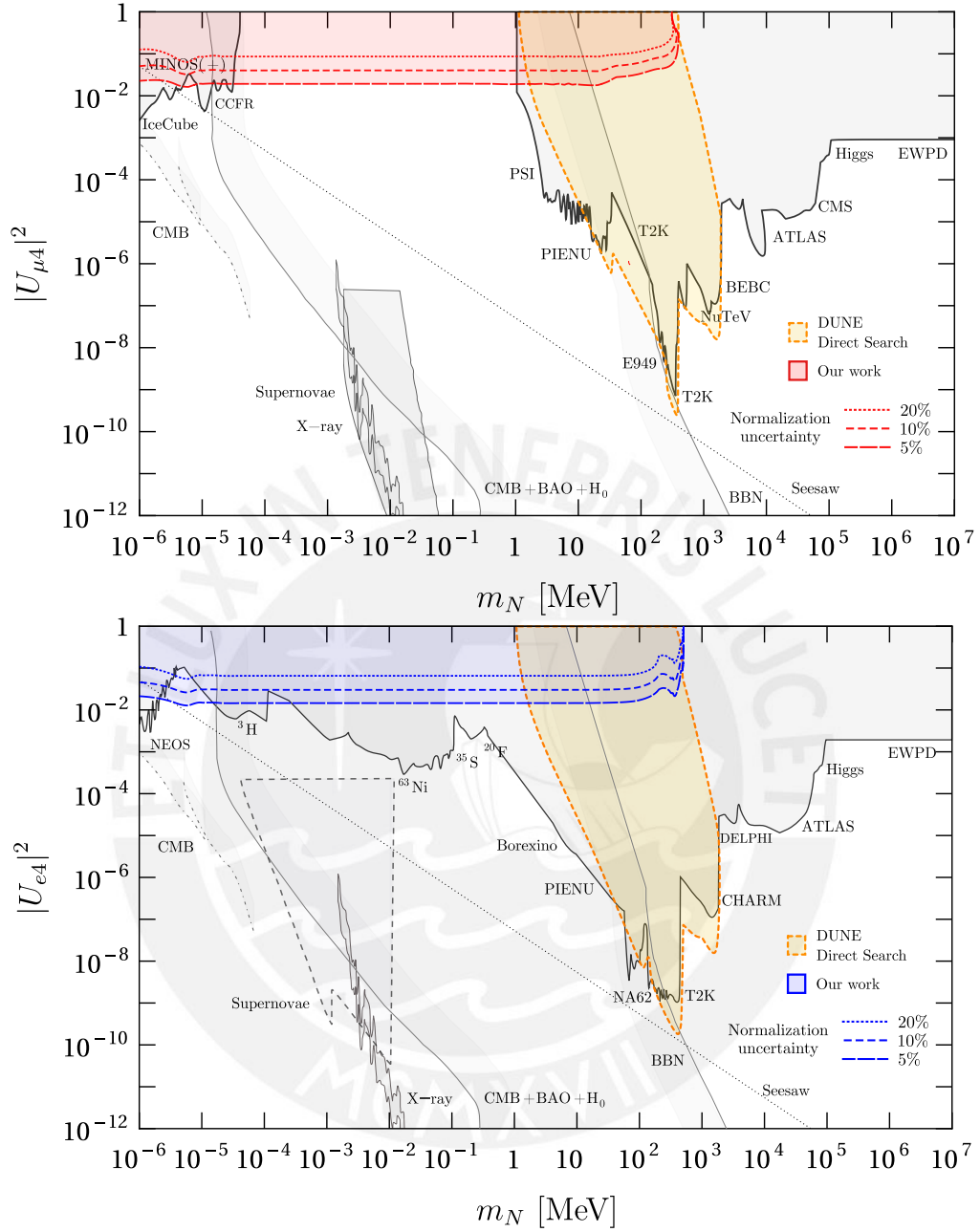
Fig. 4.30 Estimated limits of DUNE to $|U_{\mu 4}|^2$ (left, red) and $|U_{e4}|^2$ (right, blue) at 90%
confidence level by CC events disappearance at the LArTPC of the DUNEND, for 10 years
of operation (5 in neutrino and 5 in antineutrino mode) and on-axis position. The regions of
experimental constraints (gray) were taken from [32, 22, 29]. The estimated sensitivity of
DUNE obtained in [27] by direct searches of HNL decays is shown for comparison.

left plot of Fig. 4.30. We can see that close to 1 eV the sensitivity oscillates as expected, but
this effect is small and only restricted to the low tail of our sensitivity plot.
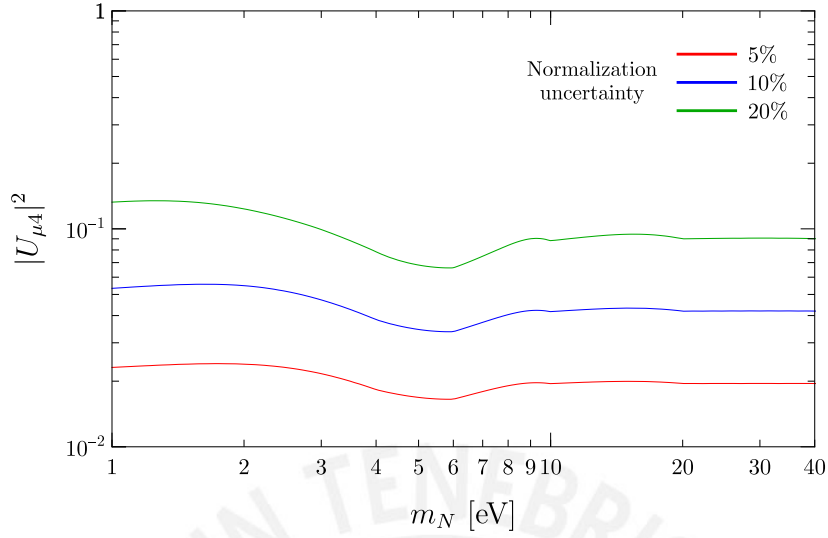
Fig. 4.31 Zoom of the sensitivy to $|U_{\mu 4}|^2$ of Fig. 4.30. The oscillation of the sensitivity near 1 eV is produced by the oscillation effects of Eq. (2.39).

We must point out that our results are blind to the Dirac or Majorana nature of the HNL. The distinction between Dirac and Majorana HNLs is usually performed in direct searches by analyzing the distributions of charged mesons and leptons produced when the HNL decays inside the detector. We are not looking into the direct search mode since it has already been discussed in [27]. Besides their decay products, Dirac and Majorana HNLs can also be differentiated by their lifetimes. However, this effect is not relevant for us because, for the mass range we studied and small mixings, almost all the HNL decays occur behind the LArTPC, as shown in Fig. 4.2. Furthermore, for very low m_N the Dirac and Majorana neutrinos are indistinguishable. Thus, we can conclude that nearly all the active neutrinos produced from the HNL decays are lost independently of the nature of neutrinos. In this way, the critical magnitude in our analysis is the production rate of HNLs, which is independent of the nature of neutrinos, so the deficit of the CC event rates is independent too. Therefore, it would not be possible to distinguish between Dirac or Majorana neutrinos through the approach presented here.

4.4.4   Off axis sensitivity

The DUNE experiment also considers the possibility of moving the DUNE near detectors horizontally, a setup known as DUNE PRISM. We move the LArTPC by up to 30 m horizontally while maintaining the rest of the simulation parameters and study the impact on our estimated sensitivities. The results are shown in Fig. 4.32, where all the lines represent the sensitivities at 90% confidence level and black dashed curves represent the on-axis

sensitivities. We see that the effect of moving the detector to an off-axis position does not affect considerably the limits. However, we see that the sensitivity increases at off-axis positions for masses close to 100 MeV.
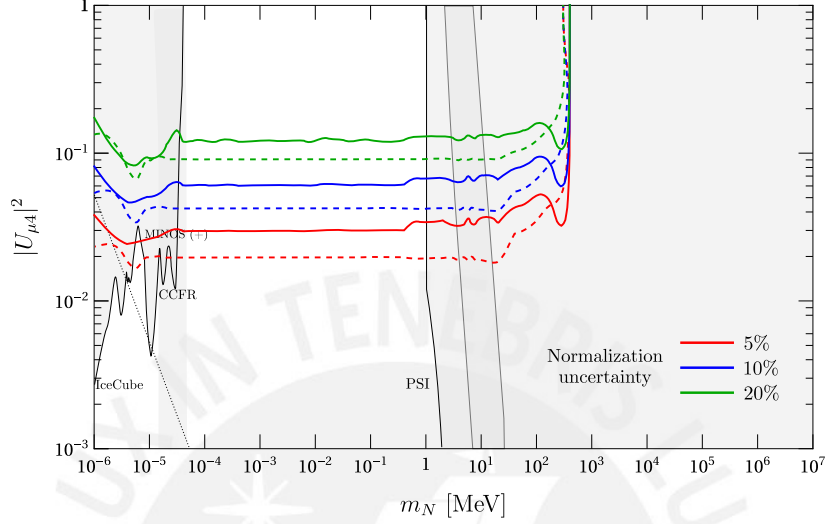
Fig. 4.32 Comparison between on-axis (black, dashed) and 30 m off-axis (solid) estimated sensitivities of DUNE to $|U_{\mu4}|^2$ at 90% confidence by neutrino CC events disappearance for 10 years of operation (5 in neutrino and 5 in antineutrino mode). The regions of experimental constraints were taken from [32, 22, 29].

4.4.5 Allowed regions for $(m_N, |U_{\alpha4}|^2)$

We also explore the potential to constraint the $(m_N, |U_{\alpha4}|^2)$ parameter space region in the context of this indirect search. So, assuming that the disappearance CC events are originated by the presence of HNLs within the neutrino beam, we perform a χ^2 analysis fixing our simulation in certain values of $(m_N, |U_{\alpha4}|^2)$. The allowed regions for $m_N = 0.1$ MeV and $|U_{\mu4}|^2 = 5 \times 10^{-2}$ are presented in Fig. 4.33 for $\sigma_a = 0.05$ (red), $\sigma_a = 0.1$ (blue) and $\sigma_a = 0.2$ (green), were we include the 90% (solid) and 95% (dashed) confidence regions. These regions are bounded to the right but extend to the left up to $m_N = 1$ eV, a mass degeneracy that reflects the fact that our approach is not sensitive to m_N for low masses. For the case $\sigma_a = 0.05$ (red) the 95% confidence region is sufficiently small that it is possible to constraint $|U_{\mu4}|^2$ within an uncertainty of 30%. However, when we include larger systematic uncertainties such as $\sigma_a = 0.2$ (green) we find that we can only constraint the value of $|U_{\mu4}|^2$ within an uncertainty of 60%.
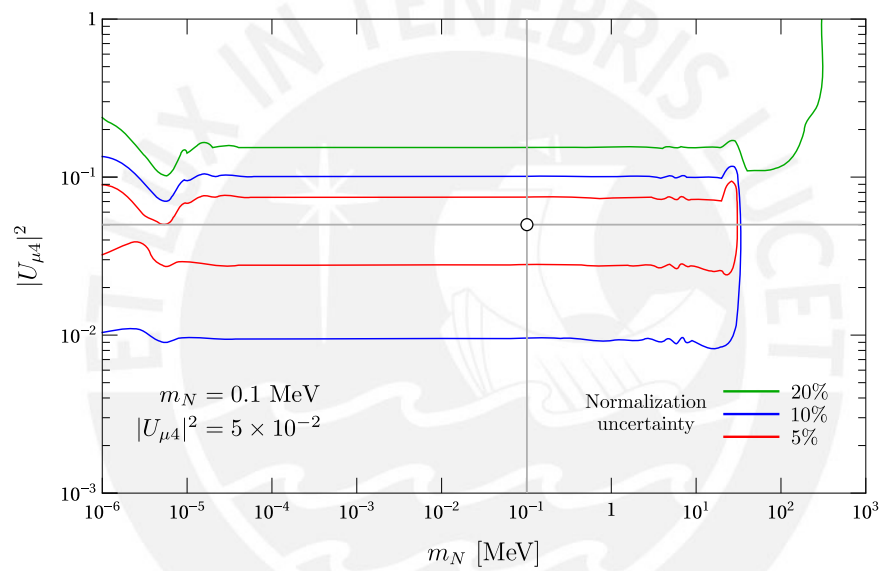
Fig. 4.33 90% confidence level regions for $m_N = 0.1$ MeV, $|U_{\mu 4}|^2 = 5 \times 10^{-2}$, 10 years of operation (5 in neutrino and 5 in antineutrino mode), on-axis position and several values of σ_a.

Chapter 5

Conclusion and outlook

This work consists of a thorough analysis of the effects that HNLs can have on the active neutrino flux produced at DUNE and the charged current event rates at the LArTPC of the DUNEND. We find that it is possible to simulate the production and decay chain of heavy neutral leptons by providing the software PYTHIA8 with all the information about the production and decay rates of the heavy neutral leptons. Since PYTHIA is a software optimized for the simulation of production and decay chains of particles, we found this approach very efficient, especially because it opens the possibility of more sophisticated analysis that exploits the capabilities of PYTHIA8. In our simulations, PYTHIA8 receives as input the positions of the lepton and meson parents of the HNLs and the relevant physical parameters of the simulation (meson decay channels and branching ratios, HNL mass, HNL lifetime, HNL decay channels and their branching ratios, among others) but the scripts also take as input the position and size of the detector. In this work, we applied our methods to the DUNE experiment; however, due to the flexibility of our analysis, it is possible to extend these results to other experiments by changing the position of the detectors and providing PYTHIA8 the initial flux of the parent particles of the experiment of interest. Although we worked mainly with cases in which the HNL mixes with electron and muon neutrinos, we were also able to parametrize the production of D mesons using PYTHIA8 and reproduce the tau neutrino flux at DUNE. Again, it is possible de repeat this calculation for other experiments at higher energies. Since DUNE is not optimized for tau neutrino production, the sensitivity of DUNE to tau channels is negligible and we could not constrain the parameter space that involves tau mixings. However, if we apply our methods to experiments with higher energies, we could study the mixing of HNLs and tau neutrinos.

After our analysis, we find that, as a rule of thumb, the production of HNls decreases the number of active neutrinos that reach the LArTPC of the DUNEND. This effect is significant

even if for $m_N \sim$ MeV, when the neutrino oscillations to HNLs are averaged out. This neutrino disappearance represents an indirect signal of HNLs at DUNE that is not due to neutrino oscillations, but rather to the kinematics of the meson and HNL decays. When combined with the effects of neutrino oscillations, it is possible to use this deficit in CC event rates to estimate limits to $|U_{e4}|^2$ and $|U_{\mu 4}|^2$. We found that these limits are very sensitive to the uncertainty of the neutrino flux prediction at the DUNEND. In order to get conservative estimates of these limits, we considered overall normalization uncertainties of up to 20%.

The main result of this work was the estimation of the sensitivity of DUNE to HNLs due to neutrino CC event rates deficit. This approach is different from the usual "direct searches", which look for the decay products of HNLs inside one detector. In this work, we did not require that the HNL decays inside a detector. In fact, most of the HNLs decay way behind the DUNEND. This phenomenon translates into a deficit of neutrino CC event rates at DUNEND and was used to set limits on the values of the HNL mass and its mixings to active neutrinos. For five years per mode (neutrino/antineutrino), on-axis configuration and a 5% overall normalization uncertainty we get limits of $|U_{\mu 4}|^2 < 9 \times 10^{-3}$ and $|U_{e4}|^2 < 7 \times 10^{-3}$ below 1.5 MeV. We also included a more pessimistic scenario of a 20% systematic uncertainty and were still able to set bounds of $|U_{\mu 4}|^2 < 4 \times 10^{-2}$ and $|U_{e4}|^2 < 3 \times 10^{-2}$ below 1.4 MeV. These limits are better than the ones predicted by DUNE direct searches or even placed in mass regions inaccessible to them. These bounds are still competitive for the off-axis configuration. Besides, we explore the capacity of determining the allowed parameter space region $(m_N, |U_{\alpha 4}|^2)$ for the specific parameter values $m_N = 0.1$ MeV and $|U_{\mu 4}|^2 = 5 \times 10^{-2}$ and found that, although there is a large degeneracy in the value of m_N, it is possible to constraint $|U_{\mu 4}|^2$ with uncertainties in the order of 30(60)% for a 5(20)% overall normalization uncertainty in the CC event rates. Finally, it is worth noting that the disappearance of CC events as a HNL signature is complementary to the direct observation or HNL decays, showing an attractive potential to be used in neutrino Near Detectors with high ν CC event rates.

References

[1] (2015). The PIP-II Reference Design Report.

[2] (2019). *Neutrino Non-Standard Interactions: A Status Report*, volume 2.

[3] Abdullahi, A. M. et al. (2022). The Present and Future Status of Heavy Neutral Leptons. In *2022 Snowmass Summer Study*.

[4] Abed Abud, A. et al. (2021). Deep Underground Neutrino Experiment (DUNE) Near Detector Conceptual Design Report. *Instruments*, 5(4):31.

[5] Abi, B. et al. (2018). The DUNE Far Detector Interim Design Report, Volume 3: Dual-Phase Module.

[6] Abi, B. et al. (2020a). Deep Underground Neutrino Experiment (DUNE), Far Detector Technical Design Report, Volume I Introduction to DUNE. *JINST*, 15(08):T08008.

[7] Abi, B. et al. (2020b). Deep Underground Neutrino Experiment (DUNE), Far Detector Technical Design Report, Volume II: DUNE Physics.

[8] Abi, B. et al. (2020c). Deep Underground Neutrino Experiment (DUNE), Far Detector Technical Design Report, Volume III: DUNE Far Detector Technical Coordination. *JINST*, 15(08):T08009.

[9] Abi, B. et al. (2020d). Deep Underground Neutrino Experiment (DUNE), Far Detector Technical Design Report, Volume IV: Far Detector Single-phase Technology. *JINST*, 15(08):T08010.

[10] Abi, B. et al. (2021). Experiment Simulation Configurations Approximating DUNE TDR.

[11] Agostinelli, S. et al. (2003). GEANT4–a simulation toolkit. *Nucl. Instrum. Meth. A*, 506:250–303.

[12] Ahmad, Q. R. et al. (2001). Measurement of the rate of $\nu_e + d \rightarrow p + p + e^-$ interactions produced by ^{8}B solar neutrinos at the Sudbury Neutrino Observatory. *Phys. Rev. Lett.*, 87:071301.

[13] Ahmad, Q. R. et al. (2002). Direct evidence for neutrino flavor transformation from neutral current interactions in the Sudbury Neutrino Observatory. *Phys. Rev. Lett.*, 89:011301.

[14] Akhmedov, E. K., Lindner, M., Schnapka, E., and Valle, J. W. F. (1996). Dynamical left-right symmetry breaking. *Phys. Rev. D*, 53:2752–2780.

[15] Aliev, T. M., Savci, M., and Ozpineci, A. (2004). Form factors of D/s+ —> phi anti-l nu decay in QCD light cone sum rule. *Eur. Phys. J. C*, 38:85–91.

[16] Allison, J. et al. (2016). Recent developments in Geant4. *Nucl. Instrum. Meth. A*, 835:186–225.

[17] Altmannshofer, W., Gori, S., Pospelov, M., and Yavin, I. (2014). Neutrino trident production: A powerful probe of new physics with neutrino beams. *Phys. Rev. Lett.*, 113:091801.

[18] Alves, G. A. et al. (1996). Feynman- x and transverse momentum dependence of D meson production in 250 gev π, K, and p interactions with nuclei. *Phys. Rev. Lett.*, 77:2392–2395.

[19] Anelli, M., Aoki, S., Arduini, G., Back, J., Bagulya, A., Baldini, W., Baranov, A., Barker, G., Barsuk, S., Battistin, M., et al. (2015). A facility to search for hidden particles (ship) at the cern sps. *arXiv preprint arXiv:1504.04956*.

[20] Antusch, S., Biggio, C., Fernández-Martínez, E., Gavela, M. B., and López-Pavón, J. (2006). Unitarity of the leptonic mixing matrix. *Journal of High Energy Physics*, 2006(10):084–084.

[21] Antusch, S., Huber, P., King, S. F., and Schwetz, T. (2007). Neutrino mixing sum rules and oscillation experiments. *JHEP*, 04:060.

[22] Argüelles, C. A., Foppiani, N., and Hostert, M. (2022). Heavy neutral leptons below the kaon mass at hodoscopic neutrino detectors. *Phys. Rev. D*, 105(9):095006.

[23] Ball, M. et al. (2017). The PIP-II Conceptual Design Report.

[24] Ballett, P., Boschi, T., and Pascoli, S. (2020). Heavy Neutral Leptons from low-scale seesaws at the DUNE Near Detector. *JHEP*, 03:111.

[25] Ballett, P., King, S. F., Luhn, C., Pascoli, S., and Schmidt, M. A. (2014). Testing atmospheric mixing sum rules at precision neutrino facilities. *Phys. Rev. D*, 89(1):016016.

[26] Bass, M. (2014). *Neutrino oscillation parameter sensitivity in future long-baseline experiments*. PhD thesis, Colorado State U., Colorado State U.

[27] Berryman, J. M., de Gouvea, A., Fox, P. J., Kayser, B. J., Kelly, K. J., and Raaf, J. L. (2020). Searches for Decays of New Particles in the DUNE Multi-Purpose Near Detector. *JHEP*, 02:174.

[28] Böhlen, T. T., Cerutti, F., Chin, M. P. W., Fassò, A., Ferrari, A., Ortega, P. G., Mairani, A., Sala, P. R., Smirnov, G., and Vlachoudis, V. (2014). The FLUKA Code: Developments and Challenges for High Energy and Medical Applications. *Nucl. Data Sheets*, 120:211–214.

[29] Bolton, P. D., Deppisch, F. F., and Bhupal Dev, P. S. (2020). Neutrinoless double beta decay versus other probes of heavy sterile neutrinos. *JHEP*, 03:170.

[30] Bondarenko, K., Boyarsky, A., Gorbunov, D., and Ruchayskiy, O. (2018). Phenomenology of GeV-scale Heavy Neutral Leptons. *JHEP*, 11:032.

[31] Breitbach, M., Buonocore, L., Frugiuele, C., Kopp, J., and Mittnacht, L. (2022). Searching for physics beyond the Standard Model in an off-axis DUNE near detector. *JHEP*, 01:048.

[32] Bryman, D. A. and Shrock, R. (2019). Improved Constraints on Sterile Neutrinos in the MeV to GeV Mass Range. *Phys. Rev. D*, 100(5):053006.

[33] Dasgupta, B. and Kopp, J. (2021). Sterile Neutrinos. *Phys. Rept.*, 928:1–63.

[34] Davidson, S., Nardi, E., and Nir, Y. (2008). Leptogenesis. *Phys. Rept.*, 466:105–177.

[35] DUNE Collaboration (2015). http://home.fnal.gov/~ljf26/DUNEFluxes/.

[36] Ferrari, A., Sala, P. R., Fasso, A., and Ranft, J. (2005). FLUKA: A multi-particle transport code (Program version 2005).

[37] Fileviez Perez, P. et al. (2022). On Baryon and Lepton Number Violation.

[38] Flanz, M., Paschos, E. A., and Sarkar, U. (1995). Baryogenesis from a lepton asymmetric universe. *Phys. Lett. B*, 345:248–252. [Erratum: Phys.Lett.B 384, 487–487 (1996), Erratum: Phys.Lett.B 382, 447–447 (1996)].

[39] Fukuda, Y. et al. (1998). Evidence for oscillation of atmospheric neutrinos. *Phys. Rev. Lett.*, 81:1562–1567.

[40] Gago, A. M., Gomes, R. A., Gomes, A. L. G., Jones-Perez, J., and Peres, O. L. G. (2017). Visible neutrino decay in the light of appearance and disappearance long baseline experiments. *JHEP*, 11:022.

[41] Gavela, M. B., Hambye, T., Hernandez, D., and Hernandez, P. (2009). Minimal Flavour Seesaw Models. *JHEP*, 09:038.

[42] Giunti, C. and Kim, C. W. (2007). *Fundamentals of Neutrino Physics and Astrophysics*.

[43] Gorbunov, D. and Shaposhnikov, M. (2007). How to find neutral leptons of the νMSM? *JHEP*, 10:015. [Erratum: JHEP 11, 101 (2013)].

[44] Gronau, M., Leung, C. N., and Rosner, J. L. (1984). Extending Limits on Neutral Heavy Leptons. *Phys. Rev. D*, 29:2539.

[45] Harris, P., Schuster, P., and Zupan, J. (2022). Snowmass White Paper: New flavors and rich structures in dark sectors. In *2022 Snowmass Summer Study*.

[46] Horiuchi, S. and Kneller, J. P. (2018). What can be learned from a future supernova neutrino detection? *J. Phys. G*, 45(4):043002.

[47] Inc., W. R. (2022). Mathematica, Version 13.1. Champaign, IL.

[48] Liberati, S. and Maccione, L. (2009). Lorentz Violation: Motivation and new constraints. *Ann. Rev. Nucl. Part. Sci.*, 59:245–267.

[49] Mavromatos, N. E. (2005). CPT violation: Theory and phenomenology. In *2nd International Conference on Exotic Atoms and Related Topics*, pages 361–372.

[50] Mirizzi, A., Tamborra, I., Janka, H.-T., Saviano, N., Scholberg, K., Bollig, R., Hudepohl, L., and Chakraborty, S. (2016). Supernova Neutrinos: Production, Oscillations and Detection. *Riv. Nuovo Cim.*, 39(1-2):1–112.

[51] Nath, P. and Fileviez Perez, P. (2007). Proton stability in grand unified theories, in strings and in branes. *Phys. Rept.*, 441:191–317.

[52] Pilaftsis, A. (1998). Baryogenesis through mixing of heavy Majorana neutrinos. *PoS*, corfu98:075.

[53] Plumacher, M. (1997). Baryogenesis and lepton number violation. *Z. Phys. C*, 74:549–559.

[54] Pontecorvo, B. (1957). Mesonium and anti-mesonium. *Sov. Phys. JETP*, 6:429.

[55] Qian, X. and Vogel, P. (2015). Neutrino Mass Hierarchy. *Prog. Part. Nucl. Phys.*, 83:1–30.

[56] Richman, J. D. and Burchat, P. R. (1995). Leptonic and semileptonic decays of charm and bottom hadrons. *Rev. Mod. Phys.*, 67:893–976.

[57] Sjöstrand, T., Ask, S., Christiansen, J. R., Corke, R., Desai, N., Ilten, P., Mrenna, S., Prestel, S., Rasmussen, C. O., and Skands, P. Z. (2015). An introduction to PYTHIA 8.2. *Comput. Phys. Commun.*, 191:159–177.

[58] Vicenzi, M. (2022). SAND - System for on-Axis Neutrino Detection - in the DUNE Near Detector Complex. *PoS*, NuFact2021:248.

[59] Weinberg, S. (1989). Larger Higgs Exchange Terms in the Neutron Electric Dipole Moment. *Phys. Rev. Lett.*, 63:2333.

[60] Wikipedia (2019). Standard model of elementary particles.

[61] Workman, R. L. and Others (2022). Review of Particle Physics. *PTEP*, 2022:083C01.

[62] Xing, Z.-z. and Zhao, Z.-h. (2021). The minimal seesaw and leptogenesis models. *Rept. Prog. Phys.*, 84(6):066201.